EVALUATION OF ^{64}Cu-ATSM FOR NON-INVASIVE IMAGING OF TUMOUR HYPOXIA BY POSITRON EMISSION

Katie A Wood

University College London, UK

Gray Cancer Institute, Middlesex, UK

Mount Vernon Cancer Centre, Northwood, UK

A thesis submitted for the degree of MD(Res)

University of London

2008

UMI Number: U593362

All rights reserved

INFORMATION TO ALL USERS
The quality of this reproduction is dependent upon the quality of the copy submitted.

In the unlikely event that the author did not send a complete manuscript
and there are missing pages, these will be noted. Also, if material had to be removed,
a note will indicate the deletion.

UMI U593362
Published by ProQuest LLC 2013. Copyright in the Dissertation held by the Author.
Microform Edition © ProQuest LLC.
All rights reserved. This work is protected against
unauthorized copying under Title 17, United States Code.

ProQuest LLC
789 East Eisenhower Parkway
P.O. Box 1346
Ann Arbor, MI 48106-1346

Declaration

I, Katie Anne Wood, confirm that the work presented in this thesis is my own. Where information has been derived from other sources, I confirm that this has been indicated in the thesis.

Katie Anne Wood

June 2008

Abstract

^{64}Cu(II)-diacetyl-bis(N^4-methyl-thiosemicarbazone) (^{64}Cu-ATSM) has been proposed as a positron emitting radiotracer to delineate tumour hypoxia using positron emission tomography (PET). In this study evaluation of this radiotracer was carried out in the P22 carcinosarcoma BD-9 rat tumour model. The distribution of ^{64}Cu-ATSM with the immunohistochemical marker of hypoxia, pimonidazole, was compared using autoradiography and pimonidazole staining at early (1 hour) and late (20.5 hours) time-points after tracer injection however no correlation was found. The impact of tumour blood flow in determining tumour distribution of ^{64}Cu-ATSM Gadolinium-enhanced MRI scanning was investigated. This showed a correlation between ^{64}Cu-ATSM and blood flow up to twenty minutes after the administration of ^{64}Cu-ATSM, an association beyond this time-point was not seen.

A further study examined the effect of increased tumour hypoxia on uptake and retention of ^{64}Cu-ATSM using the vascular disrupting agent combretastatin A4 phosphate (CA4P). No correlation between ^{64}Cu-ATSM uptake and retention and hypoxia was seen in the tumours administered ^{64}Cu-ATSM after CA4P administration, however a negative correlation between ^{64}Cu-ATSM uptake and hypoxia was seen in the tumours receiving ^{64}Cu-ATSM 10 minutes prior to CA4P administration. This strong negative association is likely to reflect the distribution of ^{64}Cu-ATSM fixed at the time of administration of the vascular disrupting agent CA4P preventing its movement elsewhere in the tumour. In this tumour model ^{64}Cu-ATSM distribution reflects tumour blood flow for twenty minutes after its administration. As

such, fixation of the distribution of ^{64}Cu-ATSM 10 minutes post-injection is likely to reflect tumour blood flow, explaining the negative association between ^{64}Cu-ATSM and hypoxia observed in this part of the study.

Evaluation of ^{64}Cu-ATSM in the P22 tumour model has demonstrated that although it is tumour-avid it does not represent tumour hypoxia.

Acknowledgements

I would like to thank;

Professor Michele Saunders, my supervisor, for setting up the project and her constant and unwavering support and advice throughout.

Dr Davina Honess and Ian Wilson for their generosity of time, advice and unending help.

Dr Ross Maxwell, for his considerable expertise in MRI and computing.

Dr Rowena Paul for her extremely hard work and long hours producing ^{64}Cu-ATSM.

Frances Daley for her hard work and advice regarding immunohistochemical staining.

Dr Wai Lup Wong and Dr Bal Sanghera in the Paul Strickland Scanner Centre at Mount Vernon Hospital and Dr Michael O'Doherty, Dr Paul Marsden and Professor Phil Blower from Guy's and St Thomas' Hospital and King's College, London, who have advised throughout the course of the project.

Finally I would like to thank my husband Hardev and daughter Lila for being so patient and understanding during this project and my parents for their support throughout.

Contents

List of figures

Chapter 1

Chapter 2

Chapter 3

Chapter 4

List of tables

CHAPTER 1

Introduction

Tumour hypoxia has been known to result in a poorer prognosis, radiation resistance and treatment failure for many years, however there is no widely available method for its measurement. Cancer treatment options are becoming increasingly sophisticated and can be tailored to the specific biological architecture of a given tumour. The ability to identify regions of hypoxia within a tumour would add to this, allowing the identification of hypoxic subvolumes for radiotherapy dose escalation using intensity modulated radiotherapy (IMRT). In addition, more informed treatment decisions could be made on the basis of whether or not a tumour is hypoxic, with improved estimates of prognosis. In providing more suitable and tailored treatment the chance of tumour control and cure will improve and the exposure to toxic treatments which are known to be ineffective in a hypoxic tumour micro-environment will be reduced.

This project has been conducted to evaluate the role of ^{64}Cu(II)-diacetyl-bis(N^4-methyl-thiosemicarbazone) (^{64}Cu-ATSM) as a positron emission tomography (PET) radiotracer of tumour hypoxia. This non-invasive technique for imaging tumour hypoxia would allow the identification of tumour hypoxia subvolumes which could inform clinicians as to the most appropriate choice of treatment, radiotherapy dose planning such that hypoxic regions are dose-escalated and provision of an additional tool to provide estimates of prognosis.

This introduction will detail the causes and effects of hypoxia within tumours, the treatment options that have so far been explored to overcome hypoxia, the methods available for determining tumour hypoxia and a review of the data currently available on ^{64}Cu-ATSM.

1.1 Biological effects of tumour hypoxia

For over half a century it has been known that within solid tumours, areas of hypoxia exist that that are not present within normal tissues (Crabtree 1933; Gray 1953). Hypoxia within a tumour has been demonstrated to increase the resistance to treatment with radiation, chemotherapy and increase metastatic potential. Tumour oxygen tensions below 2.5mmHg have been found in a variety of different tumour types: breast cancer, uterine cervix, head and neck, rectum, pancreas, brain, soft tissue sarcomas (Vaupel, Mayer 2005) and have been identified as an independent prognostic factor in squamous cell carcinomas of the head and neck, tumours of the uterine cervix and soft tissue sarcomas (Vaupel, Mayer 2005). It is thought that up to 50-60% of locally advanced solid tumours have a heterogeneous distribution of hypoxic and anoxic regions. The oxygenation of cancers of the breast, uterine cervix and head and neck is lower than their respective normal tissues prior to treatment, and this low oxygenation level is independent of tumour stage, histology and grade. Local recurrences have a higher hypoxic fraction than primary tumours although there is no apparent difference in the oxygenation status of primary tumours and metastases (Hockel 2001).

Several mechanisms have been identified in tumour cells to maintain cells in a hypoxic environment such as an increase in anaerobic glycolysis, optimisation of the oxygen carrying capacity of blood, regulation of angiogenesis to improve delivery of essential nutrients, and inhibition of apoptosis. In addition, hypoxia can induce genetic and growth factor driven cellular responses that overcome the stresses of a hypoxic environment resulting in tumour cells with a more aggressive phenotype, a greater propensity for local invasion, metastatic spread and resistance to therapy.

A definition of tissue hypoxia is the inadequate supply of oxygen such that function is compromised. A value of 10 mmHg or less is thought to represent a threshold for hypoxia on a global tissue level although this threshold does vary depending on cell type. When a cell becomes hypoxic intracellular acidosis occurs (Vaupel 1994).

Below 7mmHg cellular gene expression changes (Jiang 1996). This is the result of an adaptive response that has evolved as a result of hypoxic stress. Although hypoxia can be transient, persistent hypoxia can result in persistent alterations in gene expression. Hypoxia-inducible factor 1α (HIF-1α) is a key transcription factor regulated by oxygen (see figure 1.1). HIF-1α binds to the hypoxia-responsive element (HRE), a particular DNA sequence, and can activate more than 40 genes (Semenza 2003). HIF-1α is produced in response to hypoxic stress and one of its roles is the maintenance of cell viability in a hypoxic environment. A key part of this is facilitating the switch from oxidative metabolism to anaerobic metabolism with ATP production via glycolysis.

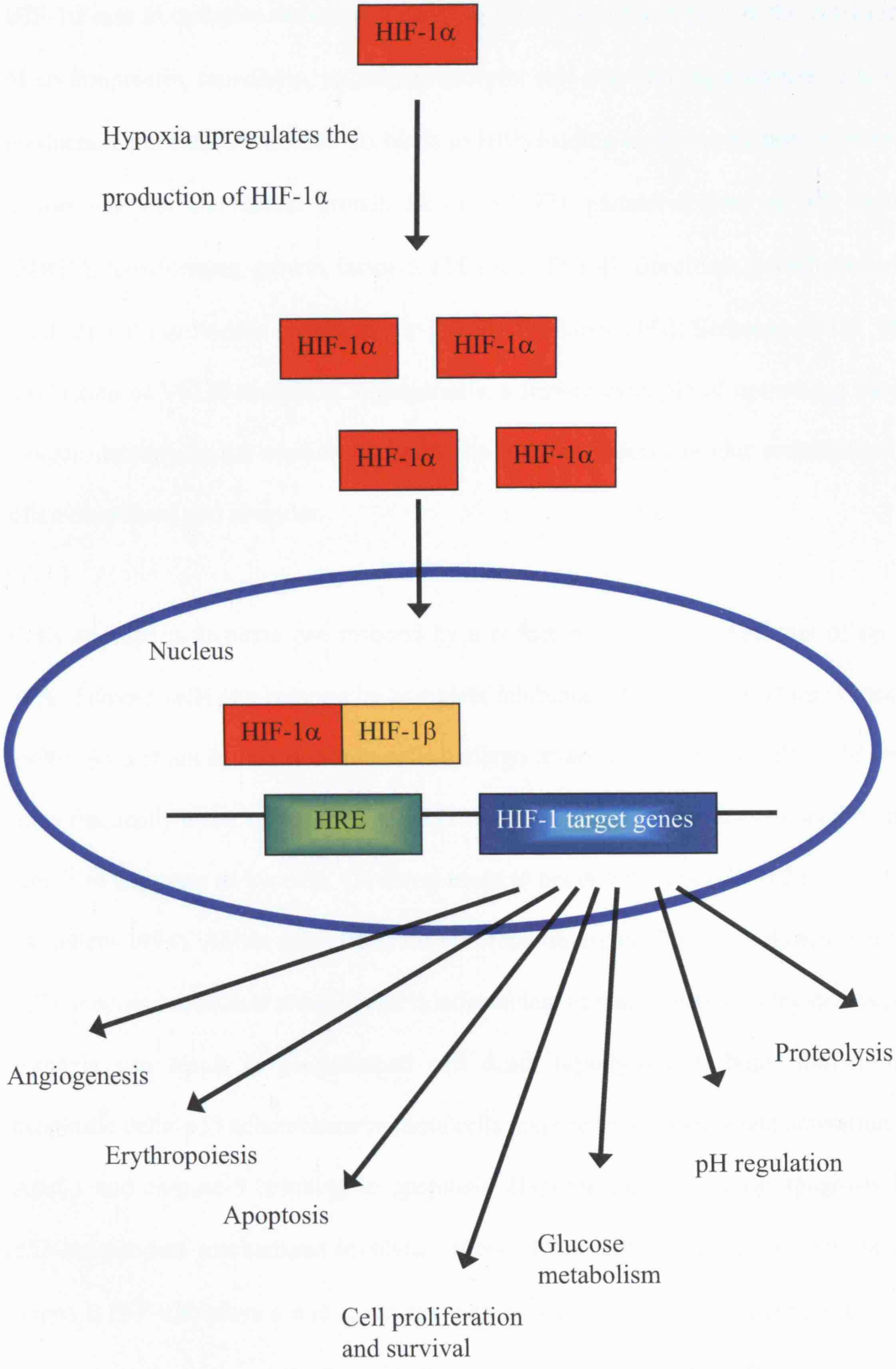

Figure 1.1 *Cellular response to HIF-1α*

HIF-1α acts to optimise the oxygen carrying capacity of the blood by the activation of erythropoietin, transferrin, transferrin receptor and rate-limiting enzymes of heme production and catabolism. HIF-1α binds to HRE leading to the production of growth factors vascular endothelial growth factor (VEGF), platelet-derived growth factor (PDGF), transforming growth factor-α (TGF-α), TGF-β, fibroblast growth factor-2 (FGF-2) and insulin-like growth factor-2 (IGF-2) (Harris 2002; Semenza 2003). The production of VEGF stimulates angiogenesis, a further example of optimising blood oxygen delivery to the tumour, although the resultant microvascular architecture is often disordered and irregular.

Cells exposed to hypoxia can respond by a reduction in protein synthesis of up to 50%. Tumour cells can respond by complete inhibition of cell proliferation (Giaccia 1996). As a result of this response cells undergo re-assortment in the cell cycle with most frequently a cell cycle arrest in the G1/s-phase, although this does depend on the length of exposure to hypoxia. G1 arrest tends to occur with a pO_2 of 0.2 to 1mmHg (Amellem 1994). Above this effects on proliferation are negligible. Below this most cells undergo immediate arrest which is independent of their position in the cell cycle. Hypoxia can result in programmed cell death (apoptosis) in both normal and neoplastic cells. p53 accumulates in these cells and causes a downstream activation of Apaf-1 and caspase-9 resulting in apoptosis. Hypoxia can also cause apoptosis by p53-independent mechanisms involving genes of the BCL-2 family. Nuclear factor kappa B (NF-κB) plays a role in the regulation of apoptosis by stimulating the over-expression of anti-apoptotic factor BCL-2. The expression of NF-κB is induced by hypoxia (Vaupel, Mayer 2005). Below a certain energy level hypoxia can cause death by necrosis (Vaupel, Mayer 2005).

HIF-1α regulates the expression of genes that have an established role in the pathophysiology of local invasion and metastasis. Cathepsin D, matrix metalloproteinase 2, urokinase plasminogen activator receptor (Patterson 2000), vimentin and transforming growth factor alpha (Krishnamachary 2003) are involved in the process of facilitating local tissue invasion and metastasis and are produced following activation of HIF-1α.

Hypoxia can cause mutagenesis in a number of ways. The point mutation rate increases as a result of diminished activity of the nucleotide repair system. Point mutations that may occur will therefore not be repaired and the passage of that genetic defect will be passed to subsequent generations of cells. Hypoxia itself may be responsible for DNA double strand breaks through the induction of a specific endonuclease. These double strand breaks may result in chromosomal aberrations and gene amplification. Often these strand breaks occur at fragile sites within regions containing oncogenes or genes that confer a more resistant phenotype. Polyploidy may be induced by hypoxia. This genetic abnormality can manifest in cells under environmental stress, thereby making the cell more resistant to cancer therapy (Vaupel and Mayer 2005). These genetic mutants occurring as a consequence of hypoxia may result in phenotypes that are more resistant to treatment, capable of surviving in circumstances that would otherwise be lethal.

1.2 Physiology of tumour hypoxia

Tumour hypoxia occurs as a result of (a) *perfusion-limited* oxygen delivery due to structural and functional abnormalities of the tumour microvasculature which can lead to transient reduction or absence of blood flow, (b) *diffusion-limited* oxygen delivery due to the loss of order of tumour vasculature such that not all regions within a tumour will be adequately perfused and (c*) disease or therapy related anaemia* leading to a reduction in the oxygen carrying capacity of the blood. Typically these failures in adequate oxygen delivery co-exist within the same tumour (Hoogsteen 2007).

Perfusion-limited hypoxia:

This is transient and also known as acute hypoxia. It is ischaemic in nature and is likely to occur as a result of the severe structural and functional abnormalities of the tumour microvasculature which can transiently shutdown or reverse the delivery of blood to parts of a tumour.

Diffusion-limited hypoxia:

This type of hypoxia is also known as chronic hypoxia and occurs as a result of diffusion distances greater than optimal for delivery of nutrients, typically cells located greater than 70-100 μm (diffusion distance of soluble oxygen in tissues) away from the nearest capillary depending on where the part of the tumour lies in relation to the arterial or venous end of the capillary. This can result in cells chronically deprived of oxygen.

Disease or therapy related hypoxia:

This relates to the reduced O_2 carrying capacity of blood and may be disease or treatment related. This is particularly seen in tumours that are supported by vessels with low perfusion pressures.

1.3 Effects of tumour hypoxia on radiotherapy

Tumour hypoxia protects against radiation damage. Radiation sensitivity declines rapidly from 30mmHg to 0mmHg (Gray 1953). It is well known that anoxic cells require up to three times the amount of radiation dose to elicit the same cell kill achieved in well-oxygenated cells (Denekamp 1989). The ratio of radiation dose required to cause the same cell kill in anoxic versus normoxic cells is known as the oxygen enhancement ratio (OER). Half maximal sensitivity to x- and γ-rays occurs at oxygen tensions of between 2-5mmHg with near maximal oxygen effects only beginning to be seen at 10-15mmHg (Hall 2006). Oxygen partial pressures below 0.5mmHg are maximally resistant to radiation however these cells are unlikely to survive due to chronic hypoxia. Clinical studies have shown that measured tumour pO_2 correlates with local control and in some cases survival following radiotherapy (Nordsmark 1996). Nordsmark et al found that a tumour pO_2 of less than 2.5mmHg was the strongest independent risk factor in predicting radiation response in squamous cell carcinoma of the head and neck and a study by Brizel et al showed that patients with squamous cell carcinoma of the head and neck with a tumour pO_2 of

less than 10mmHg had a worse disease free survival following radiotherapy (Brizel 1997).

Oxygen is required for cell damage caused by radiotherapy. Radiation produces ionizations and free radicals. These free radicals are highly reactive and can cause lethal damage to DNA, and therefore cell death. Oxygen has a high affinity for free radicals giving rise to further free radical molecules and fixing the free radical damage thereby preventing repair from taking place. Compounds containing sulphydryl (-SH) groups also have an affinity for free radicals however rather than fixing the free radicals by perpetuating their ability to cause molecular damage, they neutralise the free radicals thereby rendering them innocuous to their environment and therefore decreasing the potentially damaging radiation effects. In the absence of oxygen or in regions of hypoxia, this latter reaction will predominate, reducing the lethality of radiation.

1.4 Effects of tumour hypoxia on chemotherapy

Hypoxic cells tend to be distant to blood vessels therefore drug delivery will be limited in these areas. This in combination with the disordered array of blood vessels within a tumour and acute and chronic perfusion defects are likely to render hypoxic zones deplete of chemotherapeutic drugs. In addition, hypoxia inhibits cellular proliferation through induction of p27 which causes a cell cycle arrest in the G1/s-phase of the cell cycle in a process that is independent of the normal control of p53 (Gardener 2001). As such one would expect cell cycle specific chemotherapeutic

agents to have diminished activity in these hypoxic cells. There is evidence to demonstrate reduced activity of chemotherapy in a hypoxic environment in vitro (Teicher 1981) and in vivo (Grau 1988) in pre-clinical tumour models, however, as yet there is no data to support this clinically in humans.

1.5 Treatment methods devised to overcome impact of tumour hypoxia

A number of clinical agents have been investigated that either increase the availability of oxygen to the hypoxic tumour cells, increase the radiosensitivity of hypoxic tumour cells or are actively toxic to cells in a reduced hypoxic environment that is otherwise insensitive to the damaging effects of radiotherapy.

1.5.1 Hyperbaric oxygen

Hyperbaric oxygen therapy is the medical administration of oxygen at higher than normal atmospheric pressure. This elevated pressure results in an increased partial pressure of oxygen in the tissues of the body and therefore a resultant decrease in tissue hypoxia. Hyperbaric oxygen (HBO) administered at the same time as radiotherapy to limit diffusion limited hypoxia has a long history with variable results. Treatment of cancers of the head and neck, bladder, lung and cervix has been evaluated using this regimen with the most promising results being seen in squamous cell carcinoma of the head and neck (Henk 1986). An MRC trial of HBO in cervical cancer treatment showed a statistically significant increase in tumour control of 20%

to 24% at 5 years but this has not been repeated (Watson 1978). A meta-analysis of 17 trials of HBO defined an odds ratio of 1.3 (95% CI 1.13 to 1.48) with an absolute improvement in local control of 6.6% (Overgaard 1995). Despite this, HBO is tolerated poorly by patients resulting in reduced compliance rates and is cumbersome to administer, as such, with the development of alternative approaches such as carbogen and radiosensitisers, interest has waned.

1.5.2 Carbogen

Carbogen is a mixture of carbon dioxide (2-5%) and oxygen (98-95%) to increase the oxygen partial pressure within tissues and reduce hypoxia. Administration of carbogen at the same time as radiotherapy has proven a much more acceptable method of improving chronic hypoxia during radiotherapy versus hyperbaric oxygen. Despite promising pre-clinical studies clinical trials of carbogen breathing during radiotherapy demonstrated no benefit on local control or survival (Inch 1966; Bergsjo 1968), however the discovery of acute hypoxia and a method to reverse this has led to much better results. Nicotinamide was originally thought to sensitise tumours to radiotherapy through DNA repair inhibition, although it exerts its maximal effects when given before or during therapy as opposed to after radiotherapy when inhibition of DNA repair is most important, further investigation revealed that it improves radiation sensitivity through improved blood flow in vessels thought to become acutely ischaemic during radiotherapy. The combination of accelerated radiotherapy with carbogen and nicotinamide (ARCON) has shown promise in patients with squamous cell carcinoma of the head and neck with high tumour control rates and reasonable toxicity (Kaanders 2002), although one study reported a low compliance

(52% completed course) in taking nicotinamide due to side-effects of nausea and vomiting (Saunders 1997) A phase III trial is currently underway to look at the effects in comparing ARCON with conventional treatments.

1.5.3 Blood transfusion

Maintenance of circulating haemoglobin levels to within the 'normal' range have been studied in order to determine whether this intervention improves radiotherapy response. There are certainly data that show that haemoglobin level prior to radiotherapy treatment of cancers of the head and neck is an independent prognostic factor in determining local control and survival. An RTOG study revealed that the estimated 5 year survival rate of patients with a haemoglobin level of <14.5g/dl for men and <13g/dl for women was 21.7% compared to 35.7% in patients with haemoglobin levels above these levels (Lee 1998). Erythropoeitin was used to correct this in a randomised, double-blind, placebo-controlled trial in head and neck cancer patients undergoing radiotherapy failed to show an improvement in survival or local control, moreover loco-regional progression free survival was poorer in the erythropoietin treated arm (Henke 2003). This may reflect the associated biological activity of erythropoietin. In DAHANCA 5-85 (Overgaard 1998) 117 patients with supraglottic larynx and pharynx carcinoma had blood transfusion during treatment or not. Despite the poor local control seen in anaemic patients, transfusion did not significantly improve outcome.

1.5.4 Radiosensitisers

Nitroimidazole compounds have undergone extensive clinical investigation for evaluation of their oxygen-mimetic properties in the presence of radiation (Dische 1985; Overgaard 1994; Overgaard 1996; Overgaard 1998). They were originally developed for use as anti-protozoal agents. At the time of irradiation the nitroimidazoles undergo a rapid redox-mediated free radical process which allows them to fix radiation damage in hypoxic cells in a similar way to oxygen (Adams 1992). The daily administration of these drugs prior to radiotherapy resulted in significant toxicity in terms of nausea and vomiting and peripheral neuropathy. Despite the toxicity experienced only a small number of studies reported any clinical benefit, however, a meta-analysis of nitroimidazole radiosensitisers in radiotherapy showed that loco-regional control and overall survival were improved (Overgaard 1994). This meta-analysis examined data from more than 7000 patients in 50 randomised controlled trials. In this analysis addition of a radiosensitiser to radiotherapy resulted in an improved loco-regional control with an odds ratio of 1.17 (95% confidence interval 1.06 to 1.28). This was most notable in patients with head and neck cancer, less so for carcinoma of the bladder and no significant effect was seen in patients with tumours of the lung, cervix, central nervous system and oesophagus. Improvement in overall survival was also noted with an overall odds ratio of 1.13 (95% confidence limits 1.03 to 1.23). Since this meta-analysis was published a further randomised controlled trial on the use of nimorazole as a radiosensitiser in patients with squamous cell carcinoma of the supraglottic larynx and pharynx has been published (Overgaard 1998). This study reported a tolerable toxicity with transient nausea and vomiting being the most frequent complication.

Loco-regional control was significantly improved in the patients receiving nimorazole (49% versus 33%, p=0.002). There was a trend to improved overall survival rates in the nimorazole arm although non-significant (26% versus 16%, p=0.32). In addition to their properties as a radiosensitiser these agents are thought to have hypoxia-selective cytotoxicity in their own right and exhibit chemopotentiation (Brown 1982) such that cells have an increased sensitivity to chemotherapy following nitroimidazole exposure under hypoxic conditions. These latter effects are thought to occur as a result of the production of reactive intermediate bioreductive products and the depletion of intracellular non-protein thiols which these reactive intermediates bind to (Brown 1982).

1.5.5 Bioreductive drugs

Bioreductive drugs are prodrugs that are activated by metabolic reduction to become cytotoxins. Their use with radiotherapy is complementary such that radiation exerts its most lethal effects to cells that are normoxic and bioreductive drugs exert their lethal effects to cells that are hypoxic.

Mitomycin C is activated in a hypoxic environment by a 1-electron reduction to a semiquinone radical mainly by cytochrome P450 reductase. The resulting effector agent is capable of DNA alkylation with a hypoxic selectivity ratio of 1.5-3.0 (Cummings 1988). Mitomycin C can also undergo a 2-electron reduction to a hydroquinone, mainly via DT-diaphorase (Workman 1990; Ross 1994). DT-diaphorase has been correlated with sensitivity to mitomycin C both in vitro (Fitzsimmons 1996) and in vivo (Gan 2001), however a recent clinical study failed to show a correlation (Phillips 2000).

Tirapazamine has 50-200 times the level of cytotoxicity in hypoxic versus anoxic cells (Brown 1998; Denny 2000). It undergoes a 1-electron reduction in hypoxic conditions to form a cytotoxic free radical which is capable of producing single- and double-strand breaks in DNA. The metabolism of tirapazamine is not completely understood but there is undisputed involvement of cytochrome P450 and NADPH:cytochrome P450 reductase (Fitzsimmons 1996). Tirapazamine is not cytotoxic as a single agent but it appears to be active in combination with radiotherapy and cisplatin, the mechanism behind which appears to involve effects on the repair of platinum-DNA adducts (Goldberg 2001). Tirapazamine on its own is tolerated at higher doses than when it is used in combination with radiotherapy or cytotoxic agents. Side-effects include myelosuppression, nausea, vomiting and muscle cramps. Tirapazamine has been used in combination with cisplatin in a phase II study on the treatment of melanoma and a phase III study on the treatment of non-small cell lung cancer. In both tumour types it exhibited anticancer activity and in non-small cell lung cancer the combination versus cisplatin alone significantly prolonged median survival(von Pawel 2000). The combination of tirapazamine and radiotherapy does exacerbate radiation side-effects however local control rates look promising(Lee 1998), particularly with the addition of cisplatin in carcinomas of the head and neck and cervix where tumour responses have been quite impressive however toxicity remains of concern (Craighead 2000; Rischin 2001).

1.5.6 Particle radiotherapy

Use of proton beam radiation therapy that is less dependent on hypoxia for its effect (due to its high linear energy transfer radiation (LET)) should be considered as an

alternative to conventional photon beam radiotherapy for use in tumours that are hypoxic and resistant to conventional radiotherapy techniques.

1.6 Current methods for detection of tumour hypoxia

There are several methods available for measuring tumour oxygenation that are under evaluation. These include both invasive and non-invasive methods.

1.6.1 Polarographic needle electrodes

The Eppendorf probe is a polarographic needle electrode system that has been widely used for the measurement of tumour oxygenation. Not only has it demonstrated that hypoxia exists within tumours but that direct measurement of tumour pO_2 can predict for response to and outcome of anti-cancer treatment. Several studies have shown that low tumour pO_2 levels in squamous cell carcinomas of the head and neck have correlated with treatment outcome (Nordsmark 1996; Brizel 1997; Nordsmark 2005) The electrode consists of a 17μm gold cathode, encased in a steel needle, and a silver-silver chloride anode. A potential difference of -700mV is applied and electrochemical reduction of oxygen occurs. Electrical current generated is proportional to the partial pressure of oxygen;

$$O_2 + 4e^- + 2H_2O \rightarrow 4OH^-$$

The signal to noise ratio, and therefore accuracy, is highest at high pO_2 and lowest at low pO_2.

The Eppendorf probe has a stepper device which allows multiple measurements to be taken along a single track. The stepping movement of the probe is in the reverse direction to probe entry and insertion in order to avoid pressure artefacts. Measurements are made at 1.4-second intervals. Doll et al (Doll 2002) concluded that five measurements per track in each of four tracks were adequate to identify a tumour as hypoxic or not, with a sensitivity and specificity of 90% when compared with a complete set of Eppendorf measurements from a tumour. A tumour was designated hypoxic if the proportion of pO_2 values less than 5mmHg (HP5) was >50%, and oxic if the HP5≤50%. A limitation of the probe is that oxygen is consumed due to the electrochemical reaction, this may result in underestimation of the measured pO_2 especially at lower oxygen tensions, in addition the volume of tumour sampled is very small.

Although this device has been invaluable in determining tumour hypoxia in animal tumours its use in the clinic is limited to tumours that are accessible, i.e. palpable nodes or tumours. Therefore this device alone is not sufficient to fully assess hypoxia in the vast majority of different tumour types. In addition, it cannot distinguish necrosis from viable hypoxic tissue. The inability to distinguish viable from necrotic tissue means that measures of hypoxia are likely to be overestimates.

The Eppendorf probe can give a global estimate of tumour hypoxia from an individual tumour, therefore in addition to its role in research it could be used to

provide information with regards to prognosis in tumours that have been fully evaluated, however, at present this device and similar ones do not have a license for use in patients so they can only be used in the pre-clinical setting.

1.6.2 Exogenous tumour markers

These are markers that are administered systemically prior to tissue sampling and immunohistochemical staining. Unlike endogenous markers, these do not represent markers that are produced as a result of the normal cellular response to hypoxia, however, following administration they accumulate in regions of tumour hypoxia allowing their identification with specific antibodies.

1.6.2.1 Nitroimidazoles

Nitroimidazoles are exogenous tumour markers. They are nitro-aromatic molecules and comprise of three component parts; an imidazole ring, a nitro group capable of undergoing bioreduction in the absence of oxygen, and a side chain that determines the pharmacologic and pharmacokinetic properties of the agent (figure 1.2). Prior to their use as immunohistochemical markers of hypoxia they were investigated for use as radiation sensitisers (section 1.5.4). However the unacceptable neurotoxicity as a result of the high doses required to show a benefit versus that required for tissue staining rendered these agents unacceptable for purpose. Newer nitroimidazole radiation sensitisers such as nimorazole have a much more acceptable side-effect profile and as such have renewed interest.

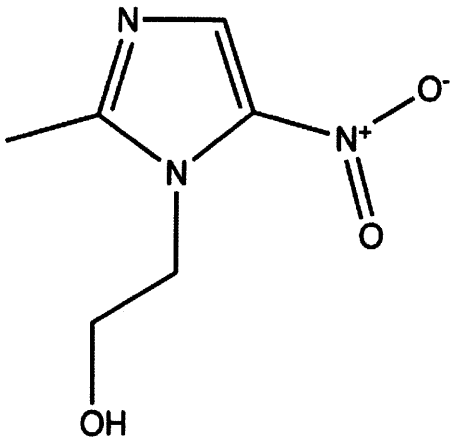

Figure 1.2 *Structure of a 2-nitroimidazole*

The 2-nitroimidazoles have become established agents for the immunohistochemical staining of tumour hypoxia. They undergo bioreductive metabolism under hypoxic conditions to form reactive intermediates, which become bound to cellular macromolecules in the hypoxic cell. These products can then be identified using immunohistochemical staining methods in order to identify their distribution and therefore the identification of cellular hypoxia. Bioreduction of the nitroimidazoles occurs involving reduction of the nitro- group. A number of reactive intermediate products are formed before the final formation of a stable 6-electron reduction product, the amine (Rauth 1984).

The process of reductive metabolism of the 2-nitroimidazoles occurs through a series of one-electron reductions (figure 1.3). The nitro-radical anion, produced by the first one-electron reduction step, avidly reacts with oxygen and is oxidised back to the parent molecule so that in well-oxygenated conditions there is effectively no substrate for the second step (Mason 1975). In low oxygen concentrations the one-electron product is further reduced to the nitroso (2 e-), hydroxylamine (4 e-), and amine (6 e-)

derivatives. Hydroxylamine, the 4-electron reduction product is unstable and highly reactive. It has a half life of 2.5 minutes under conditions of neutral pH (McClelland 1984). It is this highly reactive intermediate that is believed to be the key intermediate metabolite which undergoes a variety of reactions in addition to be reduced to the stable 6-electron product, the amine. Hydroxylamine binds to cellular macromolecules such as proteins, nucleic acids and non-protein sulphydryl compounds (Chapman 1983). These reactions occur predominantly in the cytoplasm (80%) but can occur in the nucleus (20%) (Miller 1982).

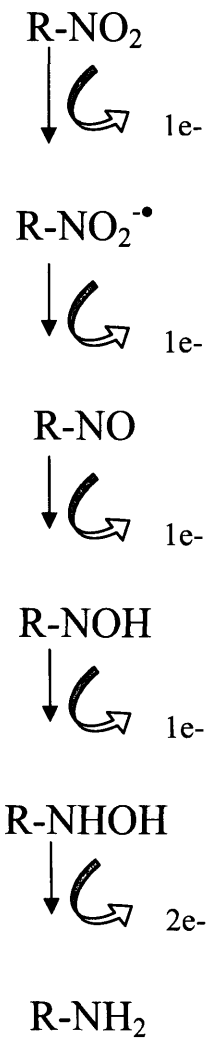

Figure 1.3 *Pathway of the nitroreductive bioactivation of nitroimidazoles*

The highly reactive nature of hydroxylamine means that these reactions will occur almost exclusively in the intracellular compartment, with little diffusion away from cells in which it was formed (Chapman 1983). Bound hydroxylamine reflects cellular hypoxia and it is this product that is thought to be detected by immunohistochemical staining techniques (Hodgkiss 1998). Alternative fates of hydroxylamine are the conjugation of hydroxylamine with the free radical scavenger glutathione (Varghese 1984), and imidazole ring fragmentation yielding glyoxal, which can form an adduct with the nucleoside guanine (Varghese 1983) (figure 1.4). It is this end-point that is thought to be the cause of normal tissue toxicity seen with the level of dose required for radiosensitisation (Whitmore 1986) but which is not seen at the lower dose requirement for marking hypoxia (figure 1.4).

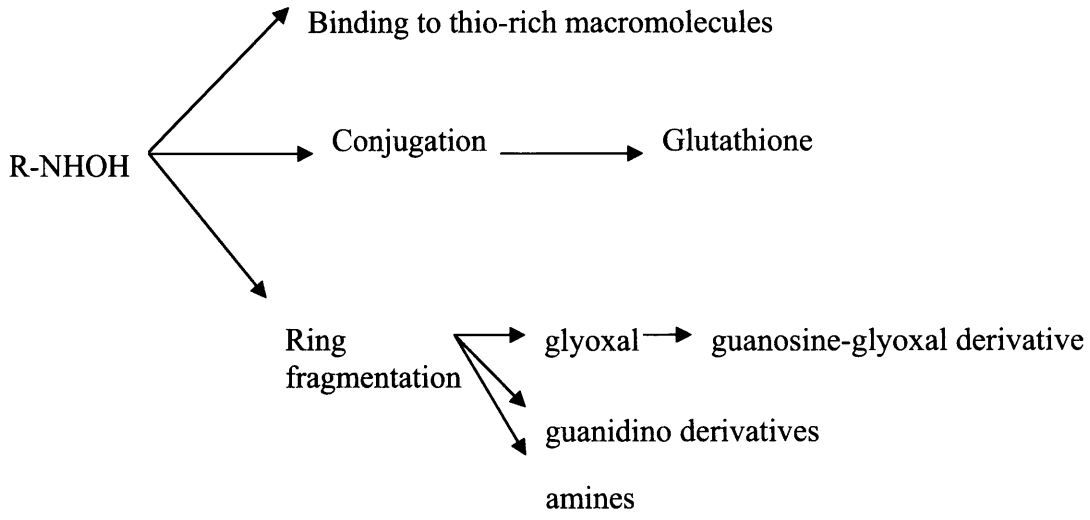

Figure 1.4 *Pathways of the hydroxylamine 4-electron product of bioreductive metabolism of nitroimidazoles*

In order for a marker to represent hypoxia it must bind to cellular components at a pO_2 level that is clinically relevant. Radiation sensitivity begins to decline at a pO_2 of less than 30mmHg, but becomes most marked at levels less than 10mmHg. Studies of EMT-6 spheroids demonstrated that there was a steep increase in the concentration of [3H]-misonidazole with a pO_2 of 10mmHg and less (Gross 1995) indicating that misonidazole and other nitroimidazoles bind and reflect cellular hypoxia at clinically relevant levels of pO_2.

Misonidazole was the first nitroimidazole to be evaluated for its role as a hypoxia marker. A study of [14C]-misonidazole administered to Balb/c mice with EMT-6 tumours demonstrated a 4-15x greater uptake in tumours than normal tissue. In this study bioreduced adducts had a half-life of 50 hours, whereas the unbound [14C]-misonidazole was cleared with a half-life of 42 minutes (Garrecht 1983). In vivo uptake of [14C]-misonidazole in the SCCVII tumour correlates with radiobiological hypoxic fraction (Kavanagh 1996) and it has been used in humans to estimate hypoxic fraction (Urtasun 1986).

Initially radiolabelling of the nitroimidazoles and autoradiography of resected tumour specimens allowed detection of the distribution of the nitroimidazoles, however immunohistochemical techniques were subsequently devised to allow the detection of these bioreduced markers without the need for radiation. Polyclonal antibodies were raised against the first nitroimidazole to be evaluated in this way, CCI-103F. These antibodies were created against the bioreduced form of CCI-103F and were found to distribute in a similar pattern to radiolabelled [3H]-CCI-103F (Raleigh 1987). For quantification of hypoxic fraction manual counting methods using light microscopy

were used (Cline 1990), however, computed image analysis can now be performed whereby the percentage cellular uptake of the nitroimidazole is determined in order to give a hypoxic fraction (Cline 1994). In order to estimate the proportion of a whole tumour that is hypoxic, using this technique, four random samples of a tumour are thought to give a measure of this to within 10% (Cline 1997).

Pimonidazole was the nitroimidazole that was subsequently taken forwards for use in humans. Unlike CCI-103F this nitroimidazole was water soluble, which allowed easier administration, and had undergone phase I testing in humans. These phase I studies showed that it had a short plasma elimination half life of 6.1 hours (Roberts 1986), a half life of >3 days in its bioreduced form in tumours (Azuma 1997) and an acceptable toxicity profile (Saunders 1984). Moreover its uptake correlated with tumour pO_2 (Raleigh 1999) and radiobiologic hypoxic fraction as determined by the comet assay (Olive 2000). Normal tissue binding of pimonidazole occurs to the sebaceous glands, keratinised squamous epithelium, epithelial linings of the lung and ducts of the parotid gland and liver surrounding centrilobular veins (Cobb 1990). These tissues possess high levels of nitroreductase enzymes which probably account for this binding. Knowledge of this normal tissue uptake should be taken in to account when interpreting results.

Pimonidazole is administered via the intra-peritoneal (i.p.) route in rodents and the intra-venous route in humans prior to surgical resection or tumour sampling. Immunohistochemical staining of pimonidazole is performed using a two-step process. In rodents, the first step uses a mouse monoclonal antibody directed against pimonidazole adducts (Hypoxyprobe^{TM}-1 Mab 1) in hypoxic tissue proteins. This

monoclonal antibody is directly labelled with fluorescein isothiocyanate (FITC) against which a second monoclonal antibody labelled with horse-radish peroxidase has been raised. This two-step approach has been developed in order to reduce the background staining that can occur as a result of the non-specific background staining. As the Mab 1 is of mouse origin, the presence of normal mouse or homologous rat immunoglobulins may result in non-specific binding of the secondary antibody.

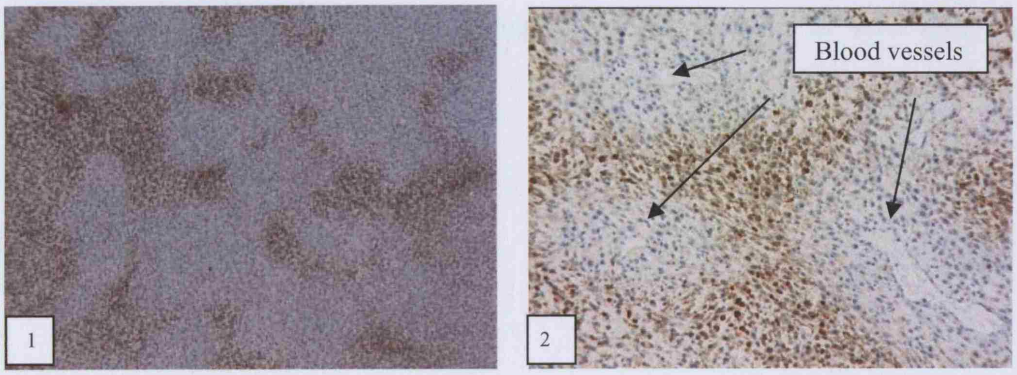

Figure 1.5 *Pimonidazole (brown) and haematoxylin (blue) stains of P22 carcinosarcoma in BD-9 rat at 2.5x magnification (1) and 20x magnification(2). Hypoxia is seen at a distance from blood vessels.*

Pimonidazole as a marker of tissue hypoxia has proven effective as a non-toxic marker of tumour hypoxia in human squamous cell carcinoma of the head and neck, cervix and prostate at a dose of 0.5 g/m^2 (Varia 1988; Kennedy 1997; Raleigh 1998; Wijffels 2000; Carnell 2006). However it is thought that there is not yet sufficient evidence to support its routine use in patients in determining clinical outcome (Nordsmark 2006). It continues to be used routinely, however, as a marker of tumour hypoxia delineation in animals (Bussink 2000) (figure 1.5). In addition,

immunohistochemical staining for pimonidazole can only be performed on resected or biopsy specimens and therefore as an invasive technique it has limitations.

2-(2-nitro-1[H]-imidazol-1-yl)-N-(2,2,3,3,3-pentafluoropropyl)-acetamide (EF-5) is a nitroimidazole that is used as a marker of tumour hypoxia. It has been used extensively in animal studies and within clinical trials in humans. It has shown oxygen-dependent uptake in EMT-6 and KHT tumours (Lee 1996; Bussink 2000) and its binding has correlated with radiobiologic hypoxic fraction in vivo (Kavanagh 1999).

1.6.3 Endogenous hypoxia markers

These are markers that are present within tissue as a result of the biological response to cellular hypoxia. Identification of these markers with staining allows regions of cellular hypoxia to be identified.

1.6.3.1 Glucose transporters (GLUT)

GLUT-1 and GLUT-3 are of interest as endogenous markers of hypoxia. Their expression allows cellular uptake of glucose thereby mediating the anaerobic glycolysis that is required in a hypoxic environment. They are expressed in normal tissue but at higher levels in tumour cells and have been identified in a number of different tissues and tumour types including squamous cell carcinoma of the head and neck (Mellanen 1994; Younes 1997). In patients with carcinoma of the cervix GLUT-1 has been shown to correlate with pO_2 measured with an Eppendorf probe. In this same series it was found that an absence of GLUT-1 is significantly associated with

the likelihood of metastasis-free survival (P = 0.022) indicating a possible use in determining prognosis (Airley 2001). GLUT-1 correlated with pimonidazole binding (r = 0.54, p = <0.001) and CA-9 expression (r = 0.40, p = <0.009) in a further study of carcinoma of the cervix (Airley 2003). Hoskin et al found that in carcinoma of the bladder there was good co-localisation of GLUT-I and CA-9 with pimonidazole and that both GLUT-1 and CA-9 were independent predictors for overall and cause specific survival (Hoskin 2003).

1.6.3.2 Hypoxia Inducible Factor-1α

Hypoxia inducible factor 1 (HIF-1) is a transcription factor that is a key regulator of oxygen homeostasis. It is composed of 2 subunits HIF-1α and HIF-1β. The HIF-1α subunit is constitutively synthesized however it undergoes proteosomal degradation in a normoxic cell. As a result HIF-1α has a short half life. In hypoxic conditions this proteosomal degradation is suppressed leading to an accumulation of the HIF-1α subunit. In response to hypoxia HIF-1α activates more than 70 genes whose protein products work towards optimising the nutritional environment of the hypoxic cell.

Although immunohistochemical analysis of HIF-1α has demonstrated an association with failure to achieve local control, poor disease free survival and overall survival in squamous cell carcinomas of the head and neck (Aebersold 2001; Koukourakis 2002) it does not correlate with pimonidazole uptake in head and neck tumours despite the strong induction of HIF-1α in hypoxic conditions (Beasley 2002; Vordermark 2005).

HIF expression does not always signify hypoxia. Its expression can be turned on following the loss of function of Von Hippel-Lindau tumour suppressor protein

resulting in constitutive activation of the HIF-1 pathway and its attendant products down stream.

1.6.3.3 Carbonic anhydrase-IX (CA-IX)

CA-IX is an endogenous marker of hypoxia. It is a carbonic anhydrase transmembrane enzyme involved in respiration and acid-base balance catalysing the reversible hydration of carbon dioxide to bicarbonate and hydrogen thereby maintaining a stable intracellular pH at the expense of extracellular acidification. Fourteen carbonic anhydrases have been identified however 2 have been found to be tumour-associated, CA-IX and CA-XII (Hoogsteen 2007). CA-IX expression is regulated through the HIF-1α pathway. In vitro studies have demonstrated that CA-IX expression is induced by hypoxia in a range of different tumour types (Wykoff 2000). The pattern of staining is in poorly perfused peri-necrotic areas consistent with regions of hypoxia (Beasley 2001) and there is considerable co-localisation with pimonidazole (Loncaster 2001), although some areas of mismatch can be found suggesting a different oxic threshold or timescale for expression of the enzyme. A study of CA-IX staining in cervical cancer have shown a correlation with radiation resistance (Olive 2001). Further studies have shown its ability to predict poor survival in patients with carcinoma of the head and neck, lung, uterine cervix and breast (Chia 2001; Giatromanolaki 2001; Koukourakis 2001; Loncaster 2001).

1.6.3.4 Other endogenous hypoxia markers

Hypoxia dependent expression of erythropoietin is regulated by HIF-1α (D'Andrea 1990). EPO is expressed by various non-erythroid tissues such as the central nervous system, endothelial cells, breast and endometrial tissues (Hoogsteen 2007). In these

tissues it is thought that EPO protects againts ischaemic injury, stimulates angiogenesis and promotes wound healing. EPO is also expressed in many human malignancies. Co-expression of EPO with HIF-1α and pimonidazole has been demonstrated in some studies in cancers of the head and neck (Arcasoy 2005), uterine cervix (Acs 2003) and breast (Acs 2004).

Osteopontin is a protein that is induced by hypoxia. One study found a correlation between osteopontin levels and tumour hypoxia measured with an eppendorf electrode (Le QT 2003). The Danish head and neck cancer study group as part of DAHANCA 5 showed that high levels of osteopontin were associated with a poor outcome after radiotherapy, that could be improved by the use of the hypoxic sensitiser nimorazole (Overgaard 2005).

1.6.4 Radiologic and nuclear medicine imaging techniques

The above methods require invasive tissue sampling for the determination of tumour hypoxia, however, hypoxia imaging techniques are non-invasive and able to provide information about the distribution of hypoxia within the whole tumour. The ability to image hypoxia within a whole tumour as opposed to histological sections or sampled averages from electrodes, together with the ability to image the same tumour at different time points in order to see how hypoxia changes will improve our understanding of hypoxia and our ability to define methods of overcoming it. Imaging techniques do have limitations. They are currently unable to provide a definitive measure of tumour pO_2 and their limits of resolution mean that regions of hypoxia can only be defined on a macroscopic scale. Despite this, development of these

techniques is required in order to aid the study of temporal changes of hypoxia within a tumour, assess the implications tumour hypoxia has with regards to resistance to therapy, determine the use of hypoxia imaging to guide therapy in terms of therapy choice and radiotherapy planning and evaluation of the usefulness of hypoxia imaging as a guide to prognosis.

The ability to image hypoxia in radiation dose-sensitive tumours such as squamous cell carcinomas of the head and neck may allow radiotherapy dose escalation to these hypoxic subvolumes and therefore improved chances of overall survival and local control. The dose-escalation to tumour subvolumes is feasible using intensity modulated radiotherapy (IMRT) and brachytherapy without escalation in toxicity. As expertise in dose painting accumulates, identification of regions that are resistant to conventional doses of radiotherapy need to be identified such that these techniques can be put in to practise.

Imaging methods that are undergoing evaluation for hypoxia imaging are the use of hypoxia-specific radiotracers in positron emission tomography (PET) and magnetic resonance imaging (MRI) techniques.

1.6.4.1 MRI

Blood oxygen level dependent (Newbold 2006) or intrinsic susceptibility weighted MRI is undergoing evaluation for use as a non-invasive technique for imaging tumour hypoxia. Oxyhaemoglobin and deoxyhaemoglobin contain iron in different states. The iron in oxyhaemoglobin is Fe^{3+} (diamagnetic) and in deoxyhaemoglobin it is Fe^{2+} (paramagnetic). This difference in charge results in differing magnetic properties

between the two types of haemoglobin. Deoxyhaemoglobin has a greater effect on ^{1}H transverse relaxation rate than oxyhaemoglobin. As a result, presence of deoxyhaemoglogin can act like an intravascular contrast agent for the blood and surrounding tissues. Changes in the deoxyhaemoglobin concentration lead to attenuation of the signal from BOLD images (T2*). The parameter R2* is used to generate BOLD image maps. R2* is the gradient of the natural log of the signal intensity plotted against echo time for each image voxel. With elevated levels of deoxyhaemoglobin the calculated R2* image appears brighter. The reciprocal of this gradient 1/R2* is T2*. BOLD imaging was first demonstrated in the brain by Ogawa and colleagues (Ogawa S 1990) and has subsequently been applied in the field of neurology for imaging stroke, degenerative brain disease, multiple sclerosis and spinal injury. It's use is still undergoing evaluation in oncology although published data has shown a correlation with pO_2 measurements taken using a microelectrode (Al-Hallaq 1998; Maxwell 1999) and immunohistochemistry (Taylor 2001; Robinson 2003; Hoskin 2007).

BOLD MRI is not a direct measure of pO_2 but a reflection of deoxyhaemoglobin levels which means it is blood volume and, in some circumstances, blood flow dependent. An area within a tumour with a higher blood volume is more likely to have a higher level of deoxyhaemoglobin present in absolute terms than an adjacent area with a lower blood volume even though the proportion of deoxyhaemoglobin is the same. This will produce images that apparently look more hypoxic in the region of high blood volume but in fact have the same pO_2. Correction for this is carried out by applying tumour perfusion maps to the BOLD maps obtained. A limitation of BOLD MRI is that it is likely to be representative of acute rather than chronic

hypoxia. It is imaging the deoxyhaemoglobin content of blood therefore regions of chronic hypoxia, distant to blood vessels will not be detected.

Dynamic contrast-enhanced MRI (DCE-MRI) is a further MRI technique that is currently being evaluated for its ability to demonstrate tumour hypoxia. A paramagnetic contrast agent such as gadolinium-DTPA is rapidly injected and generates measures of tissue perfusion, blood vessel permeability and vascular volume (Anderson 2001). Tumour oxygenation is dependent, to some degree, on vascularity (Carmeliat 2000; Hockel 2001). Therefore this technique that generates perfusion maps may be useful in delineating regions of probable hypoxia. DCE-MRI signal intensity has been correlated with cervical tumour pO_2 using a polarographic needle electrode (Cooper 2000) and has predicted outcome in patients receiving radiotherapy to head and neck (Hoskin 1999), cervix (Hawighorst 1998) and rectal tumours (De Vries 2001). This technique shows great promise however further studies are required to elucidate the precise nature of the relationship between DCE-MRI and tumour hypoxia.

1.6.4.2 Magnetic Resonance Spectroscopy (MRS)

This is a non-invasive technique that allows the characterisation of molecular tissue substituents from within an MRI image. MRI uses the magnetic properties of protons to generate images, however MRS uses this information to determine concentrations of particular metabolites within tissues. The most widely used clinical application of MRS has been in the evaluation of central nervous system disorders, of particular relevance is its ability to differentiate non-invasively between low and high grade gliomas, and separating brain neoplasms from radiation injury. ^{19}F is a para-magnetic

nucleus that can be detected using MRS (Raleigh 1991). Fluorinated 2-nitroimidazole compounds show promise as a tumour hypoxia marker in this context (Maxwell 1989; Seddon 2003) .

1.6.4.3 Single photon emission tomography (SPECT)

SPECT imaging produces a 3-dimensional distribution of a radio-labelled tracer. Unlike PET scanning, the images are generated from single photons, thereby additional spatial information is required from detection of photons by detector heads in different positions in order to precisely locate the emitting nucleotide. Iodoazomycin arabinoside (IAZA) labelled with ^{123}I is a nitroimidazole that has been used for hypoxia imaging. In a study of ten patients this imaging modality was proven feasible (Parliament 1992). Given the plasma half-life of ^{123}I-IAZA is 9.8 hours and the physical half life of ^{123}I is 13 hours imaging was carried out at 24 hours in order to reduce high background emissions. A subsequent study (Urtasun 1996) of 51 patients proposed that a tumour to normal tissue uptake of 1.1 was representative of hypoxia. Using this level as a cut-off, 40% of tumours were hypoxic. Patients with head and neck cancer had more favourable outcomes following radiotherapy if they had a low uptake versus a high uptake. As yet there are no studies that correlate direct (pO_2) or validated indirect (pimonidazole immunohistochemical staining) measures with this imaging technique.

1.6.4.4 Positron emission tomography (PET)

PET is a nuclear medicine technique that demonstrates versatility in that it is capable of imaging positron emitters used to label any active biological compound. As such use of PET in imaging functional biological processes is possibly without bounds. It

was therefore a logical step to introduce the imaging of labelled compounds that are retained within hypoxic tumour tissue. A number of radiolabelled tracers are being evaluated for their potential as hypoxia tumour markers using this technique. The ^{18}F-labelled nitroimidazoles were the first tracers to be investigated for this purpose, however, results have been so far disappointing due to the quality of the images produced. Despite this, their role as PET tracers are still undergoing evaluation. Copper bis(thiosemicarbazone) tracers have shown promise in the pre-clinical and clinical arena with rapid uptake and good tumour to background ratios, a problem that remains a recurrent theme with the nitroimidazoles. ^{18}F-FDG has also been evaluated however, there is little evidence that this should be used to identify hypoxia on its own.

1.6.4.4.1 ^{18}F-Fluorodeoxyglucose (^{18}F-FDG)

Tumours with a high metabolic activity often show enhanced proliferation rates. In the presence of sub-optimally performing tumour vasculature these tumour regions may become hypoxic. Conversely, glucose metabolism is activated under hypoxic conditions. It is for these reasons that ^{18}F-FDG has been looked at as a potential radiotracer for hypoxia. A study in a human prostate tumour cell line in mice was performed to compare the staining intensities of ^{18}F-FDG and pimonidazole which resulted in a positive correlation (Pugachev 2005). However studies comparing the distribution of ^{18}F-FDG uptake with ^{18}F-Fluoromisonidazole (^{18}F-FMISO), a nitroimidazole that represents well-documented hypoxia specific uptake in tumours, have shown some regions of overlap and disparities reflecting a likely difference in physiological mechanisms processes that are involved in taking up these radiotracers (Kubota 1999; Sorensen 2005; Thorwarth 2006). This has been further corroborated

by a group who compared ^{18}F-FDG and ^{18}F-FMISO uptake in patients with metastatic carcinoma of the head and neck with pO_2-polarography. In this study ^{18}F-FDG uptake as measured by standardised uptake value (SUV) did not correlate with tumour pO_2, however a correlation existed between maximum ^{18}F-FDG SUV and tumour to blood ratio of ^{18}F-FMISO at 2 hours (Zimny 2006). It is likely that in part ^{18}F-FDG reflects regions of hypoxia however the uptake is more complex than representing hypoxia alone.

1.6.4.4.2 2-Nitroimidazoles

The use of positron-emitting labelled nitroimidazoles to image regions of tumour hypoxia is under investigation and a variety of nitroimidazoles have been evaluated for this purpose.

^{18}F-Fluoromisonidazole (FMISO)

^{18}F-FMISO is a lipophilic compound that enters cells by passive diffusion. Once inside the cell the nitro group of the imidazole ring structure is reduced in the presence of nitroreductase activity. With high levels of oxygen the nitro group will be re-oxidised and the compound will be free to leave the cell. In the absence of adequate oxygen the reduced compound binds covalently to intracellular macromolecules trapping the ^{18}F-FMISO. ^{18}F-FMISO has a high hypoxia-specific factor, defined as the ratio of uptake in hypoxic cells compared with normoxic cells of between 20 and 50 (Chapman 1998). Retention in tumours occurs at a pO_2 of <10mmHg. Retention of ^{18}F-FMISO has been related to tissue oxygenation status as measured by pO_2-polarography (Piert 1999; Gagel 2004). Up to 1 hour after injection of ^{18}F-FMISO distribution is thought to represent blood flow, however after this it is

thought to reflect hypoxia (Rajendran 2005). The distribution of pixel values obtained following ^{18}F-FMISO PET imaging is narrow which has resulted in images with a low tumour to background ratio, however obtaining a venous blood sample mid-way through scanning allows calculation of a tumour:blood (T/B) image from which normoxic uptake (tumour:blood ratio of <1) can be subtracted to increase image contrast. A number of studies have shown that a T/B ratio of >1.2 can be used to identify the presence of hypoxia (Padhani 2007). Imaging can be carried out between 90 and 120 minutes using a dose of 3.7MBq/kg resulting in an effective total body dose equivalent of 0.0126mGy/MBq (Rajendran 2005). Interpretation of the scan can be defined by determining a fractional hypoxic volume, which is the proportion of pixels within the imaged volume having a ratio above a certain cutoff value. An alternative parameter is the total number of pixels with a tumour:blood ratio of greater than or equal to 1.2 (Rajendran 2005). ^{18}F-FMISO PET has been criticised because of the low tumour:background ratio and the time delay required for scanning. As a result of this alternative radiotracers have been sought. In particular copper labelled diacetyl-bis(N(4)-methylthiosemicarbazone) (CuATSM) appears to have a rapid uptake and distribution of hypoxia within tumours so interest has focussed on this tracer.

^{18}F-Fluoroerythronitroimidazole (FETNIM), ^{18}F-Fluoroetanidazole (FETA), ^{18}F-Fluoroazomycin arabinoside (18F-FAZA)

These nitroimidazoles are hypoxic tracers that are trapped in hypoxic tissue by the same mechanism as ^{18}F-FMISO. They have a higher tumour to background ratio than ^{18}F-FMISO (Piert 2005) and so may have greater clinical utility. There are no clinical trials that support their use at present.

2-(2-nitro-1[H]-imidazol-1-yl)-N-(2,2,3,3,3-pentafluoropropyl)-acetamide(EF-5)

EF-5 is an agent that has been used for detection of hypoxia in tissue sections. Labelled with ^{18}F it can be used to generate PET images of hypoxia. Furthermore it can be detected in tissue using immunohistochemical methods allowing correlation of imaging with hypoxia staining. Unfortunately the images produced are relatively poor because of a low tumour-background ratio (Apisarnthanarax 2005).

Copper labelled diacetyl-bis(N(4)-methylthiosemicarbazone) (Cu-ATSM)

Positron emitting isotopes of copper compounds based on thiosemicarbazone ligands have been investigated for use as surrogate markers for hypoxia. One such compound, Copper (II)-diacetyl-bis(N^4-methylthiosemicarbazone) (Cu-ATSM) has been shown to be a possible marker for delineating hypoxic, viable tissue (Fujibayashi 1997; Lewis1999; Dehdashti, Grigsby 2003; Dehdashti, Mintun 2003; Dehdashti 2008).

1.7 Cu(II)-diacetyl-bis(*N*^{4}-methyl-thiosemicarbazone) (Cu-ATSM)

1.7.1 Background

In 1997 Fujibayashi et al published the results of their investigation in to a new hypoxia imaging agent, ^{62}Cu(II)-diacetyl-bis(N^4-methylthiosemicarbazone) (^{62}Cu-ATSM) (Fujibayashi 1997). This study evaluated the effect of hypoxia on cellular retention of ^{62}Cu-ATSM in a rat heart model. It showed that ^{62}Cu-ATSM was retained in hypoxic myocardium however under conditions of normoxia or reoxygenation it was not retained. A subsequent study in the mouse mammary tumour cell line EMT6

demonstrated that ^{64}Cu-ATSM uptake increased as oxygen concentration decreased and uptake was rapid (Lewis 1999). This was also seen in the 9L gliosarcoma rodent tumour model whereby tumour oxygenation was modified using hydralazine to decrease tumour oxygenation and inhalation of 100% oxygen to increase tumour oxygenation. Again, Cu-ATSM uptake was rapid and greater in the tumours treated with hydralazine (Lewis 2001).

A number of Copper bis(thiosemicarbazones) have been investigated for the purposes of demonstrating tumour hypoxia however Copper (II)-diacetyl-bis(N^4-methylthiosemicarbazone) (Cu-ATSM) has so far been shown to be the most effective marker for delineating hypoxic viable tissue. The use of Copper radionuclides as part of these complexes promotes great versatility given the array of isotopes available, their half lives and decay products. There is potential for their use in diagnostic imaging (^{60}Cu $t_{1/2}$=23.4 mins, ^{61}Cu $t_{1/2}$=204.5 mins, ^{62}Cu $t_{1/2}$=9.7 mins, ^{64}Cu $t_{1/2}$=761.9 mins) and therapy (^{64}Cu, ^{67}Cu). These features together with the increasing availability of copper isotopes to the medical community make this copper complex an attractive option for investigation and use in clinical practise (Blower 1996).

1.7.2 Structure

In 1998, Dearling et al published details on a series of experiments performed to determine the optimal structure of bis(thiosemicarbazone) for cellular hypoxia selectivity (Dearling 1998).

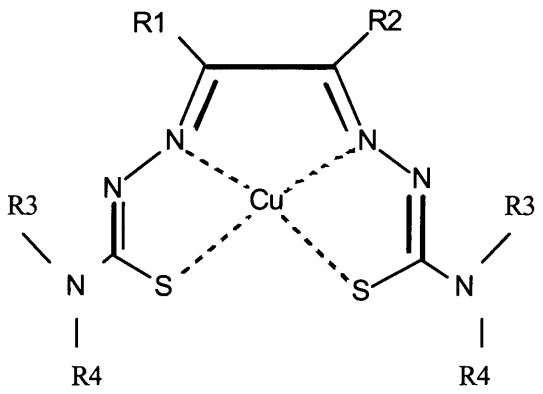

Figure 1.6 *Chemical structure of copper bis(thiosemicarbazone) complex. Alkylation patterns can be changed by substituting methyl, ethyl, phenyl and hydrogen on to R1, R2, R3, R4. This results in compounds with different redox potentials and lipophilicity. Cu-ATSM has a methyl group attached to R1, R2, R3 with a hydrogen attached to R4.*

Thirteen different complexes were synthesised differing by the combination of methyl (CH_3), ethyl (C_2H_5), phenyl (C_6H_5) and hydrogen attached to the terminal nitrogen atom (R3, R4) and the diketone backbone (R1, R2) of the bis(thiosemicarbazone) structure (figure 1.6). Hypoxia selectivity was measured using a cell suspension of mouse mammary tumour (EMT6) cells equilibrated in a hypoxic (95%N_2 - 5% CO_2) and normoxic (95% air – 5% CO_2) environment for 1 hour. The hypoxia selectivity was determined from cell uptake ratios at 1 hour and expressed as $\log_{10}$(% uptake in hypoxic cells)/(%uptake in normoxic cells). Dearling et al concluded from these experiments that hypoxia selectivity was dependent on redox potential which in turn was predicted by the number of alkyl groups on the diketone backbone. In addition

lipophilicity was required for the complex to get in to the cell. This was altered by substitution of alkyl groups but not in the same way as redox. Overall, of the complexes tested they found Cu-ATSM was found to be one of the most hypoxia selective. Its low molecular weight, planarity and lipophilicity allows it to diffuse readily in to cells, and the low redox potential results in its retention in hypoxic cells, as a result of this study the vast majority of studies have been carried out using this particular bis(thiosemicarbazone).

1.7.3 Biodistribution

Most data on the biodistribution of Cu-ATSM has been done in pre-clinical models and then extrapolated to humans. Lewis et al observed the course of ^{64}Cu-ATSM in EMT6 bearing BALB/c mice up to 40 minutes post-injection (Lewis 1999). Early uptake was seen in the heart and brain, which then diminished over the time observed consistent with vascular delivery. The same pattern was seen in the kidneys however a much greater uptake was seen initially with a proportionately smaller reduction over time. Liver uptake increased gradually during the time measured compatible with the theory that metabolism of Cu-ATSM occurs in these two organs. Tumour uptake peaked at 10 minutes post-injection and remained relatively stable thereafter. A further study has confirmed these findings (Yuan 2006), in addition ^{64}Cu-ATSM has been seen to localise to the nasal cavity and nasal sinuses (Matsumoto 2007).

Five patients with non-small cell lung cancer (NSCLC) have had whole-body imaging using ^{60}Cu-ATSM in order to obtain biodistribution data up to 2 hours post-injection (Laforest 2005). In these patients activity was seen in the liver, kidneys and

spleen, with little activity in the tumour, however, dynamic acquisitions in one bed position later revealed substantial tumour activity. Very little tracer was demonstrable in bladder and bowel despite the proposed site of metabolism being the liver and kidneys. However, failure of collection of metabolites in these organs was thought to be a result of the limited imaging time.

1.7.4 Dosimetry

Human absorbed dose estimates for Cu-ATSM have been based on rat data using ^{61}Cu-ATSM and patients with NSCLC using ^{60}Cu-ATSM. The animal data was extrapolated to estimate the human dosimetry of ^{60}Cu-ATSM, whereas the human data was used to measure organ residence times for the final calculation of organ doses using ^{60}Cu, ^{61}Cu, ^{62}Cu and ^{64}Cu (Laforest 2005). The human radiation dose estimates from the rat biodistribution data indicate that the kidney and liver are the dose-limiting organs, however, the human data shows that the kidneys actually receive a much lower dose, being just above background, suggesting that the liver should be our dose-limiting organ for dose calculations.

1.7.5 Cellular retention mechanism

Fujiyabashi and colleagues (Fujibayashi 1997) used the retention mechanism of the non-tissue-selective blood perfusion tracer Cu(II)-pyruvaldehyde-bis(N^4-methyl-thiosemicarbazone) (Cu-PTSM) as a design model for developing a hypoxia radiotracer. Cu-PTSM is a low molecular weight, planar, lipophilic compound that can move rapidly in to cells by passive diffusion. Once inside it becomes trapped,

probably as a result of mitochondrial reduction to Cu(I). It was thought that if a tracer could be designed that was only retained in cells with a more reducing environment i.e.hypoxic cells, this could lead to the generation of a hypoxic radiotracer. Cu(II)-diacetyl-bis(N^4-methyl-thiosemicarbazone) (Cu-ATSM) has a high membrane permeability and low redox potential, it was one of the first bis(thiosemicarbazone) complexes to be evaluated for its role as an agent to identify cellular hypoxia. It was initially thought that Cu-ATSM crossed the cell membrane as a result of passive transfer due to its low molecular weight and lipophilicity however it has recently been shown to be more likely taken up by an active transport mechanism using endocytosis (Pokrovska 2007). Once inside the cell a number of different mechanisms have been suggested for the retention of the copper radionuclide as a marker of cellular hypoxia (figure 1.7);

(i) Fujibayashi et al postulated that Cu(II)-ATSM is reduced selectively to Cu(I) in hypoxic cells and is irreversibly trapped following dissociation of Cu(I) from the parent compound (Fujibayashi 1997).

(ii) Dearling et al suggested that Cu(II)-ATSM reduction to Cu(I)-ATSM occurs in all cells independent of oxygen levels. In the presence of oxygen, however, Cu(I)-ATSM is reoxidised to Cu(II)-ATSM and is able to move freely out of the cell, in the absence of oxygen Cu(I) dissociates from the parent compound and is trapped intracellularly (Dearling 2002).

(iii) In a later study it was suggested that following intracellular reduction Cu(I) dissociates from the parent compound and becomes absorbed into the intracellular copper pool. Depending on the specific biology of a given tumour type, active transport mechanisms operate to expel copper from the cell. This became a real possibility following the experiments of Burgman et al who detected ^{64}Cu as $^{64}CuCl_2$

in media surrounding tumour cells exposed to ^{64}Cu-ATSM, suggesting efflux of dissociated ^{64}Cu (Burgman 2005). Cu(I) requires the presence of chaperones and transporters to maintain and protect this potentially reactive species from oxidation into reactive species. The primary cellular transporter for Cu(I) is copper transporter 1 (Ctr1), and the two primary exporters are P-type ATPases, ATP7A (Menkes protein) and ATP7B (Wilson protein) (Harris 2001). These are specific for Cu(I) transport. There may be different levels of expression of these transporters in different cell lines and hence variation in degree of Cu efflux in different tumours, a hypothesis that is supported by a study which found that overexpression of ATP7B resulted in a decrease in basal cellular Cu levels and an increase in rate of Cu efflux (Katano 2003). This description of copper handling may explain the different patterns of uptake in the different tumour cell lines, and why the validity of Cu-ATSM as a marker of hypoxia very much depends on the tumour type under investigation.

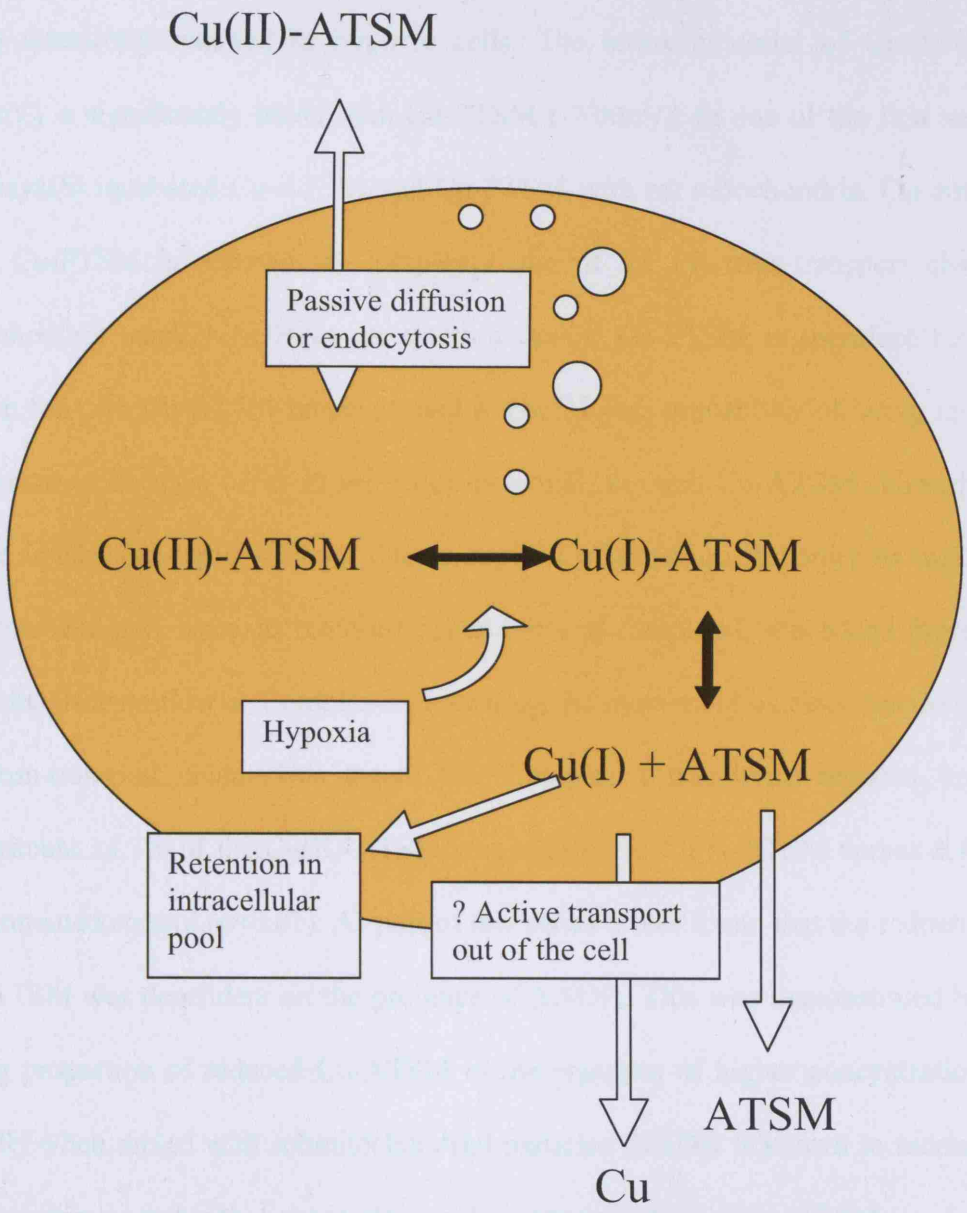

Figure 1.7 *Proposed cellular retention mechanisms for Cu-ATSM*

Intracellular reduction occurs as a result of enzymes variously identified as complex 1 of mitochondrial electron transport chain in nontumour tissue, NADH-cytochrome b5 reductase or NADPH cytochrome P450 reductase in tumour tissue, or intracellular thiols such as glutathione (Petering 1972; Minkel 1978; Obata 2001). Cu-ATSM has

a lower redox potential than the other complexes investigated and because of this it is more selectively retained in hypoxic cells. The redox potential of Cu-ATSM (-297mV) is significantly lower than Cu-PTSM (-208mV). In one of the first studies, Fujibayashi incubated Cu-ATSM and Cu-PTSM with rat mitochondria. On entering cells Cu-PTSM is reduced at Complex I site of the electron transport chain in mitochondria using NADH as an electron donor. Cu-PTSM is therefore retained within the cell. Cu-ATSM however, had a much lower probability of being reduced and retained because of its lower redox potential, as such Cu-ATSM showed high tissue uptake but rapid washout due to its lack of retention. In order to make the environment more hypoxic, rotenone, an inhibitor of complex I, was added. Rotenone disturbs electron flow at Complex I preventing the movement of electrons down the electron-transport chain. This meant that Complex I was hyper-reduced. In this experiment 14.7% of the Cu(II)-ATSM was reduced to Cu(I)-ATSM versus 3.4% of the untreated control ($p<0.01$). As part of this series it was found that the reduction of Cu-ATSM was dependent on the presence of NADH. This was demonstrated by the rising proportion of reduced Cu-ATSM in the presence of higher concentrations of NADH when mixed with submitochondrial particles. NADH is known to increase in hypoxic tissues and is thought to play a role in the reduction of Cu-ATSM.

Burgman et al (Burgman 2005) performed a study to investigate the uptake and retention mechanisms of Cu-ATSM. In this study he used 2 rodent tumour cell lines and 4 human tumour cell lines. These were the rodent prostate carcinoma (R3327-AT) and fibrosarcoma (FsaII) cell lines and the human breast cancer (MDA468, MCF7), prostate cancer (DU145) and squamous cell carcinoma (FaDu) cell lines. The different cell cultures were exposed to anoxic (<0.001% O_2), hypoxic (0.5% O_2) or

normoxic (21% O_2) conditions and incubated with ^{64}Cu-ATSM for different periods of time. Cellular uptake of ^{64}Cu-ATSM was determined by extracting the cells and lysing them, the uptake was then calculated as a percentage of the total ^{64}Cu-ATSM that was added. There was a considerable variation in ^{64}Cu-ATSM uptake and retention between the cell lines MDA468, FaDu and R3327-AT. Uptake of ^{64}Cu-ATSM in the human breast cancer MDA468 cell line was greatest with uptake being approximately 4 times greater for the anoxic and hypoxic versus normoxic cells. This uptake reached a peak at 0.5 hours and 1 hour respectively for anoxic and hypoxic cells but decreased on continued incubation. FsaII, MCF7 and DU145 demonstrated less uptake with a maximum uptake in a hypoxic environment of 1.5 times that of a normoxic environment. FaDu cells had a slower uptake with anoxic cells reaching a plateau at 1.5 hours and hypoxic and normoxic cells not reaching a steady state during the 4 hour observation period. Uptake in R3327-AT cells was broadly similar in all three oxygenation states suggesting no oxygen effect on cellular uptake.

These results show the variable nature of Cu-ATSM uptake which seems to be dependent on tumour cell type.

1.7.6 Serum stability

^{64}Cu-ATSE is thought to have similar stability to ^{64}Cu-ATSM therefore the evaluation of serum stability of ^{64}Cu-ATSE by McQuade et al provides an insight in to the likely serum stability of ^{64}Cu-ATSM (McQuade 2005). ^{64}Cu-ATSE was incubated in fresh mouse serum at 37°C. At designated time points the amount of intact complex was measured using radio thin-layer chromatography, a method that is

used to determine radiochemical purity. Protein bound ^{64}Cu was measured by removing aliquots of the solution and mixing with ethanol to precipitate the protein present. This was centrifuged and the supernatant was removed leaving the protein pellet. Both of these were then counted on a gamma counter to determine the relative activities in the supernatant and pellet. After 1 minute the amount of intact compound dropped to 80% where it remained for 30 minutes, approximately 20% of the activity was measured as being protein bound at that point. This suggests that some dissociation of ^{64}Cu from ligand occurs which may confound the proposed specific nature of ^{64}Cu-ATSM uptake and retention, and its subsequent distribution.

1.7.7 Pre-clinical studies

In 1997 Fujibayashi et al published data to show that ^{62}Cu-ATSM uptake in a rat heart model was related to oxygen tension and that it was dependent on the oxic state of the cell and not on the long-term effects of hypoxic insult (Fujibayashi 1997). In addition they reported on the the effects on ^{62}Cu-ATSM uptake in the rat heart after occlusion of the left anterior descending coronary artery and compared this with ^{201}Thallium, providing an index of myocardial perfusion. In regions of very low perfusion ^{62}Cu-ATSM uptake was low suggesting adequate blood flow is necessary to deliver this agent to hypoxic tissues, however in better perfused regions, ^{62}Cu-ATSM uptake was inversely proportional to ^{201}Tl uptake suggesting uptake in poorly perfused, therefore hypoxic regions.

A subsequent investigation in to the uptake of ^{64}Cu-ATSM in ischaemic rat myocardium compared the distribution of ^{64}Cu-ATSM and ^{11}C-acetate, a measure

of tissue perfusion (Fujibayashi 1999). In ischaemic regions with a low ^{11}C accumulation, ^{64}Cu-ATSM accumulation was disproportionately high in comparison to normally perfused areas. In rats with a large myocardial occlusion there was neither accumulation of ^{11}C nor ^{64}Cu-ATSM again suggesting that blood flow is necessary for the initial delivery of ^{64}Cu-ATSM before hypoxia can be demonstrated. In 2002 further evidence to support uptake of Cu-ATSM in hypoxic myocardium was supplied by Lewis et al with their work on canine myocardium (Lewis 2002). In their study, occlusion of the left main coronary artery resulted in a greater uptake of Cu-ATSM in ischaemic versus well oxygenated tissue. At 24 hours, by which time necrosis would have occurred to these regions, there was no uptake of Cu-ATSM, suggesting hypoxic but viable tissue is required for Cu-ATSM uptake and retention.

The evidence that Cu-ATSM could be used as a radiotracer for hypoxia was further supported by early pre-clinical studies looking at the impact of hypoxic modification on tumour uptake of Cu-ATSM. Lewis et al compared the in-vitro uptake of ^{64}Cu-ATSM and ^{18}F-FMISO in the EMT6 tumour cell line exposed to different oxygen concentrations. ^{64}Cu-ATSM and ^{18}F-FMISO uptake was significantly greater at lower oxygen tension but relative ^{18}F-FMISO uptake was approximately 10% of that compared with ^{64}Cu-ATSM. In addition, at 1 hour the uptake of ^{64}Cu-ATSM was significantly different depending on pO_2 compared with ^{18}F-FMISO which was unable to discriminate between different pO_2 levels until 2 hours (Lewis JL 1999). A further in vivo study using needle oxygen electrodes to compare ^{64}Cu-ATSM uptake with variation in oxygen delivery in a 9L gliosarcoma tumour rat model again showed a good correlation between low pO_2 and high ^{64}Cu-ATSM accumulation (Lewis 2001).

In 2005 O'Donoghue et al published an article comparing the intratumoural distribution of ^{64}Cu-ATSM with ^{18}F-FMISO, pimonidazole and the fluorescent marker of perfusion, Hoechst-33342 in rats bearing two different tumour cell lines (O'Donoghue 2005). This was the first study published that looked at the distribution of hypoxia on a cellular level using the immunohistochemical marker pimonidazole and compared this with the corresponding distribution of ^{64}Cu-ATSM detected using autoradiography. The two tumour lines used for this study were anaplastic rat prostate tumour R3327-AT and human squamous cell carcinoma FaDu. In this experiment the temporal evolution of the distribution of ^{64}Cu-ATSM was assessed by either sacrificing animals within 2 hours of radiotracer injection, or later at 16-24 hours, and determining its distribution using autoradiography. In the FaDu tumour models distribution of ^{64}Cu-ATSM closely correlated with ^{18}F-FMISO at both early and late time points, however, in the R3327-AT tumour models the distribution of ^{64}Cu-ATSM was very different to ^{18}F-FMISO at the early time point, yet at the 16 hour time-point the autoradiographic distributions of ^{64}Cu-ATSM and ^{18}F-FMISO had become similar as a result of change in the distribution of the ^{64}Cu-ATSM (the ^{18}F-FMISO distribution was unchanged over this period). Additional analysis of the R3327-AT tumour involved sacrifice at 1 and 24 hours post-injection of ^{64}Cu-ATSM. In addition to its comparison with ^{18}F-FMISO the autoradiographic pattern of uptake of this tumour model was compared with pimonidazole and the hoechst-33342 perfusion marker. Although there was no consistent correlation between ^{64}Cu-ATSM and perfusion, the early comparison between ^{64}Cu-ATSM and pimonidazole was significantly negative, whereas the 24-hour correlation was significantly positive. One may conclude that in this particular tumour type a longer period is required for ^{64}Cu-ATSM delivery, uptake and retention to reflect the underlying individual cell

biology, this may be a result of the poor perfusion to hypoxic areas, however this was not substantiated by this study.

A further study looked at the microscopic distribution of hypoxia using 2-(2-nitro-1[H]-imidazol-1-yl)-N-(2,2,3,3,3-pentafluoropropyl)-acetamide (EF-5) and compared this with ^{64}Cu-ATSM autoradiography in three rodent tumour models (Yuan 2006). At one hour post-injection of ^{64}Cu-ATSM a close spatial correlation was observed between EF-5 and ^{64}Cu-ATSM in the rodent mammary adenocarcinoma R3230Ac and 9L glioma but no correlation was seen in the fibrosarcoma (FSA) tumour cell line. A similar pattern was seen comparing autoradiography with the alternative immunohistochemical markers of hypoxia, pimonidazole and CA-IX. Interestingly, the FSA tumour cell line exhibited more uptake of ^{64}Cu-ATSM in the regions that were well perfused as seen by Hoechst fluorescence in comparison to hypoxic regions. In order to investigate the FSA tumours further the tumour bearing animals were subjected to carbogen breathing (95% O_2, 5% CO_2). In these EF5 uptake decreased, as expected, however, ^{64}Cu-ATSM uptake was unchanged, but still there remained no correlation between distribution of ^{64}Cu-ATSM and EF5. As carbogen increases blood flow in tumours it was thought that blood flow was the dominating mechanism of distribution of ^{64}Cu-ATSM in these tumours in this part of the study. The author's interpretation of the apparent tumour type specificity for ^{64}Cu-ATSM was that the redox state of FSA tumour cells was lower than other tumours despite comparable levels of hypoxia, as a result there will be a greater retention of ^{64}Cu-ATSM, a fact corroborated by the significantly higher ^{64}Cu-ATSM uptake fraction seen in FSA tumours than the other two cell lines. The redox state of FSA tumour cells is lower than other tumours as a result of the high metabolic rate of FSA

tumours which is known to have a higher glucose consumption than R3230Ac tumours (Schroeder 2005) which could explain this apparent difference in ^{64}Cu-ATSM uptake between the different tumour cell lines.

A further study by Matsumoto and colleagues on the squamous cell carcinoma SCCVII mouse model provided evidence to support the tumour specific nature of Cu-ATSM uptake and retention in hypoxic cells (Matsumoto 2007). In this study the effects of hypoxia and ^{64}Cu-ATSM uptake in the SCCVII mouse model were observed. Variation in oxygen did not result in variation of ^{64}Cu-ATSM uptake within tumour. By contrast, ^{18}F-MISO uptake increased as inspiratory oxygen levels decreased, although not significantly so. Pimonidazole staining confirmed hypoxia within tumour by showing increased staining in tumours exposed to progressively lower oxygen tensions.

These later studies have shown the variation in specificity of ^{64}Cu-ATSM as a hypoxia marker for the different tumour types, however, this does not necessarily represent a problem for the future use and development of this radiotracer. Its biological handling is different across tumour types with varying degrees of differentiation. From these pre-clinical studies we can see it represents hypoxia in some tumours and not others. Most of the tumours investigated are rodent tumours which although similar are likely to behave to a certain extent differently to human tumours. The one human tumour cell line that has been investigated is the human squamous cell carcinoma FaDu. This tumour did show a positive correlation between uptake of ^{64}Cu-ATSM and hypoxia. This is particularly reassuring as most of the

evidence for the detrimental impact hypoxia on prognosis or treatment response is on squamous cell carcinomas.

1.7.8 Clinical studies evaluating Cu-ATSM

There are currently two published studies on the use of Cu-ATSM as a hypoxia marker however a number of centres are evaluating this radiotracer in clinical trials . Both published studies looked at the relationship between ^{60}Cu-ATSM uptake and response to treatment. Dehdashti et al evaluated 14 patients with SCC cervix with ^{60}Cu-ATSM PET prior to their treatment with radical chemoradiation (Dehdashti, Grigsby 2003). A correlation was found between high uptake of ^{60}Cu-ATSM and poor response to therapy in that recurrence tended to occur in patients who had a tumour/muscle (T/M) uptake ratio of greater than 3.5. In addition, progression-free survival and overall survival were significantly longer in the patients with a tumour-to-muscle ratio of <3.5. Although it was a relatively small study with patients at different stages of disease, those with metastatic pelvic lymph nodes did have a significantly greater uptake of ^{60}Cu-ATSM in the primary tumour than those without nodal disease, suggesting a more aggressive phenotype. In a further study Dehdashti et al looked at ^{60}Cu-ATSM uptake in patients with NSCLC (Dehdashti, Mintun 2003). Nineteen patients were enrolled to this study with various stages of NSCLC. T/M activity of ^{60}Cu-ATSM was measured prior to treatment (either chemotherapy, radiotherapy or both) and compared with treatment response. Response to treatment was significantly better in patients with a lower tumour T/M (1.5±0.4) in comparison to patients with a higher T/M (3.4±0.8), which would be compatible with ^{60}Cu-ATSM being a marker of tumour hypoxia. By contrast, ^{18}F-FDG uptake using standardized

uptake value (SUV), did not discriminate between responders and non-responders suggesting a different mechanism of tracer retention.

1.7.9 Potential uses of Cu-ATSM PET

1.7.9.1 Radiotherapy planning

A PET radiotracer, such as Cu-ATSM, that delineates tumour hypoxia would have a role in radiotherapy planning, informing treatment decisions and providing additional information on disease prognosis. Already PET images can be incorporated in to radiotherapy planning systems which would make implementation of Cu-ATSM PET informed planning a relatively straightforward process. The identification of radio-resistant hypoxic subvolumes which can be treated with higher radiotherapy doses than they would receive conventionally, and incorporation of these into radiotherapy plans has the potential of improving the chances of tumour eradication. Intensity modulated radiotherapy (IMRT) allows the delivery of a number of prescribed radiation doses to subvolumes within the same tumour in an accurate and reproducible way. Use of IMRT would allow radiotherapy dose escalation to these hypoxic subvolumes, at the same time maintaining conventional dosage to the rest of the tumour. Such proof of principle has been demonstrated in a recent study. An IMRT radiotherapy plan was formulated using PET co-registered to CT for a patient with locally advanced squamous cell carcinoma of the right tonsil/tongue base metastasising to a neck node. The hypoxic gross tumour volume (hGTV) based on ^{60}Cu-ATSM PET was planned to be dose escalated to 80Gy/35#, the gross tumour volume (GTV) simultaneously planned to receive 70Gy/35#, the clinical target

volume on plan received 60Gy and more than one-half of the parotid glands were spared to less than 30Gy (Chao 2001).

1.7.9.2 Use of ^{64}Cu-ATSM PET scanning for determining prognosis

Tumour to muscle ratio has been used as a measure of prognosis in patients with carcinoma of the cervix (Dehdashti, Grigsby, 2003). In this group both progression-free survival and overall survival were significantly longer in the patients with a tumour-to-muscle ratio of <3.5. In patients with non-small-cell lung cancer (NSCLC) response to treatment (either chemotherapy, radiotherapy or both) was significantly better in patients with a lower tumour T/M (1.5±0.4) in comparison to patients with a higher T/M (3.4±0.8) (Dehdashti, Mintun et al. 2003).

1.7.9.3 Use of ^{64}Cu-ATSM PET scanning to aid treatment decisions

In addition to radiotherapy planning and prognostic predictions, knowledge of tumour hypoxia may inform regards the most appropriate treatment choice. A tumour that is known to be hypoxic that could be treated equally with either radiotherapy, chemotherapy or surgery may be best suited to surgical treatment. Both radiotherapy and chemotherapy work less well in a hypoxic environment. This information would very much assist faced with such treatment choices.

1.8 Summary and aims of thesis

Tumour hypoxia is a cause of radiation resistance, insensitivity to chemotherapy and more aggressive tumour biology with increased likelihood of local invasion and distant metastasis. Despite this there are no simple non-invasive procedures available to inform clinicians about the presence of tumour hypoxia or its distribution within the tumour. With the advent of IMRT and the development of an ever growing array of novel drug therapies, cancer treatments are more focussed and specific than ever before. Knowledge of tumour hypoxia is becoming more relevant in order to choose the most specific therapy. Cu-ATSM shows promise as a radiotracer for delineating tumour hypoxia although it is unlikely to be useful across the whole range of tumour types however, the same can be said for ^{18}F-FDG, currently our most readily available and widely used PET tracer. In this thesis I will evaluate this non-invasive PET imaging marker using the rodent tumour model bearing P22 carcinsarcoma and compare its distribution with immunohistochemically derived hypoxia. In addition I propose to modulate tumour hypoxia with the vascular targeting agent combretastatin and assess the impact of tumour blood flow on the distribution of ^{64}Cu-ATSM with Gadolinium-enhanced MRI techniques.

References

Acs G, Chen M., Xu X, Acs P, Verma A, Koch CJ (2004). "Autocrine erythropoietin signalling inhibits hypoxia-induced apoptosis in human breast carcinoma cells." Cancer Lett(214): 243-251.

Acs G, Zhang P, Mcgrath CM, Acs P, McBroom J, Mohyeldin A, Liu S, Lu H, Verma A (2003). "Hypoxia-inducible erythropoietin signalling in squamous dysplasia and squamous cell carcinoma of the uterine cervix and its potentia role in cervical carcinogenesis and tumour progression." Am J Pathol(162): 1789-1806.

Adams G. (1992). "Fallia Memorial Lecture: Redox, radiation and reductive bioactivation." Radiat Res(132): 129-139.

Aebersold DM, Burri P, Beer KT, Laissue J, Djonov V, Greiner RH, Semenza GL (2001). "Expression of hypoxia-inducible factor 1α: a novel predictive and prognostic parameter in the radiotherapy of oropharyngeal cancer." Cancer res(61): 2911-2916.

Airley R, Loncaster J, Davidson S, Bromley M, Roberts S, Patterson A, Hunter R, Stratford I, West C (2001). "Glucose Transporter Glut-1 Expression Correlates with Tumor Hypoxia and Predicts Metastasis-free Survival in Advanced Carcinoma of the Cervix." Clin Cancer Res **7**(4): 928-934.

Airley RE, Loncaster J, Raleigh JA, Harris AL, Davidson SE, Hunter RD, West CM, Stratford IJ (2003). "GLUT-1 and CAIX as intrinsic markers of hypoxia in carcinoma of the cervix: Relationship to pimonidazole binding." Int J Cancer 104(1): 85-91.

Al-Hallaq HA, River J, Zamora M, Oikawa H, Karczmar GS (1998). "Correlation of magnetic resonance and oxygen microelectrode measurements of carbogen-induced changes in tumour oxygenation." Int J Radiat Oncol Biol Phys(41): 151-159.

Amellem O, Loffler M, Pettersen EO. (1994). "Regulation of cell proliferation under extreme and moderate hypoxia: the role of pyrimidine (deoxy) nucleotides." Br J Cancer(70): 857-866.

Anderson H, Price P, Blomley M, Leach MO, Workman P (2001). "Measuring changes in human tumour vasculature in response to therapy using functional imaging techniques." Br J Cancer(85): 1085-1093.

Apisarnthanarax S, Chao KS (2005). "Current imaging paradigms in radiation oncology." Radiat Res 163(1): 1-25.

Arcasoy M O, Amin K, Chou SC, Haroon ZA, Varia M, Raleigh JA (2005). "Erythropoietin and erythropoietin receptor expression in head and neck cancer: relationship to tumor hypoxia." Clin Cancer Res 11(1): 20-7.

Azuma C, Raleigh J, Thrall DE (1997). "Longevity of pimonidazole adducts in spontaneous canine tumours as an estimate of hypoxic cell lifetime." Radiat Res(148): 35-42.

Beasley N J, Leek R, Alam M, Turlet H, Cox GK, Katter K, Millard P, Fuggle S, Harris AL (2002). "Hypoxia-inducible factors HIF-1alpha and HIF-2alpha in head and neck cancer: relationship to tumor biology and treatment outcome in surgically resected patients." Cancer Res 62(9): 2493-7.

Beasley NJ, Wykoff CC, Watson PH, Leek R, Turley H, Gatter K, Pastorek J, Cox GJ, Ratcliffe P, Harris AL (2001). "Carbonic anhydrase IX, an endogenous hypoxia marker, expression in head and neck squamous cell carcinoma and its

relationship to hypoxia, necrosis, and microvessel density." Cancer Res 61(13): 5262-7.

Bergsjo P, Evans J. (1968). "Tissue oxygen tension of cervix cancer. Comparison of effects of breathing a carbon dioxide mixture and pure oxygen." Acta Radiol Ther Phys Biol 7(1): 1-11.

Blower PJ, Lewis J., Zweit J (1996). "Copper radionuclides and radiopharmaceuticals in nuclear medicine." Nuclear Medicine & Biology.(23): 957-980.

Brizel DM, Sibley GS, Prosnitz LR, Scher RL, Dewhirst MW. (1997). "Tumor hypoxia adversely affects the prognosis of carcinoma of the head and neck." Int J Radiat Oncol Biol Phys 38(2): 285-9.

Brown J (1982). "The mechanisms of cytotoxicity and chemosensitisation by misonidazole and other nitroimidazoles." Int J Radiat Oncol Biol Phys(8): 675-682.

Brown JM, Wang L. (1998). "Tirapazamine: laboratory data relevant to clinical activity." Anti-Cancer Drug Design 13: 529-539.

Burgman P, O'Donoghue JA, Lewis JS, Welch MJ, Humm JL, Ling C (2005). "Cell line-dependent differences in uptake and retention of the hypoxia-selective nuclear imaging agent Cu-ATSM." Nucl Med Biol 32: 623-630.

Bussink J, Kaanders J., Strik AM, Vojnovic B, van der Kogel AJ (2000). "Optical sensor-based oxygen tension measurements correspond with hypoxia marker binding in three human tumour xenograft lines." Radiat Res(154): 547-555.

Carmeliat P, Jain RK. (2000). "Angiogenesis in cancer and other diseases." Nature(407): 249-257.

Carnell DM, Smith R, Daley FM, Saunders MI, Bentzen SM, Hoskin PJ (2006). "An immunohistochemical assessment of hypoxia in prostate carcinoma using

pimonidazole: Implications for radioresistance." Int J Radiat Oncol Biol Phys **1**(65): 91-99.

Chao KS, Bosch WR, Mutic S, Lewis JS, Dehdashti F, Mintun MA, Dempsey JF, Perez CA, Purdy JA, Welch MJ (2001). "A novel approach to overcome hypoxic tumor resistance: Cu-ATSM-guided intensity-modulated radiation therapy." Int J Radiat Oncol Biol Phys 49(4): 1171-82.

Chapman JD, Baer K., Lee J (1983). "Characteristics of the metabolism-induced binding of misonidazole to hypoxic mammalian cells." Cancer Res 4(43): 1523-1528.

Chapman JD, Engelhardt EL, Stobbe CC, Schneider RF, Hanks GE. (1998). "Measuring hypoxia and predicting tumor radioresistance with nuclear medicine assays." Radiother Oncol 46(3): 229-37.

Chia SK, Wykoff CC, Watson PH, Han C, Leek RD, Pastorek J, Gatter KC, Ratcliffe P, Harris AL. (2001). "Prognostic significance of a novel hypoxia-regulated marker, carbonic anhydrase IX, in invasive breast carcinoma." J Clin Oncol 19(16): 3660-8.

Cline JM, Raleigh JA, Thrall DE (1997). "Quantification of CCI-103F labelling heterogeneity in canine solid tumours." Int J Radiat Oncol Biol Phys(37): 655-662.

Cline JM, Thrall D., Page RL, Franko AJ, Raleigh JA (1990). "Immunohistochemical detection of a hypoxia marker in spontaneous canine tumours." Br J Cancer(62): 925-931.

Cline JM, Thrall D., Rosner JL, Raleigh JA (1994). "Distribution of the hypoxia marker CCI-103F in canine tumours." Int J Radiat Oncol Biol Phys(28): 921-933.

Cobb LM, Nolan J., Butler SA (1990). "Distribution of pimonidazole and RSU 1069 in tumour and normal tissues." Br J Cancer(62): 915-918.

Cooper RA, Carrington BM, Loncaster JA, Todd SM, Davidson SE, Logue JP, Luthra AD, Jones AP, Stratford I, Hunter RD, West CM. (2000). "Tumour oxygenation levels correlate with dynamic contrast-enhanced magnetic resonance imaging parameters in carcinoma of the cervix." Radiother Oncol 57(1): 53-9.

Crabtree HG(1933). "The action of radium on cancer cells. Some factors determining the susceptibility of cancer cells to radium." Proc R Soc Ser B(113): 238-250.

Craighead PS, Pearcey R., Stuart G (2000). "A phase I/II evaluation of tirapazamine administered intravenously concurrent with cisplatin and radiotherapy in women with locally advanced cervix cancer." Int J Radiat Oncol Biol Phys 48: 791-795.

Cummings J, Spanswick V., Tomacz M, Smyth JF (1988). "Enzymology of mitimycin C metabolic activation in tumour tissue: implications for enzyme-directed bioreductive drug development." Biochem Pharmacol 56: 405-414.

D'Andrea AD, Zon L. (1990). "Erythropoietin receptor. Subunit structure and activation." J Clin Invest(86): 681-687.

De Vries AF, Griebel J., Kremser C, Judmaier W, Gneiting T, Kreczy A, Ofner D, Pfeiffer K-P, Brix G, Lukas P (2001). "Tumour microcirculation evaluated by dynamic magnetic resonance imaging predicts therapy outcome for primary rectal carcinoma." Cancer Res(61): 2513-2516.

Dearling JLJ, Lewis J, McCarthy DW, Welch MJ, Blower PJ (1998). "Redox-active metal complexes for imaging hypoxic tissues: structure-activity relationships in copper(II) bis(thiosemicarbazone) complexes." Chem Commun(2531-2532).

Dearling JLJ, Lewis J., Mullen GED, Welch MJ, Blower PJ (2002). "Copper bis(thiosemicarbazone) complexes as hypoxia imaging agents: structure-activity relationships." J Biol Inorg Chem 7: 249-259.

Dehdashti F, Grigsby P, Lewis JS, Laforest R, Siegel BA, Welch MJ (2008). "Assessing tumour hypoxia in cervical cancer by PET with [60Cu]-labeled diacetyl-bis(N4-methylthiosemicarbazone)." Journal of nuclear medicine 49(2): 201-205.

Dehdashti F, Grigsby PW, Mintun MA, Lewis JS, Sigel BA, Welch MJ (2003). "Assessing tumor hypoxia in cervical cancer by positron emission tomography with 60Cu-ATSM: relationship to therapeutic response-a preliminary report." Int J Radiat Oncol Biol Phys 55(5): 1233-8.

Dehdashti F, Mintun MA, Lewis JS, Bradley J, Govindan R, Laforest R, Welch MJ, Siegel BA. (2003). "In vivo assessment of tumor hypoxia in lung cancer with 60Cu-ATSM." Eur J Nucl Med Mol Imaging 30(6): 844-50.

Denekamp J. (1989). Physiological hypoxia and its influence on radiotherapy. Amsterdam, Elsevier Sciencwe.

Denny WA, Wilson W. (2000). "Tirapazamine: a bioreductive drug that exploits tumour hypoxia." Exp Opin Invest Drugs 9: 2889-2901.

Dische S. (1985). "Chemical sensitizers for hypoxic cells: a decade of experience in clinical radiotherapy." Radiother Oncol 3(2): 97-115.

Doll CM, Milosevic M., Pintilie M, Hill RP, Fyles AW (2002). "Estimating hypoxic status in human tumors: A simulation using Eppendorf oxygen probe data in cervical cancer patients." Int J Radiat Oncol Biol Phys 5(55): 1239-1246.

Fitzsimmons SA, Workman P, Grever M, Paull K, Carnalier R, Lewis AD (1996). "Reductase enzyme expression across the National Cancer Institute Tumour Cell

Line Panel: Correlation with sensitivity to mitomycin C and EO9." J Natl Cancer Inst 88: 259-269.

Fujibayashi Y, Cutler C., Anderson CJ, McCarthy DW, Jones LA, Sharp T, Yonekura Y, Welch MJ (1999). "Comparative studies of Cu-64-ATSM and C-11-Acetate in an acute myocardial infarction model: Ex vivo imaging of hypoxia in rats." Nucl Med Biol 26: 117-121.

Fujibayashi Y, Taniuchi H, Yonekura Y, Ohtani H, Konishi J, Yokoyama A. (1997). "Copper-62-ATSM: a new hypoxia imaging agent with high membrane permeability and low redox potential." J Nucl Med 38(7): 1155-60.

Gagel B, Reinartz P, Dimartino E, Zimny M, Pinkawa M, Maneschi P, Stanzel S, Hamacher K, Coenen HH, Westhofen M, Bull U, Eble MJ. (2004). "pO(2) Polarography versus positron emission tomography ([(18)F] fluoromisonidazole, [(18)F]-2-fluoro-2'-deoxyglucose). An appraisal of radiotherapeutically relevant hypoxia." Strahlenther Onkol 180(10): 616-22.

Gan Y, Mo Y., Kalns JE, Lu J, Danenberg K, Danenberg P, Wientjes MG, Au JL-S (2001). "Expression of DT-diaphorase and cytochrome P450 reductase correlates with mitomycin C activity in human bladder tumours." Clin Cancer Res 7: 1313-1319.

Gardener LB, Li Q., Park MS, Flanagan WM, Semenza GL, Dang CV (2001). "Hypoxia inhibits G1/S transition through regulation of p27 expression." J Biol Chem 276: 7919-7926.

Garrecht BM, Chapman J. (1983). "The labelling of EMT-6 tumours in BALB/C mice with [14C]-misonidazole." Br J Radiol(56): 745-753.

Giaccia AJ (1996). "Hypoxic Stress Proteins: Survival of the Fittest." Semin Radiat Oncol 6(1): 46-58.

Giatromanolaki A, Koukourakis M., Sivridis E, Pastorek J, Wykoff CC, Gatter KC, Harris AL (2001). "Expression of hyopxia-inducible carbonic anhydrase-9 relates to angiogenic pathways and independently to poor outcome in non-small cell lung cancer." Cancer Res(61): 7992-7998.

Goldberg Z, Evans J., Birrell G, Brown JM (2001). "An investigation of the molecular basis for the synergistic interaction of tirapazamine and cisplatin." Int J Radiat Oncol Biol Phys 49: 175-182.

Grau C, Overgaard J. (1988). "Effect of cancer chemotherapy on the hypoxic fraction of a solid tumour measured using a local tumour control assay." Radiother Oncol 13: 301-309.

Gray HL, Conger A., Ebert M, Hornsey S (1953). "Concentration of oxygen dissolved in tissues at the time of irradiation as a factor in radiotherapy." Br J Radiol(26): 638-648.

Gross MW, Karbach U., Groebe K, Franko AJ, Mueller-Klieser W (1995). "Calibration of misonidazole labelling by simultaneous measurement of oxygen tension and labelling density in multicellular spheroids." Int J Cancer(61): 567-573.

Hall EJ, Giaccia A. (2006). Oxygen effect and reoxygenation, Lippincott Williams and Wilkins.

Harris A (2002). "Hyoxia - a key regulatory factor in tumour growth." Nat Rev Cancer(2): 38-47.

Harris E (2001). "Copper homeostasis: the role of cellular transporters." Nutr Rev **59**: 281-285.

Hawighorst H, Knapstein P., Knopp MV, Weikel W, Brix G, Zuna I, Schonberg SO, Essig M, Vaupel P, van Kaick G (1998). "Uterine cervical carcinoma: comparison

of standard and pharmacokinetic analysis of time-activity curves for assessment of tumour angiogenesis and patient survival." Cancer Res(58): 3598-3602.

Henk J. (1986). "Late results of a trial of hyperbaric oxygen and radiotherapy in head and neck cancer: a rationale for hypoxic cell radiosensitizers." Int J Radiat Oncol Biol Phys(12): 1339-1341.

Henke M, Rube C, Schafer U (2003). "Erythropoietin to treat head and neck cancer patients with anaemia who are undergoing radiotherapy: randomised, double blind, placebo controlled trial." Lancet 9392(362): 1255-1260.

Hockel M, Vaupel P. (2001). "Tumour hypoxia: definitions and current clinical, biologic, and molecular aspects." J Natl Cancer Inst(93): 266-276.

Hodgkiss R J (1998). "Use of 2-nitroimidazoles as bioreductive markers for tumour hypoxia." Anticancer Drug Des 13(6): 687-702.

Hoogsteen IJ, Marres H, Bussink J, van der Kogel AJ, Kannaders J (2007). "Tumour microenvironment in head and neck squamous cell carcinomas: Predictive value and clinical relevance of hypoxic markers. A review." Head Neck: Epub ahead of print.

Hoskin P, Taylor N, et al (2007). "Hypoxia in prostate cancer: correlation of BOLD-MRI with pimonidazole immunohistochemistry." Int J Radiat Oncol Biol Phys(In Press).

Hoskin PJ, Sibtain A, Daley FM, Wilson GD. (2003). "GLUT1 and CAIX as intrinsic markers of hypoxia in bladder cancer: relationship with vascularity and proliferation as predictors of outcome of ARCON." Br J Cancer 89(7): 1290-7.

Hoskin PJ, Saunders M., Goodchild K, Powell MEB, Taylor NJ, Baddeley H (1999). "Dynamic contrast-enhanced magnetic resonance scanning as a predictor of

response to accelerated radiotherapy for advanced head and neck cancer." Br J Radiol(72): 1093-1098.

Inch WR, McCredie J, Kruuv J (1966). "Effect of breathing 5 per cent carbon dioxide and 95 per cent oxygen at atmospheric pressure on tumour radiocurability." Acta Radiol Ther Phys Biol 4(1): 17-25.

Jiang BH, Semeza G., Bauer C, Marti HH (1996). "Hypoxia-inducible factor 1 levels vary exponentially over a physiologically relevant range of O2 tension." Am J Physiol(271): C1172-C1180.

Kaanders, J. H., L. A. Pop, Marres HA, Bruaset I, Van den Hoogen FJ, Merkx MA, Van der Kogel AJ. (2002). "ARCON: experience in 215 patients with advanced head-and-neck cancer." Int J Radiat Oncol Biol Phys 52(3): 769-78.

Katano K, Safaei R., Samimi G, Holzer A, Rochdi M, Howell SB (2003). "The copper export pump nATP7B modulates the cellular pharmacology of carboplatin in ovarian carcinokma cells." Mol Pharmacol 64: 466-473.

Kavanagh M-C, Sun A., Hu Q, Hill RP (1996). "Comparing techniques of measuring tumour hypoxia in different murine tumours: Ellendorf pO2 histograph, [3H]-misonidazole binding and paired survival assay." Radiat Res(145): 491-500.

Kavanagh M-C, Tsang V., Chow S, Koch CJ (1999). "A comparison in individual murine tumours of techniques for measuring oxygen levels." Int J Radiat Oncol Biol Phys(44): 1137-1146.

Kennedy AS, Raleigh J., Perez GM, Calkins DP, Thrall DE, Novotny DB, Varia MA (1997). "Proliferation and hyopxia in human squamous cell carcinoma of the cervix: first report of combined immunohistochemical assays." Int J Radiat Oncol Biol Phys(37): 897-905.

Koukourakis MI, Giatromanolaki A, Liberis V, Sivridis E. (2002). "Hypoxia-inducible factor (HIF1A and HIF2A), angiogenesis, and chemoradiotherapy outcome of squamous cell head-and-neck cancer." Int J Radiat Oncol Biol Phys 53(5): 1192-202.

Koukouraki MI, Giatromanolaki A, Sivridis E, Simopoulos K, Pastorek J, Wykoff CC, Gatter KC, Harris AL (2001). "Hypoxia-regulated carbonic anhydrase-9 (CA9) relates to poor vascularization and resistance of squamous cell head and neck cancer to chemoradiotherapy." Clin Cancer Res 7(11): 3399-403.

Krishnamachary B, Berg-Dixon S., Kelly B, Agani F, Feldser D, Ferreira G, Iyer N, LaRush J, Pak B, Taqhavi P, Semenza GL (2003). "Regulation of colon carcinoma cell invasion by hypoxia-inducible factor 1." Cancer Res 5(63): 1138-1143.

Kubota K, Tada M, Yamada S, Hori K, Saito S, Iwata R, Sato K, Fukuda H, Ido T. (1999). "Comparison of the distribution of fluorine-18 fluoromisonidazole, deoxyglucose and methionine in tumour tissue." Eur J Nucl Med 26(7): 750-7.

Laforest R, Dehdashti F, Lewis JS, Schwarz SW. (2005). "Dosimetry of 60/61/62/64Cu-ATSM: a hypoxia imaging agent for PET." Eur J Nucl Med Mol Imaging 32(7): 764-70.

Le QT, Sutphin P, Raychaudhuri S (2003). "Identification for osteopontin as a prognostic plasma marker for head and neck squamous cell carcinomas." Clin Cancer Res(9): 59-67.

Lee DJ, Trottis A., Spencer S (1998). "Concurrent tirapazamine and radiotherapy for advanced head and neck carcinomas: A phase 2 study." Int J Radiation Onc Biol Phys(41): 811-815.

Lee J, Siemann DW, Koch CJ, Lord EM (1996). "Direct relationship between radiobiological hypoxia in tumors and monoclonal antibody detection of EF5 cellular adducts." Int J Cancer 67(3): 372-8.

Lee WR, Berkey B, Marcial V, Fu KK, Cooper JS, Vikram B, Coia LR, Rotman M, Ortiz H (1998). "Anaemia is associated with decreased survival and increased locoregional failure in patients with locally advanced head and neck carcinoma: a secondary analysis of RTOG 85-27." Int J Radiat Oncol Biol Phys 5(42): 1069-1075.

Lewis J, Laforest R, Buettner T, Song S, Fujibayashi Y, Connett J, Welch M (2001). "Copper-64-diacetyl-bis(N4-methylthiosemicarbazone): An agent for radiotherapy." Proc Natl Acad Sci U S A 98(3): 1206-11.

Lewis JL, McCarthy D., McCarthy TJ, Fujibayashi Y, Welch MJ (1999). "Evaluation of ^{64}Cu-ATSM in vitro and in vivo in a hypoxic tumour model." J Nuc Med(40): 177-183.

Lewis JS, Herrero P, Sharp TL, Engelbacj JA, Fujibayashi Y, Laforest R, Kovacs A, Gropler RJ, Welch MJ. (2002). "Delineation of hypoxia in canine myocardium using PET and copper(II)-diacetyl-bis(N(4)-methylthiosemicarbazone)." J Nucl Med 43(11): 1557-69.

Lewis JS, Sharp TL, Laforest R, Fujibayashi Y, Welch MJ. (2001). "Tumor uptake of copper-diacetyl-bis(N(4)-methylthiosemicarbazone): effect of changes in tissue oxygenation." J Nucl Med 42(4): 655-61.

Loncaster JA, Harris AL, Davidson SE, Logue JP, Hunter RD, Wycoff CC, Pastorek J, Ratcliffe PJ, Stratford IJ, West CM. (2001). "Carbonic anhydrase (CA IX) expression, a potential new intrinsic marker of hypoxia: correlations with tumor

oxygen measurements and prognosis in locally advanced carcinoma of the cervix." Cancer Res 61(17): 6394-9.

Mason RP, Holtzman J. (1975). "The mechanism of microsomal and mitochondrial nitroreductase. Electron spin resonance evidence for nitroaromatic free radical intermediates." Biochemistry 8(14): 1626-1632.

Matsumoto K, Szajek L, Krishna MC, Cook JA, Seidel J, Grimes K, Carson J, Sowers AL, English S, Green MV, Bacharach SL, Eckelman WC, Mitchell JB. (2007). "The influence of tumor oxygenation on hypoxia imaging in murine squamous cell carcinoma using [64Cu]Cu-ATSM or [18F]Fluoromisonidazole positron emission tomography." Int J Oncol 30(4): 873-81.

Maxwell RJ, Robinson S., McIntyre DJO (1999). "Comparison of changes in gradient-echo 1H MR image intensity and pO2 in rodent tumours in response to carbogen breathing." Proc I S M R M 7th Annual meeting (Abstract): 495.

Maxwell RJ, Workman P., Griffiths JR (1989). "Demonstration of tumour selective retention of fluorinated nitroimidazole probes by 19F magnetic resonance spectroscopy in vivo." Int J Radiat Oncol Biol Phys(16): 925-929.

McClelland RA, Fuller J., Seaman NE (1984). "2-hydroxylaminoimidazoles - unstable intermediates in the reduction of 2-nitroimidazoles." Biochem Pharmacol(33): 303-309.

McQuade P, Martin KE, Castle TC, Went MJ, Blower PJ, Welch MJ, Lewis JS. (2005). "Investigation into 64Cu-labeled Bis(selenosemicarbazone) and Bis(thiosemicarbazone) complexes as hypoxia imaging agents." Nucl Med Biol 32(2): 147-56.

Mellanen P, Minn H., Grenman R, Harkonen P (1994). "Expression of glucose transporters in head-and-neck tumours." Int J Cancer(56): 622-629.

Miller GG, Ngan-Lee J., Chapman JD (1982). "Intracellular localisation of radioactively labelled misonidazole in EMT-6 tumour cells in vitro." Int J Radiat Oncol Biol Phys(8): 741-744.

Minkel DT (1978). "Initial reaction of 3-ethoxy-2-butyraldehyde bis(thiosemicarbazonato) copper(II) with Ehrlich ascites tumour cells." Cancer Res(38): 117-123.

Newbold K, Partridge M et al(2006). "Advanced imaging applied to radiotherapy planning in head and neck cancer: a clinical review." Br J Radiol 79(943): 554-61.

Nordsmark M, Bentzen SM et al. (2005). "Prognostic value of tumor oxygenation in 397 head and neck tumors after primary radiation therapy. An international multi-center study." Radiother Oncol 77(1): 18-24.

Nordsmark M, Loncaster J, Aquino-Parsons C, Chou SC, Gebski V, West C, Lindegaard JC, Havsteen H, Davidson SE, Hunter R, Raleigh JA, Overgaard J. (2006). "The prognostic value of pimonidazole and tumour pO2 in human cervix carcinomas after radiation therapy: a prospective international multi-center study." Radiother Oncol 80(2): 123-31.

Nordsmark M, Overgaard M, Overgaard J. (1996). "Pretreatment oxygenation predicts radiation response in advanced squamous cell carcinoma of the head and neck." Radiother Oncol 41(1): 31-9.

O'Donoghue JA, Zanzonico P, Pugachev A, Wen B, Smith-Jones P, Cai S, Burnazi E, Finn RD, Burgman P, Ruan S, Lewis JS, Welch MJ, Ling CC, Humm JL. (2005). "Assessment of regional tumor hypoxia using 18F-fluoromisonidazole and 64Cu(II)-diacetyl-bis(N4-methylthiosemicarbazone) positron emission tomography: Comparative study featuring microPET imaging, Po2 probe

measurement, autoradiography, and fluorescent microscopy in the R3327-AT and FaDu rat tumor models." Int J Radiat Oncol Biol Phys 61(5): 1493-502.

Obata A, Miono Y, Waki A, Yonekura Y, Welch MJ (2001). "Enzymes for reductive retention of Cu-diacetyl-bis(N4-methylthiosemicarbazone) in tumour cells and their localisation in mice." J Labelled Compd Radiopharm(42): S273-S275.

Ogawa S, Lee T. (1990). "Magnetic resonance imaging of blood vessels at high fields: in vivo and in vitro measurements and image simulation." Reson Med(16): 9-18.

Olive PL, Aquino-Parsons C, MacPhail SH, Liao SY, Raleigh JA, Lerman MI, Stanbridge EJ. (2001). "Carbonic anhydrase 9 as an endogenous marker for hypoxic cells in cervical cancer." Cancer Res 61(24): 8924-9.

Olive PL, Durand R., Raleigh JA, Luo C, Aquino-Parsons C (2000). "Comparison between the comet assay and pimonidazole binding for measuring tumour hypoxia." Br J Cancer(83): 1525-1531.

Overgaard J. (1994). "Clinical evaluation of nitroimidazoles as modifiers of hypoxia in solid tumors." Oncol Res **6**(10-11): 509-18.

Overgaard J. (1995). "Modification of hypoxia - from Gottwald Schwarz to nicotinamide. Have we learned the lesson?" Proceedings 5th International Meeting on Progress in Radio-Oncology: 469.

Overgaard J, Eriksen JG, Nordsmark M, Alsner J, Horsman MR. (2005). "Plasma osteopontin, hypoxia, and response to the hypoxia sensitiser nimorazole in radiotherapy of head and neck cancer: results from the DAHANCA 5 randomised double-blind placebo-controlled trial." Lancet Oncol 6(10): 757-64.

Overgaard, J., H. S. Hansen, Overgaard M, Bastholt L, Berthelsen A, Specht L, Lindelov B, Jorgensen K. (1998). "A randomized double-blind phase III study of

nimorazole as a hypoxic radiosensitizer of primary radiotherapy in supraglottic larynx and pharynx carcinoma. Results of the Danish Head and Neck Cancer Study (DAHANCA) Protocol 5-85." Radiother Oncol 46(2): 135-46.

Overgaard J, Horsman MR (1996). "Modification of Hypoxia-Induced Radioresistance in Tumors by the Use of Oxygen and Sensitizers." Semin Radiat Oncol 6(1): 10-21.

Padhani AR, Krohn KA, Lewis JS, Alber M. (2007). "Imaging oxygenation of human tumours." Eur Radiol 17(4): 861-72.

Parliament MB, Chapman J, Urtasun RC, McEwan AJ, Golberg JR, Mercer JR, Mannan RH, Wiebe LI (1992). "Non-invasive assessment of human tumour hypoxia using 123I-Iodoazomycin arabinoside: preliminary report of a clinical study." Br J Cancer(65): 90-95.

Patterson LH, McKeown SR, Ruparelia K, Double JA, Biddy MC, Cole S, Stratford IJ. (2000). "Enhancement of chemotherapy and radiotherapy of murine tumours by AQ4N, a bioreductively activated anti-tumour agent." Br J Cancer 82(12): 1984-90.

Petering D. (1972). "The reaction of 3-ethoxy-2-oxobutyraldehyde bis(thiosemicarbazone) copper(II) with thiols." Bioinorg Chem(1): 273-288.

Phillips RM, Burger A., Loadman PM, Jarrett CM, Swaine DJ, Fiebig H-H (2000). "Activity or drug metabolism by tumour homogenates: Implications for enzyme-directed bioreductive drug development." Cancer Res 60: 6384-6390.

Piert, M., H. Machulla, Becker G, Stahlschmidt A, Patt M, Aldinger P, Dissmann PD, Fischer H, Bares R, Becker HD, Lauchart W. (1999). "Introducing fluorine-18 fluoromisonidazole positron emission tomography for the localisation and quantification of pig liver hypoxia." Eur J Nucl Med 26(2): 95-109.

Piert M, Machulla HJ, Picchio M, Reischl G, Ziegler S, Kumar P, Wester HJ, Beck R, McEwan AJ, Wiebe LI, Schwaiger M. (2005). "Hypoxia-specific tumor imaging with 18F-fluoroazomycin arabinoside." J Nucl Med 46(1): 106-13.

Pokrovska T, Christlieb M., Churchill GC (2007). "Seminar: ZnATSM as a model for CuATSM." Personal communication at Oxford University Gray Cancer Institute.

Pugachev A, Ruan S., Carlin S (2005). "Dependence of FDG uptake on tumour microenvironment." Int J Radiat Oncol Biol Phys(62): 545-553.

Rajendran, J. G. and K. A. Krohn (2005). "Imaging hypoxia and angiogenesis in tumors." Radiol Clin North Am 43(1): 169-87.

Raleigh JA, Calkins-Adams D., Rinker LH, Ballenger CA, Weissler MC, Fowler WC Jr, Novotny DB, Varia MA (1998). "Hypoxia and vascular endothelial growth factor receptor in human squamous cell carcinomas using pimonidazole as a hypoxic marker." Cancer Res(58): 3765-3768.

Raleigh JA, Chou SC, Arteel GE, Horsman MR. (1999). "Comparisons among pimonidazole binding, oxygen electrode measurements, and radiation response in C3H mouse tumors." Radiat Res 151(5): 580-9.

Raleigh JA, Franko A., Kelly DA (1991). "Development of an in vivo 19F magnetic resonance method for measuring oxygen deficiency in tumours." Magn Reson Med(22): 451-466.

Raleigh JA, Miller G., Franko AJ, Koch CJ, Fuciarelli AF, Kelly DA (1987). "Fluorescence immunohistochemical detection of hypoxic cells in spheroids and tumours." Br J Cancer(56): 395-400.

Rauth A. (1984). "Pharmacology and toxicology of sensitisers: mechanism studies." Int J Radiat Oncol Biol Phys(10): 1293-1300.

Rischin D, Peters L., Hicks R, Hughes P, Fisher R, Hart R, Sexton M, D'Costa I, von Roemeling R (2001). "Phase I trial of concurrent tirapazamine, cisplatin and radiotherapy in patients with advanced head and neck cancer." J Clin Oncol 19: 535-542.

Roberts JT, Bleehan N., Walton MI, Workman P (1986). "A clinical phase I toxicity study of Ro 03-8799:plasma, urine, tumour and normal brain pharmacokinetics." Br J Radiol(59): 107-116.

Robinson SP, Rijken P., Howe FA (2003). "Tumour vascular architecture and function evaluated by non-invasive susceptibility MRI methods and immunohistochemistry." J Magn Reson Imaging(17): 445-454.

Ross D, Beall H., Travers RD, Siegel D, Phillips RM, Gibson N (1994). "Bioactivation of quinones by DT-diaphorase, molecular, biochemical and chemical studies." Oncol Res 6: 493-500.

Saunders MI, Anderson P, Bennett MH, Dische S, Minchington A, Stratford M, Tothill M (1984). "The clinical testing of Ro 03-8799 - pharmacokinetics, toxicology, tissue and tumour concentrations." Int J Radiat Oncol Biol Phys(10): 1759-1763.

Saunders MI, Pigott K., Powell ME, Goodchild K, Dische S, Denekamp J, Stratford M, Dennis MF, Rojas AM (1997). "Accelerated radiotherapy, carbogen and nicotinamide (ARCON) in locally advanced head and neck cancer: a feasibility study." Radiother Oncol 2(45): 159-166.

Schroeder T, Yuan H., Viglianti (2005). "Saptial heterogeneity and oxygen dependence of glucose consumption in R3230Ac and fibrosarcomas of the Fischer 344 rat." Cancer Res(65): 5163-5171.

Seddon BM, Payne G., Simmons L, Ruddle R, Grimshaw R, Tan S, Turner A, Raynaud F, Halbert G, Leach MO, Judson I, Workman P (2003). "A phase I study of SR-4554 via intravenous administration for noninvasive investigation of tumour hypoxia by magnetic resonance spectroscopy in patients with malignancy." Clin Cancer Res 14(9): 5101-5112.

Semenza, G. (2003). "Targeting HIF-1 for cancer therapy." Nat Rev Cancer(3): 721-732.

Sorensen M, Horsman MR, Cumming P, Munk OL, Keiding S. (2005). "Effect of intratumoral heterogeneity in oxygenation status on FMISO PET, autoradiography, and electrode Po2 measurements in murine tumors." Int J Radiat Oncol Biol Phys 62(3): 854-61.

Taylor NJ, Baddeley H., Goodchild KA, Powell ME, Thoumine M, Culver LA, Stirling JJ, Saunders MI, Hoskin PJ, Phillips H, Padhani AR, Griffiths JR (2001). "BOLD MRI of human tumour oxygenation during carbogen breathing." J Magn Reson Imaging(14): 156-163.

Teicher BA, Lazo J., Sartorelli AC (1981). "Classification of antineoplastic agents by their selective toxicities toward oxygenated and hypoxic tumour cells." Cancer Res 41: 73-81.

Thorwarth D, Eschmann S., Holzner F, Paulsen F, Alber M (2006). "Combined uptake of [18F]FDG and [18F]FMISO correlates with radiation therapy outcome in head-and-neck cancer patients." Radiother Oncol(80): 151-156.

Urtasun RC, Chapman J., Raleigh JA, Franko AJ, Koch CJ (1986). "Binding of [3H]-misonidazole to solid human tumours as a measure of tumour hypoxia." Int J Radiat Oncol Biol Phys(12): 1263-1267.

Urtasun RC, Parliament M., McEwan AJ, Mercer JR, Mannan RH, Wiebe LI, Morin C, Chapman JD (1996). "Measurement of hypoxia in human tumours by non-invasive SPECT imaging of iodoazomycin arabinoside." Br J Cancer(74(Suppl. XXVII)): S209-S212.

Varghese AJ, W. G. (1983). "Modification of guanine derivatives by reduced 2-nitroimidazoles." Cancer Res(43): 78-82.

Varghese AJ, Whitmore G. (1984). "Misonidazole-glutathione conjugates in CHO cells." Int J Radiat Oncol Biol Phys(10): 1341-1345.

Varia MA, Calkins-Adams D., Rinker LH, Kennedy AS, Novotny DB, Fowler WC Jr, Raleigh JA. Gynecol Oncol, 71: 270-277, 1988 (1988). "Pimonidazole: a novel hypoxia marker for complementry study of tumour hyopxia and cell proliferation in cervical carcinoma." Gynecol Oncol(71): 270-277.

Vaupel P, Mayer A (2005). "Effects of anaemia and hypoxia on tumour biology." European School of Oncology, Scientific updates 6: 47-66.

Vaupel P, Mayer A (2005). "Hypoxia and anemia: effects on tumor biology and treatment resistance." Transfus Clin Biol 12(1): 5-10.

Vaupel P, Schaefer C., Okunieff P (1994). "Intracellular acidosis in murine fibrosarcomas coincides with ATP depletion, hypoxia, and high levels of lactate and total P_i." NMR Biomed(7): 128-136.

von Pawel J, von-Roemeling R., Gatzemeier U, Boyer M, Elisson LO, Clark P, Talbot D, Rey A, Butler TW, Hirsch V, Olver I, Bergman B, Ayoub J, Richardson G, Dunlop D, Arcenas A, Vesico R, Viallet J, Treat J (2000). "Tirapazamine plus cisplatin versus cisplatin in advanced non-small-cell lung cancer: a report of the international CATAPULT I study group. Cisplatin and tirapazamine in subjects

with advanced previously untreated non-small-cell lung tumours." J Clin Oncol 18: 1351-1359.

Vordermark D, Kraft P., Katzer A, Bolling T, Willner J, Flentje M (2005). "Glucose requirement for hypoxic accumulation of hypoxia-inducible factor 1α." Cancer Lett(230): 122-133.

Watson ER, Halnan K., Dische S, Saunders MI, Cade IS, McEwen JB, Wiernik G, Perrins DJ, Sutherland I (1978). "Hyperbaric oxygen and radiotherapy: a Medical Research Council trial in carcinoma of the cervix." Br J Radiol 611(51): 879-87.

Whitmore GF, Varghese A. (1986). "The biological properties of reduced nitroheterocyclics and possible underlying biochemical mechanisms." Biochem Pharmacol(35): 97-103.

Wijffels KIEM, Kaanders J., Rijken PFJW, Bussink J, van den Hoogen FJA, Marres HAM, de Wilde PCM, Raleigh JA, van der Kogel AJ (2000). "Vascular architecture and hypoxic profiles in human head and neck squamous cell carcinomas." Br J Cancer(83): 674-683.

Workman P, Waltman M. (1990). Enzyme-directed bioreductive drug development. New York, USA, Plenum Press.

Wykoff CC, Beasley N., Watson PH (2000). "Hypoxia-inducible expression of tumour associated carbonic anhydrases." Cancer Res(60): 7075-7083.

Younes M, Lechago L., Somoano JR, Mosharaf M, Lechage J (1997). "Immunohistochemical detection of Glut 3 in human tumours and normal tissues." Anticancer Res(17): 2747-2750.

Yuan H, Schroeder T, Bowsher JE, Hedlund LW, Wong T, Dewhirst MW (2006). "Intertumoral differences in hypoxia selectivity of the PET imaging agent 64Cu(II)-diacetyl-bis(N4-methylthiosemicarbazone)." J Nucl Med 47(6): 989-98.

Zimny M, Gagel B, Dimartino E, Hamacher K, Coenen HH, Westhofen M, Eble M, Buell U, Reinartz P. (2006). "FDG-a marker of tumour hypoxia? A comparison with [(18)F]fluoromisonidazole and pO (2)-polarography in metastatic head and neck cancer." Eur J Nucl Med Mol Imaging 33(12): 1426-31.

CHAPTER 2

Materials and methods

2.1 Positron emission tomography

2.1.1 Theory

2.1.1.1 Positron detection

Positron emission tomography (PET) generates images of the distribution of positron-emitting radiotracers. These proton-rich radiotracers are unstable and reach a more stable state by positron decay. Once emitted the positron slows down as a result of interactions before it finally interacts with an electron, its antiparticle, in an annihilation reaction. The masses of the positron and electron are converted into two photons of 511keV each that travel in opposite directions from one another at an angle of 180 degrees. This photon pair is detected by a PET scanner and used to generate a functional image of the distribution of a radiotracer.

Scintillation crystals detect this photon pair and become excited with the incident photons. When the atoms within the crystal return to their ground state they emit light photons, the number emitted being proportional to the incident photon energy. A photomultiplier is adjacent to the scintillation crystals which converts light in to electric current. If this indicates arrival of a 511 keV photon the event and time is

recorded. If two detectors register an event at the same time an annihilation must have happened on the line between the two crystals involved, as such a coincidence event is recorded on the line of response. Short time windows are set that will accept a photon pair, called coincidence windows. As photons travel at the speed of light the difference in arrival times of a photon from an annihilation pair at one detector at closer proximity versus another will be short. PET scanners are currently unable to detect a difference in photon arrival times of less than 0.3 ns, this means a time of flight resolution of 5cm, however, reconstruction methods using back projection can approximately localise annihilation reactions to where the event occurred (Mullani 1980).

Following absorption of a photon by a scintillation crystal it is unable to register further strikes until the process of detection is complete. This is known as system dead time. When working with high count rates many coincidence events will be lost. Mathematical corrections can be applied to compensate for this, however, beyond a certain activity the system will be flooded and corrections will be less accurate. The creation of scanners with a shorter dead time is likely to improve this limitation leading to the ability to measure a wider range of activities.

2.1.1.2 Image reconstruction

During a PET scan, coincidence events are continually recorded. At the end of an acquisition, prior to reconstruction, the acquired coincidences are stored in the form of sinograms. The sinogram describes the offset of the line of response and projection angle of any given annihilation event. The sinogram data is corrected for detector and photomultiplier non-uniformity and the attenuation of photons as they pass through

the body. Non-uniformity is corrected by the use of phantom acquistions which are transformed into correction maps. Photon attenuation can result in a decrease in detected photons by a factor of 20 and is measured (in a PET-only scanner) by performing a transmission scan either at the beginning or end of the PET acquisition scan. This scan is performed using a single photon source (e.g.^{57}Cobalt) that travels around the subject. The attenuation correction factor is determined by the photon energy detected compared with that expected if the subject were not present. This correction factor can then be applied to the PET acquistion data to generate more accurate images. For a PET-CT scanner the attenuation correction is derived from X-ray CT image data.

2.1.1.3 Scatter

True coincidences represent a pair of photons being detected along the line of response from which they were generated. Other types of coincidence events however do occur that are not true and need to be corrected for as much as possible (figure 2.1). These scattered coincidence events superimpose noise on the image thereby losing contrast. Scattering of photons away from the line of response can result in the detection of two photons along a different line of response that is not that of the annihilation reaction, thereby misplacing the event. Alternatively random coincidences may occur such that single photon acquisitions occurring within the same narrow time window will be accepted and a line of response generated even though they do not come from the same annihilation reaction. As the daughter nucleus de-excites after emission of a positron or electron capture gamma-rays are emitted. These can be of a variety of energies and can occasionally fall within the detected range of coincidence pairs in the energy window of the scanner. This can

result in triple events, in which the random gamma ray is detected at the same time as a coincidence pair, these triple events are rejected by the scanner reducing sensitivity, random events, in which two non-coincidence gammas are detected at the same time which the scanner interprets as a coincidence pair, and scatter-like events that whereby one of a pair of annihilation gammas is detected in coincidence with an associated gamma from the same decay.

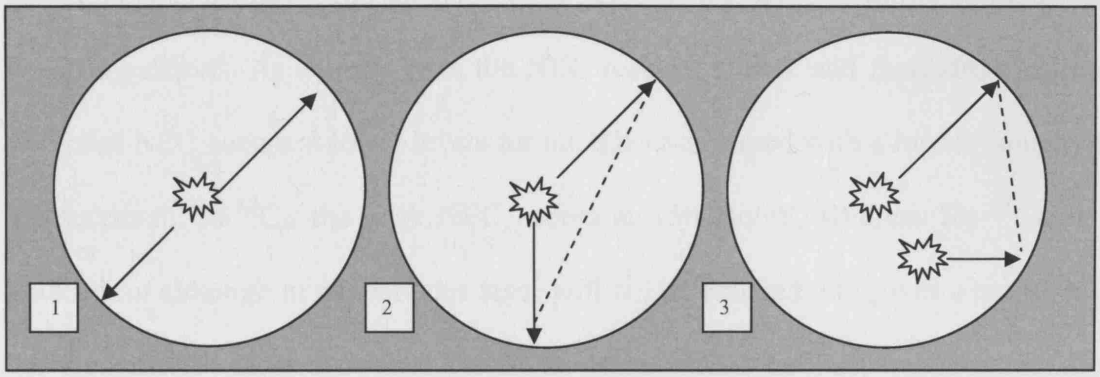

Figure 2.1 *True line of response from an annihilation event (1). Scattered photons from an annihilation event result in misplaced line of response (2). A random coincidence occurs when photons from two separate events are detected within the set time and energy windows. A corresponding line of response may be generated (3).*

The production of positron decay is close to unity for ^{60}Cu, ^{61}Cu and ^{62}Cu, however ^{64}Cu produces positrons from only 17.4% of nuclei. This has been shown to influence sensitivity directly even though scatter fractions are slightly higher for ^{60}Cu and ^{61}Cu because of their associated gammas (Williams 2005). The noise equivalent count rate (NEC) takes in to account the true (T), random (R) and scattered (S) coinicidences and provides a measure of the effects random and scattered coincidences have on

image quality, it was originally defined in order to compare the performances of different scanners;

$$NEC=T^2 \div (T + R + S)$$

The NEC shows an initial rise in total and scattered event rates with increasing activity, but as the dose rises the number of randoms increases resulting in significant dead time effects. As activity rises the NEC reaches a peak and thereafter declines. The peak NEC occurs at lower levels for nuclides associated with a higher sensitivity measurement. In ^{62}Cu the peak NEC occurs at 150kBq/ml, whereas for ^{64}Cu it is 820kBq/ml although in patients this level will not be reached, but gives a measure of the theoretically ideal dose that should be administered for best image acquisition although NEC does not take spatial resolution in to account (figure 2.2).

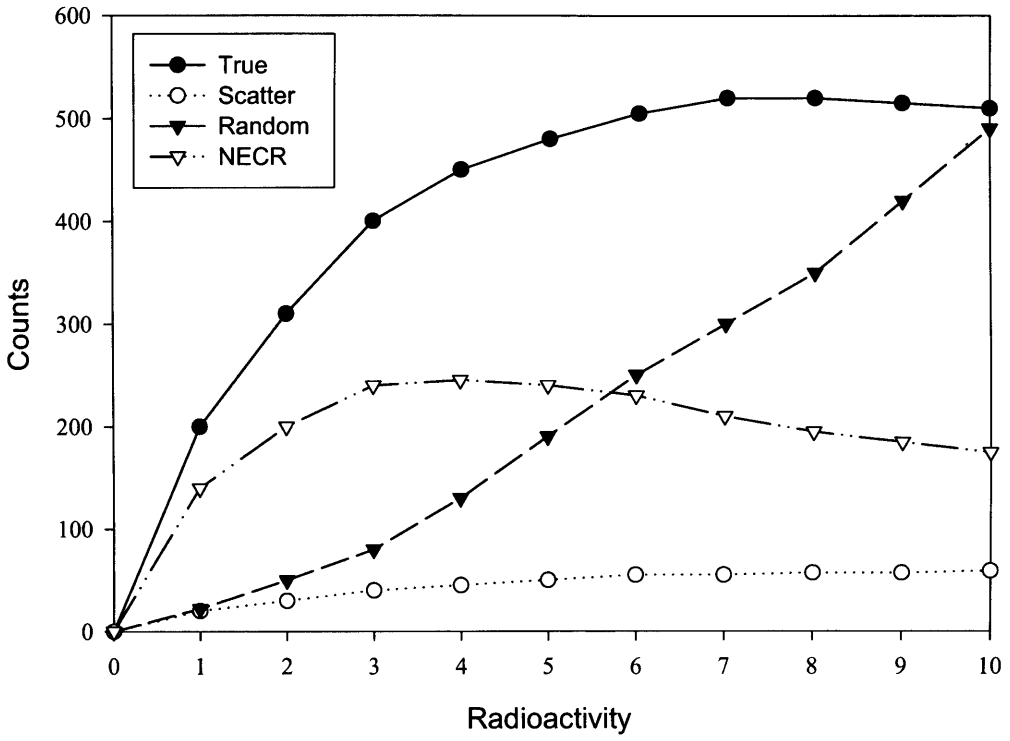

Figure 2.2 *Impact of scatter on true count rate with increasing dose as seen from NECR*

Techniques for reducing scatter include the recognition of photons by a detector within a narrow energy window, i.e 511keV, with rejection of all others. Although too narrow a window may result in the rejection of many true coincidences thereby reducing the efficiency of the machine. Introduction of lead or tungsten septa shields between rings of a PET scanner significantly reduces scatter (Cherry 1996). Use of septa means that photons generated as a result of a coincidence reaction will not be detected in adjacent imaging planes, making reconstruction possible in only 2-dimensions. Three-dimensional reconstruction of images is possible with removal of septa with a 10-fold increase in efficiency of the scanner. This improves the image quality in low count rate studies, reduces the radioactive dose required and scan time.

However, scattered events may account for up to 45% of events recorded in 3-D PET unlike 2-D reconstructions when scattered events account for only 15% of recorded events. Mathematic methods for compensating for scattered events are also possible. These include convolving images with a deblurring filter, or more complex computational methods based on Monte Carlo simulations and the Klein-Nishina formula (Budinger 1998).

2.1.1.4 Spatial resolution

Resolution is measured by the scanner's ability to distinguish 2 radioactive sources of a defined size placed at a small distance from each other. Measuring the full width at half maximum (FWHM) count provides information about the spatial resolution (figure 2.3). This can be obtained from an intensity-distance plot through the centre of a point source. The FWHM is a value that provides us with the possible resolution of the scanner such that sources placed closer together than this distance will not be discernable as two separate points. The spatial resolution of a PET scanner is dependent on detector size, non-collinearity of the coincidence pair and the positron range. An opposing pair of detectors provide a channel width for detection of coincidence pairs, objects smaller than the channel width will not be visualised as smaller due to the limitation imposed by the detector size. Small crystals are sometimes grouped in to blocks resulting in a further deterioration of event localisation (block effect). Reducing the size of detectors improves resolution which has been an important factor in the improvement of PET scanner resolution. Non-collinearity of photon pairs occurs as a result of the residual momentum of the positron, electron or both as they annihilate. This means the coincidence photons are not always at 180 degrees from each other, in fact sometimes there may be a

deviation by as much as 0.5 degrees. The impact of this depends on the diameter of the detector ring having a larger impact on scanners with a larger diameter of detector ring. Positron path length determines the intrinsic resolution of the radiotracer. Following emission of the positron from the unstable nucleus the positrons travels a short but variable distance (mm) before its annihilation reaction with an electron. As the line of response is generated from the point of annihilation rather than atomic nucleus from which it is released an intrinsic limit of resolution is present dependent on the isotope used.

Putting together all of these factors the FWHM and therefore the spatial resolution of a PET scanner can be determined by:

$$FWHM = k_r\sqrt{(C^2 + c^2 + R^2 + B^2)}$$

Where C = non-collinearity effect, c = crystal size, R = positron range, B = block effect, and k_r is a constant depending on the reconstruction algorithm used.

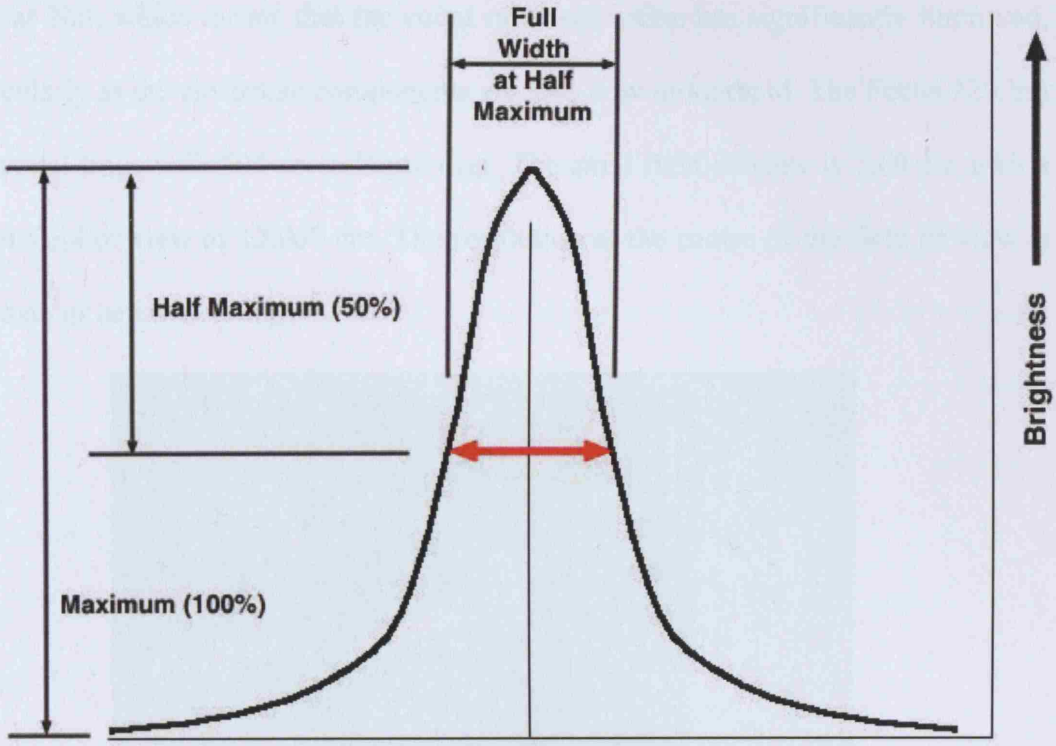

Figure 2.3 *Full width at half maximum (FWHM) can be used to measure spatial resolution. The brightness of a point source is plotted against distance through the centre of the source. The FWHM is the width of source detection at 50% of the maximum intensity. Sources placed closer together than this will not be resolved.*

2.1.2 Hardware

The PET scanner used for this study was the Siemens MicroPET Focus 220 (Concorde Microsystems Incorporated) suitable for imaging rodents (figure 2.4). Lutetium Oxyorthosilicate (LSO) is the scintillation crystal in this system with each crystal measuring 1.5mm (axial) x 1.5mm (transaxial) x 10mm (depth). LSO has a

faster scintillation emission in comparison to the scintillation crystals originally used, such as NaI, which means that the count rate acquisition has significantly improved, particularly as the electronic components are also now more rapid. The Focus 220 has 48 crystal rings with 504 crystals per ring. The axial field of view is 7.69 cm with a radial field of view of 12.067 cm. The resolution at the centre of the field of view is less than or equal to 1.4mm.

Figure 2.4 *Siemens MicroPET Focus 220 (Concorde Microsystems Incorporated)*

2.1.3 PET imaging acquisition and reconstruction parameters

Imaging data was acquired dynamically from the time of injection of ^{64}Cu-ATSM over the course of 1-2 hours using MicroPET Manager 2.2.4.0 (CTI Concorde

Microsystems) and stored as list-mode data. The list-mode format includes a record of all coincidence events, which can subsequently be processed in to sinograms and then images for any required set of time frames. A single bed position was used for the acquisition with the scan centred on the mid-point of the tumour. The energy discrimination window was set at 350keV to 750 keV with a 6ns timing window. Histograms were framed in to variable time segments depending on the information required. As the list mode data was stored framing could be altered for an individual study in order to generate further information from the same data set. The sinogram rebinning algorithm used was the Fourier rebinning algorithm. Data was reconstructed using the ordered-subsets expectation maximization (OSEM) 2-D iterative algorithm.

2.1.4 Transmission scans

These were performed for 15 minutes with the object to be scanned in field using single photon emitting Co-57 transmission sources either before or after the ^{64}Cu-ATSM acquisition scan. The resulting attenuation file was then applied to the corresponding ^{64}Cu-ATSM acquisition during image reconstruction.

2.1.5 Standardised uptake value (SUV) analysis

In order to get an absolute measure of ^{64}Cu-ATSM uptake that allowed comparison across tumours and with alternative imaging modalities we measured mean tumour SUV. This parameter was chosen to give a measure of ^{64}Cu-ATSM uptake in the whole tumour region-of-interest (ROI) rather than the point measurements obtained if

we had measured maximum SUV. The mean tumour SUV was compared directly with tumour blood blood flow per unit area using Gadolinium AUC90 of the same tumour cross-section and percentage tumour pimonidazole uptake. Similar measures of SUV have been used previously as described in the literature (McQuade 2005; Yuan 2006; Matsumoto 2007). Alternative parameters such as maximum tumour SUV were not thought to be reflective of the tumour uptake of ^{64}Cu-ATSM for such comparative purposes and were therefore not used in this analysis. Tumour to muscle (T/M) ratio has been used clinically to determine ^{64}Cu-ATSM uptake (Dehdashti, Mintun 2003; Dehdashti 2008) however due to the possible inaccuracy in delineating muscle because of the absence of CT imaging measurement of this parameter was felt to be unreliable in this context. SUV is corrected for variations in dose injected and body weight, it can therefore be used to compare different tumours directly;

SUV= ^{64}CuATSM uptake in MBq per unit volume/ Administered activity per unit weight of rat

For image analysis ASIPro VM^{TM} (CTI Concorde Microsystems) software was used. The image output was displayed as a voxel value. Therefore a calibration factor was needed that could be applied to the voxel value in order to get an output in MBq/ml. To determine the calibration factor, the voxel value for a known activity of ^{64}Cu-ATSM per unit volume was measured. For this calculation a cylindrical perspex phantom was used with an internal volume of 296.20mls. In the phantom 31.74 MBq of ^{64}Cu-ATSM was diluted to a volume of 296.20mls with distilled water. This phantom was placed centrally in the microPET scanner and PET data acquired over the course of 15 hours. Following decay corrected reconstruction of the data a

cylindrical 3-dimensional region of interest (ROI) was drawn within the visible image structure. For this ROI the mean voxel value was calculated. In order to see how this mean voxel value compared with activity concentration, the mean activity per unit volume (31.74 MBq/296.20 mls = 0.11 MBq/ml) was divided by the mean voxel value per unit volume (0.00021) to give the calibration factor for conversion of voxel output to activity. Thereafter, for determination of tumour SUV the voxel values were multiplied by this calibration factor (520.4) and divided by injected dose per unit animal weight;

SUV = [voxel value x calibration factor (520.4)] / [^{64}Cu-ATSM dose injected(MBq)/weight of animal(g)]

For comparison of tumour SUV with MRI and immunohistochemistry the central tumour axial slice was used (figure 2.5). This central axial slice was identified prior to imaging with the animal in the imaging cradle. The animal would remain in the same cradle without movement throughout the PET and MRI imaging process. The slice was determined using the alignment lasers in the microPET scanner and drawn on to the animal using an indelible marker. Imaging was centred on this slice in the MRI and microPET and after sacrifice, the tumour was bisected at this level for immunohistochemistry and autoradiography of the central axial slice. Following histogramming and reconstructing of the microPET image an ROI was drawn around the tumour at the level of the axial centre. Tumour uptake of ^{64}Cu-ATSM was avid aiding identification of the tumour ROI which was delineated at the level at which ^{64}Cu-ATSM uptake was significantly different to background (figure 2.5). The tumour ROI was drawn on the MRI on the same axial slice using T1 images to

delineate the tumour region accurately. Fiducial markers were used latterly in the course of the experiment to aid co-registration of the microPET and MRI images and confirm the comparative nature of the central axial PET and MRI slices.

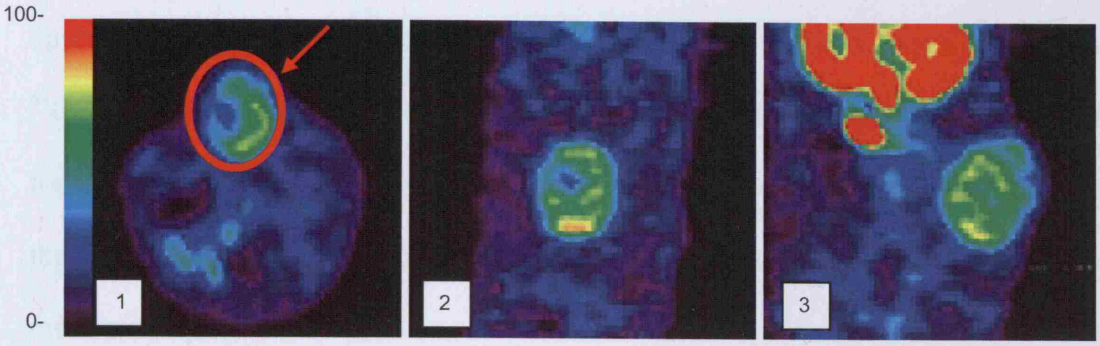

Figure 2.5 *^{64}Cu-ATSM microPET images of BD-9 rat bearing P22 carcinosarcoma. (1) Axial image of tumour through mid-point, ROI outlined in red. (2) Coronal tumour section, (3) sagittal tumour section.*

2.2 ^{64}Cu-ATSM

2.2.1 Choice of isotope

Copper is available in a number of different isotopic forms. Each has a different half-life and radiation emission spectrum emitting some combination of γ-ray, β^- particle or β^+ positron (table 2.1). In addition, for each copper isotope producing positrons, the positron branching fractions are different as are the positron path lengths. These features combine to form isotopes with quite different imaging qualities. A prerequisite for this project was the need for a positron emitting isotope, as such we were able to choose from ^{60}Cu, ^{61}Cu, ^{62}Cu or ^{64}Cu.

The decay half-life is an important aspect in determining which copper isotope to use in imaging. Copper isotopes with short half lives ^{60}Cu (23.4 minutes) and ^{62}Cu (9.7 minutes) can be used in imaging biological processes that rapidly establish tracer uptake, for instance perfusion (Cu-PTSM), the shorter half lives also allow the opportunity to perform dual tracer analyses. Longer lived isotopes such as ^{61}Cu and ^{64}Cu are more suitable for imaging biological processes that take longer to establish, for instance the labelling of cellular processes. In addition, a longer half-life means the production of the isotope can occur off site and be delivered without loss of too much activity.

The distance travelled by the positron prior to annihilation with an electron is known as the positron path length or range. This is different for different isotopes and reflects the energy of the emitted positron. Positron path length determines the intrinsic resolution possible for an isotope used in positron emission tomography. The positron range spectra can be sought for each isotope and comes from a detailed analysis of their decay schemes. ^{64}Cu decays by positron emission with a branching fraction of 17.4%, a maximum β^+ energy of 0.653MeV and a positron path length of 0.57mm. This is similar to ^{18}F (0.634MeV) with a mean positron range in water of 0.5mm. ^{60}Cu has a maximum β^+ energy of 3.772MeV with an average positron range in water of 3.09mm. This, together with its production of γ-rays with an energy mostly greater than 0.826MeV which may be detected as part of a coincidence pair they are likely to limit its imaging potential. ^{61}Cu has a maximum β^+ energy of 1.215MeV which produces an average positron range of 1.32mm (Ruangma 2006). Of the copper isotopes, ^{64}Cu has one of the shortest ranges meaning less discrepancy

between the true and assumed location of the positron emitter, leading to less image blurring and a better resolution.

The final choice of ^{64}Cu was based on its longer half-life (12.7 hours), shorter positron path length and ability to be produced by a small biomedical cyclotron within a medical facility. The compromise with ^{64}Cu versus the other copper isotopes is that its sensitivity is low due to the relatively low branching fraction of 17.4%, although this can be corrected for by longer imaging times and higher doses.

Nuclide	Half-life (min)	Radiation	Positron energy(MeV)	Positron branching ratio (%)
^{60}Cu	23.4	β^+ (93%), electron capture (7%)	2.940	93
^{61}Cu	204.5	β^+, electron capture	1.159	62
^{62}Cu	9.7	β^+ (98%), electron capture (2%)	2.925	98
^{64}Cu	761.9	Electron capture (45%), β^- (37%), β^+ (18%)	0.657	18
^{66}Cu	5.1	β^- (100%)	N/A	N/A
^{67}Cu	3720	β^- (100%)	N/A	N/A

Table 2.1 *Half-lives and decay of the copper radionuclides (Blower 1996)*

2.2.2 Radionuclide and ^{64}Cu-ATSM synthesis

The production of ^{64}Cu-ATSM was performed by Dr Rowena Paul in the Clinical PET Centre, St Thomas's Hospital, London, UK.

2.2.2.1 Production of ^{64}Cu.

The production of ^{64}Cu was performed on the CTI RDS-112 cyclotron within the Cyclotron Facility at The Clinical PET Centre, St Thomas's Hospital. The CTI RDS-112 is a positive ion machine which accelerates protons to 11.5 MeV. These protons bombard a ^{64}Ni plated target to form ^{64}Cu by the nuclear reaction ^{64}Ni(p,n)^{64}Cu;

(28,64) Ni + proton → (29,64) Cu + neutron

The ^{64}Ni plated gold bullet target is irradiated for 1-4 hours in a specially designed target holder in the cyclotron.

2.2.2.2 Nuclide Separation and Purification

After bombardment the ^{64}Cu is separated from the target nickel and other contaminants. The ^{64}Ni (containing the ^{64}Cu) is dissolved in 3 x 0.2 µl of 9.0M HCl with heating to evaporation each time. The final solid $^{64}CuCl_2$ is then dissolved in 0.5 ml 9.0 M HCl and transferred to a Bio-Rad (Hercules, CA) glass ion exchange column to separate the ^{64}Cu from the contaminants nickel and ^{61}Co. Elution of the column is carried out with the nickel and other reaction by-products collected immediately in the first 4 ml fraction of the 9.0M HCl. The ^{64}Cu is then collected in approximately 2 – 12 mL of 0.5M HCl. Radionuclidic purity is confirmed by gamma

spectroscopy (Ortec Ge detector, *DSPEC jr* 2.0) (McCarthy 1997; McCarthy 1999; Welch 2000).

2.2.2.3 Production of H_2ATSM

The non-radioactive portion of the drug is diacetyl bis(N^4-methylthiosemicarbazone) (H_2ATSM). H_2ATSM is a yellow, air stable solid material. H_2ATSM is produced by the following procedure, which is based on literature methods (Petering 1964; Petering 1972). 4-Methyl-3-thiosemicarbazide is dissolved in 50 ml 5% acetic acid and maintained at a temperature of 50-60°C with constant stirring. 2,3-Butanedione is taken up in 10 mL MilliQ® ultrapure H_20 and added drop-wise to the 4-methyl-3-thiosemicarbazide solution over a 45 minute period. Soon after the butanedione addition is begun, a precipitate begins to form in the light yellow solution. The mixture is left stirring for an additional 30 minutes at 60°C, and then the hot solution is filtered through a course fitted-glass filter to isolate the solid product. The isolated H_2ATSM is washed with 2 x 50 mL H_2O and then 2 x 50 mL ethanol and dried at 75°C in the oven overnight. H_2ATSM is taken up into 100 mL 80% acetic acid and is heated under reflux for 30 min. The solution is then filtered hot. Any undissolved material is collected and dried overnight at 75°C. H_2ATSM is characterized fully by the use of elemental analysis, NMR and mass spectrometry.

2.2.2.4 Production of ^{64}Cu-ATSM

H_2ATSM (1mg) is prepared by dissolving in 1 ml of dimethyl sulfoxide (DMSO). Ten μL of the H_2ATSM/DMSO solution is added to the $^{64}CuCl_2$ in 150 μL 3M HCl solution and vortexed immediately. The resulting ^{64}Cu-ATSM containing solution is transferred onto a prewashed C_{18} SepPak® Light cartridge to extract the ^{64}Cu-ATSM from aqueous solution. The C_{18} SepPak® Light cartridge is then washed with 10 mL

MilliQ® ultrapure water and the ^{64}Cu-ATSM eluted from the cartridge in 0.1 mL fractions of ethanol. The fractions containing the peak amounts of activity are combined and the ethanol fraction is diluted with 0.9% sodium chloride for injection such that the composition contains no more than 10 % ethanol. A higher concentration would be toxic to the animals in the study.

2.3 Animal models

2.3.1 Tumour model

Male BD9 rats produced by the Gray Cancer Institute, Northwood, UK, were used for this study. The P22 carcinosarcoma rat allograft was used as the tumour model. This tumour was originally produced following the irradiation of the cervical spinal cord in a male BD9 rat (Tozer 1993). The tumour model was chosen for a number of different reasons;

1. A rat tumour was chosen so a larger tumour could be imaged versus a mouse tumour model. Given the resolution of the MicroPET scanner in particular it was felt the larger tumour size would be better for analysis.
2. The P22 carcinosarcoma is more oxic than many animal tumours and as such it was felt to be a better model for human tumours.
3. The Gray Cancer Institute, where the study was performed, were vastly experienced in the study and maintenance of this tumour model and this model has been used for the extensive evaluation of the vascular targeting agent, combretastatin, in this institution.

4. The P22 tumour is a solid tumour, more cystic tumours typical of rat tumours would have made analysis difficult.

2.3.2 Tumour implantation

The P22 carcinosarcoma rat allograft was used as the tumour model which was implanted subcutaneously over the left flank. Initiation of the tumour line involved the subcutaneous implantation of 1-2mm^3 tumour pieces of an early passage tumour from frozen stock. Experiments were performed on the 2nd to 8th passage tumours. Following halothane inhalation a tumour-bearing rat was sacrificed by cervical dislocation. The tumour was then resected and sectioned using cross scalpel blades in to 1-2mm^3 pieces. These were then implanted in the recipient rats using inhalational halothane anaesthesia. The left flank was shaved and cleaned, then a small incision was made and a subcutaneous pocket formed in the connective tissue with sterile forceps in to which the tumour piece was placed. The incision was then closed using autoclips (Clay Adams). The tumour models were used for experimentation after 10-14 days when they reached a size of approximately 1.5 cm in diameter. The mean tumour weight of the resected tumours was 3.10g (range 1.16 – 5.82g).

2.3.3 Experimental procedure

On the day of the experiment the rat was anaesthetised using inhalational halothane. The rat was subsequently weighed for the determination of intra-peritoneal anaesthetic dosage. The intra-peritoneal anaesthesia used was a combination of midazolam (5mg/ml; Hypnovel, Roche, Welwyn Garden City, UK), fentanyl citrate

(0.312mg/ml) and fluanisone (10mg/ml; obtained together as Hypnorm, Vetapharma Ltd, Leeds, UK). Hynorm (1ml) and Hypnovel (1ml) were mixed with sterile water (2ml) to produce the anaesthetic which was then administered at a dose of 3.2ml/kg. A further dose of 0.1ml was administered intraperitoneally at 45 minutes and thereafter at 25 minute intervals as necessary until the rat was connected up to a syringe pump delivering anaesthesia continuously via the intra-peritoneal line at a dose rate of 4.2µl/min. When used, pimonidazole was administered via the intra-peritoneal route at a dose of 60mg/kg (Hypoxyprobe™-1,Chemicon International). This was injected 4 hours prior to the anticipated time of sacrifice because in this tumour model a minimum of 4 hours was needed between injection and sacrifice for adequate tissue staining to occur. Single venous and arterial cannulation of the tail artery and vein were carried out using sterile procedures (figure 2.6). Polythene tubing with an internal diameter of 0.58mm and an external diameter of 0.96mm (SIMS Portex Ltd, UK) was used to cannulate the vessels which were kept patent with heparinised saline. During this procedure the rats core temperature was maintained using a heating mat with negative feedback from a rectal temperature probe.

The rat was the placed in a rigid cradle for imaging in both the MRI and MicroPET scanners so that the position of the rat was not changed whilst moving between scans (figure 2.7). The cradle was made out of PTFE that was not visible by either of the two imaging techniques. Fiducial markers, when used, were fitted to the cradle at the level of the axial centre of the tumour (see 2.5.3), in addition a heating mat with feedback from a rectal temperature probe was fitted to the cradle in order to monitor

the body temperature of the rat. For further information about imaging techniques please refer to section 2.1 and 2.5.

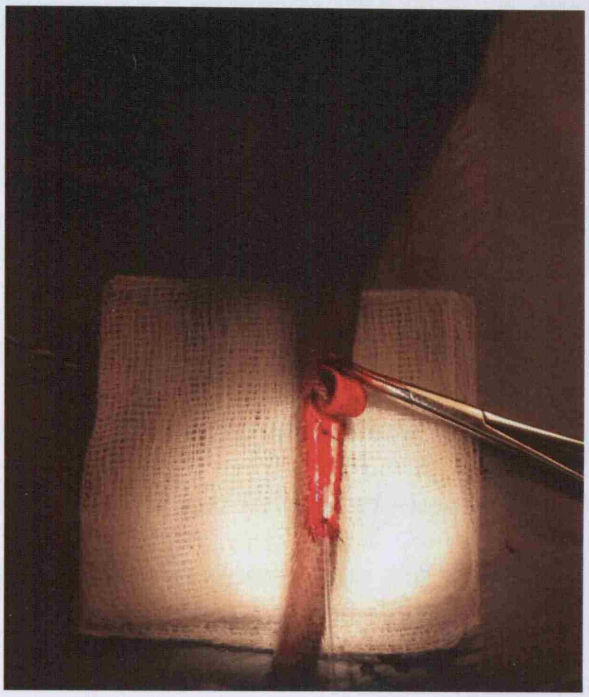

Figure 2.6 *Cannulation of tail artery.*

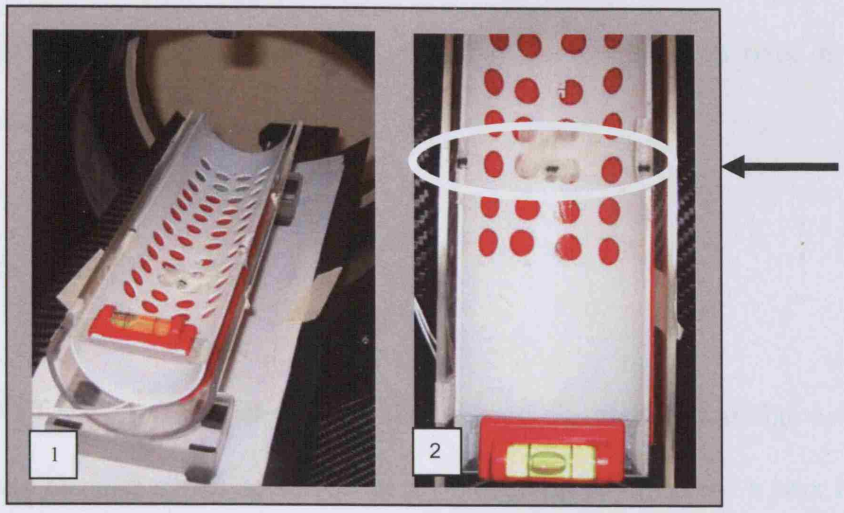

Figure 2.7 *(1) Rat cradle for imaging in both MRI and microPET scanners. (2) Rat positioned identically in both scanners using the spirit level and fiducial markers (see arrows). The fiducial markers were aligned using the microPET set-up laser, see arrow.*

Following imaging the rat was sacrificed using 0.2ml (200mg/ml) of intravenous pentobarbital sodium (Euthatal, Vericore Ltd, Dundee, UK) and then carefully moved to a bench such that the position of the rat was unchanged to allow bisection of the tumour in an axis perpendicular to the axis of scanning. The tumour was resected behind a lead glass shield to protect against continuing radioactive emissions. The tumour was revealed by dissecting the skin back, it was then inked laterally along the length of the tumour to identify the dorso-lateral aspect of the tumour following sectioning and immunohistochemical staining. Once the ink had dried the tumour was removed from the body of the rat and bisected at the tumour mid-point along the axis perpendicular to its movement through the scanners. This resulted in a histological cross section representing the central axial tumour that corresponded to images obtained by both the PET and MRI. Upon bisecting the tumour the half tumours were

further bisected parallel to the cut surface, placed in cassettes and in fixed in 10% Neutral Buffered Formalin.

2.3.4 Histological processing

One tumour half was left in 10% Neutral Buffered Formalin until the level of radioactivity has reached a safe level (10 days) before processing into a wax block. These tumour specimens were transferred to a container of 70% alcohol after 48 hours. The other half was placed in a cassette and transferred to an enclosed automated tissue processor to run a 12-hour schedule to enable rapid tumour sectioning for autoradiography while maintaining good tissue architecture for later immunohistochemical staining. The rapid processing technique involved fixation of tissue in 10% Neutral Buffered Formalin (2.5 hours) dehydration with alcohol (4.5 hours), clearing in xylene (3 hours) and infiltration of the sample with wax (2 hours). The specimens were then embedded in a wax block and serial sections were taken of the cut surface using the microtome of slice thicknesses 4, 10 and 25μm. These were floated out on a warm water bath before being picked up on to a glass slide and left to dry using a slide heater.

2.3.5 Frozen sections

A number of specimens had frozen sections cut in order to expose the tumour section to the autoradiography plate with minimal delay. Following resection of the tumour it was bisected and frozen immediately in Tissue-Tek®OCT (optimal cutting temperature) medium, at –40 degrees in isopentane. The blocks were then cut in to 8

μm sections using a cryostat, fixed with acetone and left to dry before placing on the autoradiography plate for a ten day exposure (section 2.3.7). After this they were stained using the techniques described in section 2.3.6.

2.3.6 Immunohistochemical staining

Formalin fixed paraffin embedded sections were de-waxed in xylene for five minutes prior to re-hydration through graded alcohols (100, 90 70%) to water. Antigen retrieval was performed on the slides by placing them in a bath of 10mM citric acid pH 6.0 and boiling for 8 minutes using an 800W microwave oven (2450 MHz Panasonic NN-6453BBPQ). The volume of fluid was topped up to its original level and the slides were then left to stand for 20 minutes at room temperature before being washed in running tap water.

2.3.6.1 Pimonidazole

Staining comprised of the following steps:

1. The slide was rinsed in Tris Buffer Saline (TBS) followed by the application of Dako Protein Block (DakoCytomation Ely Cambs X0909) for 5 mins.
2. Hypoxyprobe-1 antibody (Chemicon Europe Ltd Hamps HP2-100) was applied diluted 1/100 in antibody diluent (DakoCytomation S2022) for 60 mins, following which it was washed in TBS for 3 minutes.
3. Anti- fluorescein isothiocyanate (FITC) Mono-clonal antibody (Mab) (Chemicon Europe Ltd) was applied diluted 1/100 in Dako antibody diluent for 30 mins and then washed three times in TBS for 3 minutes.

4. 3,3'-diaminobenzidine (DAB) substrate (DakoCytomation K3467) was applied for 5 mins followed by rinsing with TBS and washing in running tap water.
5. The slide was then counterstained in Mayers haematoxylin (Surgipath Europe Ltd Peterborough UK Cat No 01582E) for 10-60 seconds then washed again in running tap water.
6. Finally it was dehydrated through graded alcohols, washed in xylene and mounted with a coverslip in DPX (Surgipath Europe Ltd 08600E)

2.3.6.2 GLUT-1

GLUT-1 required microwave pre-treatment in 10mM citric acid pH 6.0 on high power for a total of 12 min (4x3min). The staining method comprised of the following steps:

1. The slides were de-waxed and re-hydrated through graded alcohols to water then transferred to a plastic rack and microwaved in 10mM Citric acid for a total of 12mins (3x4 min pulses). They were then left to stand at room temperature for 20 minutes then washed in running tap water followed by TBS.
2. Dako H_2O_2 block was applied for 5 minutes followed by rinsing in distilled water and TBS.
3. Dako protein block was applied for 5 mins and the excess removed.
4. Glut-1 antibody diluted 1/200 in TBS (Dako A3536) was applied for 60 minutes, then washed three times in TBS (3 minutes) and the excess fluid removed.

5. Envision ^{TM} HRP Rabbit polymer (Dako K4010) was applied for 30 minutes followed by washing in TBS (3 minutes) and removal of excess fluid.

6. DAB substrate was applied for 5 minutes then the slides were washed well in running tap water.

7. The slides were then counterstained for 10-60 seconds in Mayers haematoxylin (Surgipath), washed well in tap water before dehydrating clearing and mounting in DPX.

2.3.7 Autoradiography

Following the rapid fixation described above the slides were placed in a cassette containing a storage phosphor screen (GE Healthcare, UK). This was left undisturbed at ambient temperature for 10 days at which point the storage phosphor screen was removed and digitised using a Storm^{TM} phosphor imaging system and ImageQuant^{TM} software (Amersham Biosciences Ltd, UK). The images obtained were converted to 8-bit greyscale and each pixel assigned an intensity value of 0-255 depending on concentration of ^{64}Cu-ATSM. The relationship between ^{64}Cu-ATSM concentration and greyscale intensity value is linear.

2.4 Histological analysis

2.4.1 Digitisation of slide

Analysis of immunohistochemistry first involved digitisation of the histology slides. The steps involved in the process of digitisation are as follows:

1. All sides had coverslips to protect from dust and debris.
2. The slide was mounted on a Nikon eclipse TE2000-E microscope and microscopy was performed at x40 (x4 objective lens and x10 eyepiece).
3. Background corrections were made to compensate for any artefact caused by particles on the lens, or discolouration of the slide. The 'white average' was created by using a clean area of slide adjacent to specimen. The 'black average' was taken by blocking the light source.
4. The region of interest was defined on the computer screen using x and y coordinates.
5. The focal plane was defined by focussing on three coordinates in a triangular pattern within the region of interest (chosen by the computer). The computer then calculated and compensated for any variations in thickness of the specimen.
6. Multiple images were acquired using the computer controlled motorised microscope stage. In order that no part of the specimen was omitted a 10% overlap between each image was specified.

The separate images were then stitched together using an in-house program ('image stitching,' Gray Cancer institute, Northwood, Middlesex, UK). The programme used

pixel data that aligned at a cellular level. The 10% overlap was removed at this stage. The resulting image was a .tif file.

Every pixel of the image contained information in an 8-bit format with a value between 0-255 for each of the colours red, green and blue (RGB). 0 indicating a total absence of colour and 255 indication complete saturation. This provided quantification of colour and allowed subsequent analysis of each histology image on the basis of colour.

2.4.2 Linear unmixing

This process allowed the separation of the immunohistochemical colour stain from the rest of the slide in order to determine the precise uptake of the immunohistochemical stain. For this the digitised RGB colour image was used (figure 2.8). This was resampled by 50% for ease of processing. The tumour was then outlined and a mask generated to exclude the region of outside of the tumour, as well as areas of necrosis, acellularity and stroma (Varia 1998; Raleigh 2000). Using the microscope for visual inspection, cells were identified that stained positively for pimonidazole. This colour of positive staining was selected and using linear unmixing software (TRI 2, in-house software, Gray Cancer Institute) a separated reference map of cells staining for this colour only was produced. Following reapplication of the mask of the excluded region a colour intensity histogram was generated and normalised to calculate the total area delineated (T). The upper and lower thresholds of colour intensity were then altered to exclude regions that were not genuinely staining and thought to represent background staining or artefact. As a result of this a

value for the stained area was obtained (S). The percentage area of tumour section staining positively for immunohistochemical stain, the hypoxic fraction, was then generated;

S/T x 100% = Hypoxic fraction

Figure 2.8 *Process of using linear unmixing to separate out a colour reference. (1) is the digitised histology slide stained with pimonidazole (brown) and haematoxylin (blue). A mask is drawn to generate a region of interest (2). Any area of necrosis, accellularity, stroma, artefact was exluded from this. The representative colour for positive staining is chosen and a separated reference image is produced (3). Using the miscroscope, colour reference thresholds are set to exclude any staining that is thought to not represent true staining or artefact.*

Similar computerised analysis methods are in routine use elsewhere (Wijffels K2000; Raleigh 2001; Janssen 2002).

2.4.3 Co-registration of autoradiography with stained slides

Following the generation of .tif files for the autoradiography images and immunohistochemical images of the same slide the images were oriented using the layer palette of Jasc Paint Shop Pro ™.

2.4.4 Methodology for comparison of autoradiography with stained slides

Comparison of the autoradiography and histology images was performed using two different methods;

1. Pixel by pixel analysis comparing intensity of immunohistochemical stain and tracer uptake.
2. Grid analysis comparing percentage uptake of immunohistochemical stain with ^{64}Cu-ATSM mean intensity per unit grid square.

2.4.4.1 Pixel analysis

Intensity of pimonidazole staining is not representative of the level of hypoxia and is variable within and between tissue sections. This variability is not thought to occur as a result of staining, which has been described as being very reproducible over a period of years (Raleigh 2001). However it is thought to reflect different redox capacities within the same tumour and between tumours, variable pharmacokinetic handling of pimonidazole amongst tumours, a fluctuating oxygen concentration in the time following pimonidazole administration and tumour resection, and a different rate of decay of the marker adduct. As ^{64}Cu-ATSM is retained in the cell as a result of

similar redox processes, and as ^{64}Cu-ATSM uptake is being compared with pimonidazole in the same tissue section which has been subject to the same changes in tissue oxygenation, one would expect the paired images to act as their own control. It is for this reason it was felt there was a sound basis for comparing autoradiography and immunohistochemistry of the same tumour slice on a pixel by pixel basis, following conversion of the immunohistochemistry separated colour reference image to an 8-bit greyscale and comparing this with our 8-bit autoradiograph. This meant comparing individual pixel intensities with each other (figure 2.9).

Each pixel was assigned a value of 0-255 based on the greyscale intensity of that pixel, which in turn represented intensity of immunohistochemical stain or tracer uptake. Using Image J 1.35s (NIH, USA) both the autoradiography and histology slides were converted in to approximately 50x50 pixel images and each pixel coordinate was assigned its intensity value. The pixel coordinates were compared and any that didn't match were discarded, in addition to any regions of necrosis, acellularity and stroma. The resulting coordinate matched pixel values were compared to determine the correlation. A similar method of analysis has been used previously (O'Donoghue 2005; Yuan 2006).

GLUT-I is an intinsic marker of hypoxia and and therefore not subject to the same pharmacologic handling variability as pimonidazole, its expression is likely to vary within and between tumours, and its expression will be subject to the same changes in tumour microenvironment as the radiotracer. As such the pixel analysis described above was also used as a method for comparing the distribution of ^{64}Cu-ATSM with GLUT-I.

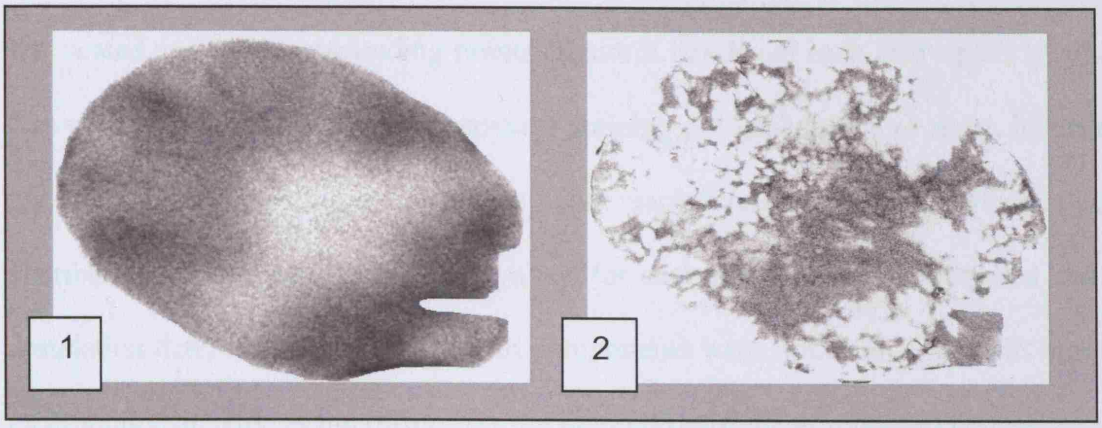

Figure 2.9 *(1) ^{64}Cu-ATSM autoradiograph of the same histology slide that was later immunohistochemically stained for pimonidazole from which a separated colour reference was generated. This was then converted to 8-bit greyscale (2) for pixel-by-pixel comparison between the two.*

2.4.4.2 Grid analysis

Although immunohistochemistry of pimonidazole and ^{64}Cu-ATSM autoradiography of a tumour section act as their own control, for the purposes of completeness pimonidazole and GLUT-1 staining were compared using percentage staining per unit grid square with ^{64}Cu-ATSM autoradiography using greyscale mean intensity per unit grid square. Comparing the large grid square elements used for this analysis rather than pixels is less likely to be subject to errors as a result of mis-coregistration. The autoradiography images were not thresholded in order to get a corresponding area of uptake of ^{64}Cu-ATSM as methods to do this were very subjective. In order to do this comparison, the histology slices were prepared using the images generated from the TRI2 program with the threshold levels applied such that the only pixels counted were those that stained positively for pimonidazole. The autoradiography image was

called up at the same time in TRI2. A 10 x 10 grid was applied to both images that was scaled to fit at corresponding points (figure 2.10). From each grid square a value was generated that gave either percentage staining per grid square or mean intensity per grid square depending on the image being respectively the immunohistochemical distribution or autoradiography. The values for each grid were then compared and a correlation determined. Values for grid components were not used if the grid square incorporated an edge as the result may not be correct for the purposes of comparison.

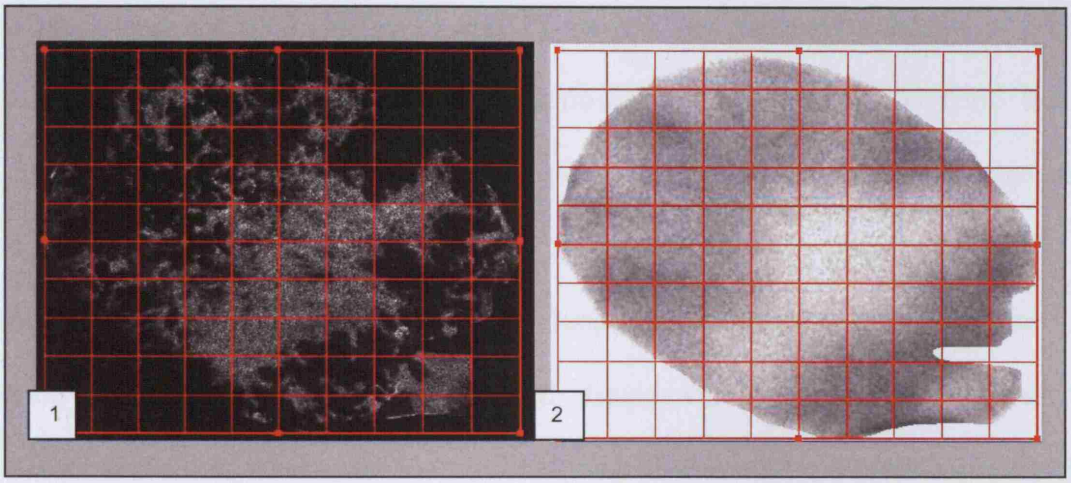

Figure 2.10 *The separated colour reference image for the immunohistochemical distribution of our marker (1) was compared with ^{64}Cu-ATSM autoradiography of the same slide (2). Identical grids were placed over the co-registered images and the percentage of grid square staining positively for immunohistochemical marker compared with ^{64}Cu-ATSM mean intensity per grid square.*

2.5 Dynamic contrast enhanced magnetic resonance imaging (DCE-MRI)

2.5.1 Theory

MRI produces images that delineate the differing response of protons in different tissues to a changing magnetic field. These images can provide quite detailed tissue structure.

Tissues have characteristic ^{1}H T1 and T2 values. The magnetic moments of protons align themselves in a longitudinal direction when an external magnetic field is applied. The effect of a radiofrequency pulse on proton alignment is to change its direction such that the net direction is in a transverse direction. When the radiofrequency pulse is switched off longitudinal magnetization increases and transversal magnetization decreases and disappears. T1 is a time constant that describes the time it takes for longitudinal magnetization after a radiofrequency (RF) pulse to recover, it is defined as the time taken when 63% of this original magnetization is reached. T2 is a time constant describing the transversal relaxation time, it is defined as the time taken for transversal magnetization to decrease to 37% of its original value. In absolute terms tissue ^{1}H T1 is 300 to 2000 msec and T2 is 30 to 150 msec. Liquids have a long T1 and T2, fat has a shorter T1 and T2. Tumours tend to have a relatively high water content therefore tend to have a longer T1 and T2 than normal tissues. In order to create an image a particular sequence of RF pulses and magnetic field gradients is applied. The size, direction, timing and frequency of the pulses can be used to manipulate the individual tissue signal intensities in order to create an image of sufficient contrast for diagnosis.

Image contrast can be enhanced by the use of an intra-venous low molecular weight paramagnetic contrast agent, gadopentate dimeglumine (Gd-DTPA, Magnevist®). In shortening the T1 relaxation time the use of Gd-DTPA increases the signal intensity on a T1-weighted image, thereby enhancing the definition of fluids which become extremely bright. This provides higher sensitivity for the detection of vascular tissues such as tumours. Low molecular weight contrast agents such as Gd-DTPA pass in to the capillary bed and the extravascular-extracellular space (EES). This occurs at a rate determined by the permeability of microvessels, surface area and blood flow (Padhani 2002). In tumours a variable 12%-45% of the contrast media leaks in to the EES during first pass (Daldrup 1998). Although the assumption is that changes in signal intensity are directly proportional to tissue contrast, this is not so, as there is a non-linear relationship between the two, particularly when the contrast agent concentration is large (Hoffman 1995).

Dynamic contrast enhanced (DCE) MRI involves the acquisition of a set of images as an intravenous contrast agent such as Gd-DTPA is injected. The bolus of Gd-DTPA will briefly be confined within the vascular space before diffusing rapidly in to the tumour EES. The change in signal intensity over time following injection of the contrast agent can be used to provide semi-quantitative parameters such as maximum gradient, maximum amplitude or area under the signal intensity-time curve (AUC). This can be used to provide information about the tumour microcirculation such as tumour perfusion, vascular permeability and vessel surface area (Mayr NA 1996; Beauregard DA 1998; Hawighorst H 1999).

The AUC (units mM.min or mM.s) is a measure of how much contrast has been taken up by the tumour in the first 60 or 90 seconds post-Gd-DTPA injection and is influenced by tumour blood flow rate and vessel permeability (Evelhoch 1999; Evelhoch 2004). AUC has the advantage that it does not require either mathematical modelling or arterial input function. AUC values can be easily and robustly calculated for individual voxels in the tumour region of interest after quantification of baseline T1. From these an average AUC for the tumour can be determined. For this experiment the AUC at 90s (AUC90) was chosen as the tumour blood flow parameter. This parameter has been used previously in the same tumour model (Maxwell 2002).

DCE-MRI was the technique chosen for this study to evaluate the impact of tumour blood flow on the distribution of ^{64}Cu-ATSM, and how the vascular targeting agent, combretastatin, modified this.

2.5.2 Experimental procedure

Following venous and arterial cannulation the rats were placed in the custom-built cradle for imaging designed to allow movement-free transfer between the bore of the Varian 4.7 T MR scanner and the bed of the Siemens MicroPet Focus 220 scanner.

Gadolinium-enhanced MRI imaging was performed immediately prior to dynamic ^{64}Cu-ATSM PET scanning. Rats were placed in a 4.7 T 30cm diameter horizontal-bore magnet of an Inova MR spectroscopy imaging system (Varian, Palo Alto, CA) using a 6cm diameter quadrature birdcage coil that was used as both transmitter and

receiver. A hot air blower with continuous temperature monitoring was used to maintain body temperature. A sequence of 100 gradient echo images was obtained with each image generated every 6 seconds. After the first 30 seconds the contrast agent Gadolinium-DTPA (Magnevist, Schering Health Care Ltd, Burgess Hill, UK) was administered at a dose of $0.1 mMol.kg^{-1}$ which was delivered by an infusion pump over the course of 5 seconds in to the tail vein at a rate of 20 $ml.min^{-1}Kg^{-1}$.

For the subsequent analysis of these images an in-house programme (Dr Ross Maxwell) was used which was applied to Matlab version 5 software (The Mathworks, Nantick, MA, USA). The process included the following stages: (i) calculation of T1; (ii) determination of pre-contrast signal intensity; (iii) calculation of gadolinium concentration for each post-contrast image from the initial T1 and the change in signal intensity. The region of interest was drawn on each central tumour slice using T1 data acquired prior to the contrast-enhanced data acquisition. These pre-injection images were then averaged to improve the signal to noise ratio and subtracted from the post-injection images to give enhancement images. The AUC90 was calculated on a voxel-wise basis which was then used to provide a mean tumour value per unit area.

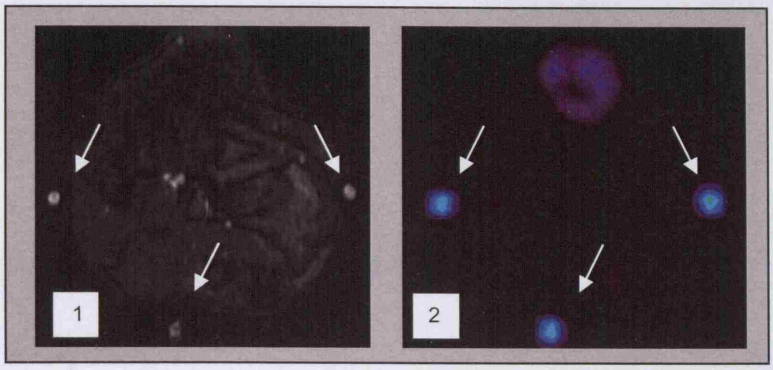

Figure 2.11 *A T1 MRI image with fiducial markers arrowed at axial mid-point of tumour (1). Corresponding ^{64}Cu-ATSM microPET image (2)*

2.5.3 Fiducial markers

Fiducial markers were used in later experiments (9 rats) to provide further assurance that identical tumour slices were being compared from MRI and microPET imaging. The fiducial markers comprised 1mm diameter blind ending plastic tubes containing 30µl of a dimeglumine gadopentetate(Magnevist ^{TM})/^{64}Cu-ATSM solution. This solution contained dimeglumine gadopentatate at a concentration of 8.27mg/ml, and nominally .25MBq/ml of ^{64}Cu-ATSM. Following instillation of the solution the open end was closed using beeswax. Three fiducial markers were used for each experiment to align the central tumour slice. These were fixed on the jig at the level of the mid-point of the tumour and aligned using the laser alignment system on the microPET scanner. A spirit level attached to the animal cradle was used to make sure there was no discrepancy in rotation between the two scans. Following MRI imaging the

animal was transferred across to the microPET scanner on the same jig with fiducial markers remaining in place (figure 2.11).

2.6 Eppendorf polarographic needle electrode

Eppendorf pO_2 histograph (Helzel Messtechnik Gmbh, Germany) measurements of tumour oxygenation were taken to provide additional information for the study with regards to tumour pO_2 and ^{64}Cu-ATSM uptake. Moreover it was used to provide a direct measure of tumour pO_2 in animals pre-treated with combretastatin (CA4P), a vascular targeting agent used to modify tumour pO_2. The pO_2 in P22 tumour bearing BD-9 control rats (see section 2.3.2 for tumour implantation method) was compared to those pre-treated with combretastatin in order to confirm tumour oxygen levels. It was unknown whether CA4P would compromise vascular delivery of pimonidazole and ^{64}Cu-ATSM to the tumour, Eppendorf measurements were therefore felt to be prudent in order to confirm the hypoxia inducing effects of CA4P using a technique that did not depend on tumour blood flow. In the treatment arm, animals received an i.p. injection of CA4P (10mg/kg) 2 hours prior to Eppendorf probe measurements. For Eppendorf probe measurements the animals were anaesthetised as described in section 2.3.3. A small incision was made in the skin overlying the tumour and the needle electrode was inserted. Three tracks were made radiating out from the point of entry with 14 measurements taken per track. The stepper device was set to use the 'pilgrim step method' whereby for each measurement the probe was moved forwards by 0.9mm followed by a retraction of 0.3mm to avoid pressure artefacts. The process

was repeated at the opposite pole of the tumour. Following completion of the measurements the animals were sacrificed using cervical dislocation.

2.7 Statistics

The statistics software package used for the statistical analysis of this thesis was StatsDirect version 2.4.1 (StatsDirect Limited). Graphs were generated using SigmaPlot 2000 version 6.00 (SPSS Inc.).

The Shapiro-Wilk test was used to objectively assess whether or not data was normally distributed before further statistical analysis could be performed.

For the calculation of correlation coefficients Pearson's correlation coefficient was used when at least one of the two variables was normally distributed based on the distribution of residuals being the difference between the observed and predicted values. Spearman's rank correlation was used when neither variable was normally distributed. For the comparison of two groups either the unpaired t-test (parametric) or Man-Whitney U test (non-parametric) was used depending on whether or not the data was normally distributed.

References

Beauregard DA, Thelwall P., Chaplin DJ, Hill SA, Adams GE, Brindle KM (1998). "Magnetic resonance imaging and spectroscopy of combretastatin A4 pro-drug-induced disruption of tumour perfusion and energetic status." Br J Cancer 77: 1761-1767

Blower PJ, Lewis J, Zweit J (1996). "Copper radionuclides and radiopharmaceuticals in nuclear medicine." Nuclear Medicine & Biology.(23): 957-980.

Budinger, T. (1998). "PT instrumentation: what are the limits?" Semin Nucl Med(28): 247-267.

Cherry SR, Phelps M. (1996). Positron emission tomography: methods and instrumentation. Baltimore, Williams and Wilkins.

Daldrup HE, Shames D., Husseini W, Wendland MF, Okuhata Y, Brasch RC (1998). "Quantification of the extraction fraction for gadopentetate across breast cancer capillaries." Magn Reson Med 40: 537-543.

Dehdashti F, Grigsby P., Lewis JS, Laforest R, Siegel BA, Welch MJ (2008). "Assessing tumour hypoxia in cervical cancer by PET with [60Cu]-labeled diacetyl-bis(N4-methylthiosemicarbazone)." Journal of nuclear medicine 49(2): 201-205.

Dehdashti F, Mintun MA, Lewis JS, Bradley J, Govinfan R, Laforest R, Welch MJ, Siegel BA. (2003). "In vivo assessment of tumor hypoxia in lung cancer with 60Cu-ATSM." Eur J Nucl Med Mol Imaging 30(6): 844-50.

Evelhoch J. (1999). "Key factors in the acquisition of contrast kinetic data for oncology." J Magn Reson Imaging 10: 254-259.

Evelhoch JL, LoRusso P., He Z, Delproposto Z, Polin L, Corbett TH, Langmuir P, Wheeler C, Stone A, Leadbetter J, Ryan AJ, Blakey DC, Waterman JC (2004).

"Magnetic resonance imaging measurements of the response of murine and human tumours to the vascular-targeting agent ZD6126." Clin Cancer Res 10(3650-3657).

Hawighorst H, Libicher M., Knopp MV, Moehler T, Kauffmann GW, Gv K (1999). "Evaluation of angiogenesis and perfusion of bone marrow lesions: role of semiquantitative and quantitative dynamic MRI." J Magn Reson Imaging 10: 286-294.

Hoffman U, Brix G., Knopp MV, Hess T, Lorenz WJ (1995). "Pharmacokinetic mapping of the breast: a new method for dynamic MR mammography." Magn Reson Med 33: 506-514.

Janssen HL, Haustermans KM, Sprong D, Blommestijn G, Hofland I, Hoebers FJ, Blijweert E, Raleigh JA, Semenza GL, Varia MA, Balm AJ, van Velthuysen ML, Delaere P, Sciot R, Begg AC. (2002). "HIF-1A, pimonidazole, and iododeoxyuridine to estimate hypoxia and perfusion in human head-and-neck tumors." Int J Radiat Oncol Biol Phys 54(5): 1537-49.

Matsumoto K, Szajek L, Krishna MC, Cook JA, Seidel J, Grimes K, Carson J, Sowers AL, English S, Green MV, Bacharach SL, Eckelman WC, Mitchell JB. (2007). "The influence of tumor oxygenation on hypoxia imaging in murine squamous cell carcinoma using [64Cu]Cu-ATSM or [18F]Fluoromisonidazole positron emission tomography." Int J Oncol 30(4): 873-81.

Maxwell RJ, Wilson J., Prise VE, Vojnovic B, Rustin GJ, Lodge MA, Tozer GM (2002). "Evaluation of the anti-vascular effects of combretastatin in rodent tumours by dynamic ontrast enhanced MRI." NMR Biomed 15: 89-98.

Mayr NA, Yuh W., Magnotta VA, Ehrhardt JC, Wheeler JA, Sorosky JI, Davis CS, Wen BC, Martin DD, Pelsang RE, Buller RE, Oberley LW, Mellenberg DE, Hussey DH (1996). "Tumour perfusion studies using fast magnetic resonance imaging

technique in advanced cervical cancer: a new noninvasive predictive assay." Int J Radiat Oncol Biol Phys 36: 623-633.

McCarthy DW, Bass LA, Cutler PD, Shefer RE, Klinlowstein RE, Herrero P, Lewis JS, Cutler CS, Anderson CJ, Welch MJ. (1999). "High purity production and potential applications of copper-60 and copper-61." Nucl Med Biol 26(4): 351-8.

McCarthy DW, Shefer RE, Klinkowstein RE, Bass LA, Margeneau WH, Cutler CS, Anderson CJ, Welch MJ. (1997). "Efficient production of high specific activity 64Cu using a biomedical cyclotron." Nucl Med Biol 24(1): 35-43.

McQuade P, Martin KE, Castle TC, Went MJ, Blower PJ, Welch MJ, Lewis JS. (2005). "Investigation into 64Cu-labeled Bis(selenosemicarbazone) and Bis(thiosemicarbazone) complexes as hypoxia imaging agents." Nucl Med Biol 32(2): 147-56.

Mullani NA, Markham J., Ter-Pogossian MM (1980). "Feasibility of time of flight reconstruction in positron emission tomography." J Nuc Med(21): 1095-1097.

O'Donoghue JA, Zanzonico P, Pugachev A, Wen B, Smith-Jones P, Cai S, Burnazi E, Finn RD, Burgman P, Ruan S, Lewis JS, Welch MJ, Ling CC, Humm JL.. (2005). "Assessment of regional tumor hypoxia using 18F-fluoromisonidazole and 64Cu(II)-diacetyl-bis(N4-methylthiosemicarbazone) positron emission tomography: Comparative study featuring microPET imaging, Po2 probe measurement, autoradiography, and fluorescent microscopy in the R3327-AT and FaDu rat tumor models." Int J Radiat Oncol Biol Phys 61(5): 1493-502.

Padhani A. (2002). "Dynamic contrast-enhanced MRI in clinical oncology: Current status and future directions." J Magn Reson Imaging 16: 407-422.

Raleigh JA, Chou S.-C., Bono EL, Thrall DE, Varia MA (2001). "semiquantitive immunohistochemical analysis for hypoxia in human tumour." Int J Radiat Oncol Biol Phys 49(2): 569-574.

Raleigh JA, Chou S.-C., Calkins-Adams DP (2000). "A clinical study of hypoxia and metallothionein protein expression in squamous cell carcinoma." Clin Cancer Res 6: 855-86.

Ruangma A, Bai B, Lewis JS, Sun X, Welch MJ, Leahy R, Laforest R. (2006). "Three-dimensional maximum a posteriori (MAP) imaging with radiopharmaceuticals labeled with three Cu radionuclides." Nucl Med Biol 33(2): 217-26.

Varia MA, Calkins-Adams D., Rinker LH, Kennedy AS, Novotny DB, Fowler WC Jr, Raleigh JA. Gynecol Oncol, 71: 270-277, 1988 (1998). "Pimonidazole: a novel hypoxia marker for complementry study of tumour hyopxia and cell proliferation in cervical carcinoma." Gynecol Oncol(71): 270-277.

Welch MJ, McCarthy DW, Shefer RE, Klinkostein RE (2000). Production of ^{64}Cu and other radionuclides using a charged-particle accelerator. Washington University. United States of America. 6,011,825.

Wijffels KIEM, Kaanders J, Rijken PFJW, Bussink J, van den Hoogen FJA, Marres HAM, de Wilde PCM, Raleigh JA, van der Kogel AJ (2000). "Vascular architecture and hypoxic profiles in human head and neck squamous cell carcinomas." Br J Cancer(83): 674-683.

Williams HA, Robinson S., Julyan P, Zweit J, Hastings D (2005). "A comparison of PET imaging characteristics of various copper radioisotopes." Eur J Nucl Med Mol Imaging 32(12): 1473-1480.

Yuan H, Schroeder T, Bowsher JE, Hedlund LW, Wong T, Dewhirst MW (2006). "Intertumoral differences in hypoxia selectivity of the PET imaging agent 64Cu(II)-diacetyl-bis(N4-methylthiosemicarbazone)." J Nucl Med 47(6): 989-98.

CHAPTER 3

^{64}Cu–ATSM uptake and retention in a rat tumour model

3.1 Introduction

A number of studies have demonstrated that an increase in tumour hypoxia results in an increase in tumour retention of ^{64}Cu-ATSM (Lewis 1999; Lewis 2001; Lewis 2002; Matsumoto 2007). However, only a small number have looked at the specific cellular distribution of ^{64}Cu-ATSM and compared this with tumour hypoxia markers at a cellular level (O'Donoghue 2005).

Defining the nature of the microscopic retention pattern of ^{64}Cu-ATSM in tumours is central to the evaluation of this tracer if it is to be used in order to delineate hypoxic sub-volumes and provide information about the status of tumour oxygenation. In addition the effect of blood flow and its contribution to uptake and retention of ^{64}Cu-ATSM needed evaluation. Dynamic contrast-enhanced (DCE) MRI was chosen for this purpose. Validated as a method for determining tumour blood flow this technique meant that MRI imaging could take place immediately prior to MicroPET imaging

with the animal maintained in exactly the same position for the robust comparison of corresponding image slices. Other methods for assessing blood flow and ^{64}Cu-ATSM retention at the cellular level include comparison of the fluorescent vascular perfusion marker Hoechst 33342 with ^{64}Cu-ATSM autoradiography and the vascular endothelial membrane protein CD31 with ^{64}Cu-ATSM autoradiography. Both of these techniques were attempted however the Hoechst 33342 fluorescence was not representative of the rich profusion of vasculature in this tumour and CD31 staining was very non-specific with abundant background staining (possibly as a result of the protein rich extra-cellular matrix) making the identification of vessels unreliable.

3.2 Aims

The aim of this study was to look at the biodistribution of ^{64}Cu-ATSM in a tumour bearing rat model and to compare the distribution of ^{64}Cu-ATSM at a cellular level with the well-validated tumour marker of hypoxia, pimonidazole. Evaluation of ^{64}Cu-ATSM as a tumour hypoxia marker was performed 1.25h and a mean of 20.5 hours (range 16.00-21.75 hours) after its administration. As part of this study the Eppendorf polarographic needle electrode was used to measure baseline tumour oxygenation in the P22 carcinosarcoma.

DCE-MRI using gadopentate dimeglumine (Gd-DTPA, Magnevist®) was used to determine tumour blood flow in a single cross-sectional tumour slice. The reliable and reproducible parameter Gadolinium AUC90 was chosen to represent tumour blood flow in the tumours imaged. This was compared with uptake of ^{64}Cu-ATSM in

the same tumour slice in order to determine a possible relationship between the radiotracer and tumour blood flow.

3.3 Materials and methods

3.3.1 Eppendorf probe measurement of tumour oxygenation

3.3.1.1 Experimental models

Three tumour bearing rats were chosen for this procedure. Tumour implantation and anaesthesia was carried out as described in sections 2.3.2 and 2.3.3. Following completion of the experiment the animals were sacrificed by cervical dislocation.

3.3.1.2 Experimental practise

The measurements were taken as described in section 2.7

3.3.2 ^{64}Cu-ATSM uptake in tumour model

A time-activity curve was generated for 4 tumour-bearing rats in order to observe the dynamics of tracer uptake in the tumour as compared with background tissues. For this experiment an i.v. activity of 9.96-34.91MBq (mean 20.34MBq) of ^{64}Cu-ATSM was administered to the tumour model prior to a dynamic 2 hour microPET acquisition. The rat was imaged in a single bed position with the centre of the field at the mid-point of the tumour. Following data acquisition the rat was sacrificed using an i.v. injection of pentobarbital sodium (Euthatal, Vericore Ltd, Dundee, UK).

Histogramming and reconstruction of the list mode data acquired was carried out as described in section 2.1.3. The data was reconstructed using the following time frame starting at the beginning of microPET imaging; 2 x 5 seconds (s), 29 x 10s, 30 x 30s, 40 x 60s, 30 x 120s. Time-activity data was generated using the 'region of interest' ROI tool of ASIPro VM™ (CTI Concorde Microsystems). A 3-dimensional ROI of the whole tumour was drawn together with a region of background adjacent to the tumour. Time-activity curves were generated from the two ROIs using ASIPro VM™ software.

A single whole body scan of a rat was obtained in order to determine the distribution of radiotracer within the rat. An activity of 24.0 MBq was administered intravenously at the same time as starting image acquisition. For this scan three bed positions were required with imaging times of 20 minutes for each position starting with the head and moving down. Following histogramming and reconstruction as described (section 2.1.3) the resulting images were stitched together using the ASIPro VM™ bed-stitching tool.

3.3.3 Comparison of tumour uptake of ^{64}Cu-ATSM with immunohistochemical markers of hypoxia

3.3.3.1 Comparison of Standardised uptake value (SUV) of ^{64}Cu-ATSM PET with pimonidazole staining

^{64}Cu-ATSM PET images were obtained of sixteen tumour bearing rats. Pimonidazole was administered (60mg/kg i.p.) 4 hours prior to the anticipated time of sacrifice. Each rat was imaged for 1 hour commencing at the same time as i.v. injection of ^{64}Cu-ATSM (mean activity 31.10MBq, range 9.96-55.95MBq). Imaging occurred in a single bed position with the mid-point of the tumour at the centre of the field. A 15-minute attenuation scan was performed following the ^{64}Cu-ATSM PET acquisition. On completion of imaging the rat was sacrificed using 0.2 mls (200mg/ml) intravenous pentobarbital sodium (Euthatal, Vericore Ltd, Dundee, UK) after which the tumour was resected, fixed and wax embedded as described in sections 2.3.4 and 2.3.5. The 4μm slide mounted central axial tumour sections were stained for pimonidazole (section 2.3.6.1) and digitised (section 2.4.1) from which the percentage of the tumour cross section staining positively for pimonidazole (section 2.4.2) was determined for comparison with the microPET images. The microPET data acquired was reconstructed in to 6 x 10 minute time frames from 0-60 minutes, and also a single time frame of 60 minutes (section 2.1.3). The 10-minute time frames were performed to see if correlation of ^{64}Cu-ATSM and pimonidazole changed over the course of 1 hour that may suggest an optimal time point for imaging hypoxia using ^{64}Cu-ATSM. From the reconstructed images the mean SUV of the central axial tumour slice was determined as described in section 2.1.5. This SUV was then compared with the corresponding pimonidazole stained histological section to see if

there was a correlation between tumour SUV and hypoxic fraction i.e. percentage of tumour cross section staining positively for pimonidazole.

Both the SUV and pimonidazole uptake were normally distributed therefore Pearson's correlation coefficient was used.

3.3.3.2 Pixel-by-pixel comparison of ^{64}Cu-ATSM autoradiography with pimonidazole distribution

^{64}Cu-ATSM autoradiography and pimonidazole distribution of the same tumour section were compared on a pixel-by-pixel basis in order to obtain a precise measure of the degree of co-localisation of ^{64}Cu-ATSM with tumour regions designated hypoxic by pimonidazole retention. The P22 carcinosarcoma was implanted in to 7 rats as described in section 2.3.2. Pimonidazole was administered as described in section 2.3.3. ^{64}Cu-ATSM was injected in to the tail vein cannula at the start of scanning 75 minutes (1 hour PET acquisition + 15 minute attenuation scan) prior to sacrifice with i.v. pentobarbitol sodium (Vericore Ltd, Dundee). The mean dose of ^{64}Cu-ATSM injected was 40.66MBq (range 24.58-55.95MBq). Following sacrifice the tumour was resected, fixed, wax embedded and sectioned as described in 2.3.3 and 2.3.4. The slides were then placed on an autoradiography plate for 10 days and digitised, detailed in section 2.3.7. On completion of the autoradiography process the slides were stained with haematoxylin and had immunohistochemical staining for pimonidazole, described in section 2.3.6. The stained slides were digitised and separated brown pimonidazole reference images were created (section 2.4.1 and 2.4.2). The separated pimonidazole reference image was then rotated and resized to have an identical orientation to the autoradiography image of the same slide, see

2.4.3. Both the autoradiography and separated brown reference image were converted to greyscale images. Fifty by fifty pixel images were generated and the greyscale values compared as described in section 2.4.4.1. Spearman's rank correlation coefficient was used for purposes of comparison as greyscale pimonidazole intensity and ^{64}Cu-ATSM intensity were not normally distributed.

3.3.3.3 Grid comparison of ^{64}Cu-ATSM autoradiography with pimonidazole distribution

The separated brown pimonidazole reference slide and autoradiography images of the same tissue section were prepared as described above (section 3.3.3.2). Using TRI2 grid comparison software (in-house software, Gray Cancer Institute) a 10 x 10 grid was positioned over the identically oriented paired separated reference slide and autoradiography image such that the edges of the grid touched the edges of the specimen, for further details see section 2.4.4.2. In the case of the autoradiography images, values generated for the grid squares were greyscale mean intensity, representing ^{64}Cu-ATSM uptake mean intensity. For the pimonidazole images the grid square values represented the proportion of that grid square staining positively for pimonidazole i.e. hypoxic fraction. Spearman's rank correlation was applied to generate a correlation coefficient as the values generated did not follow a normal distribution.

3.3.3.4 Prolonged tumour exposure to ^{64}Cu-ATSM uptake and its comparison with pimonidazole

A previous study described the statistically significant correlation of ^{64}Cu-ATSM with pimonidazole following resection of tumour 24 hours after administration of

^{64}Cu-ATSM (O'Donoghue 2005). This was studied in the R3327-AT anaplastic rat prostate tumour. This additional time point was used because a correlation was not seen between ^{64}Cu-ATSM and pimonidazole when they were compared after tumour resection at 1 hour.

For our study 5 tumour bearing rats were injected with i.v. ^{64}Cu-ATSM (mean dose 81.61MBq) a mean of 20.50 hours prior to sacrifice with cervical dislocation.

Three of the tumours had frozen sections cut immediately (section 2.3.5). The quality of these frozen sections was insufficient for a detailed pixel-by-pixel or grid analysis, however two tumour sections were prepared using rapid formalin fixation and wax embedding prior to exposure to the autoradiography plate as described in section 2.3.4, and 2.3.7. Both pixel-by-pixel analysis and grid analysis could be performed on these to determine a correlation between ^{64}Cu-ATSM uptake and pimonidazole distribution as described in section 2.4.4.

3.3.4 Dynamic contrast-enhanced MRI

Fourteen P22-bearing BD-9 rats had Gadolinium-enhanced MRI immediately prior to microPET imaging. The rats had both venous and arterial access to monitor the blood pressure of the rat throughout the procedure. The rats were anaesthetised throughout using intra-peritoneal anaesthesia described in section 2.3.3

The imaging process was carried out with the rat in a cradle that could be moved between scanners without movement, a pre-requisite for optimal comparison of PET

and MRI images. Furthermore, fiducial markers were used latterly in the experimental process to increase our confidence that the MRI and microPET images to be compared were indeed of the same slice (see section 2.5.3). Following completion of Gadolinium-enhanced MRI (section 2.5.2) the rat was transferred across to the microPET scanner for a one-hour dynamic list mode data acquisition that began at the same time as intravenous delivery of ^{64}Cu-ATSM (section 2.1.3 and 2.1.4). Attenuation scans were performed for 15 minutes after ^{64}Cu-ATSM PET acquisition. Following completion of the microPET scan the animal was sacrificed using pentobarbital sodium (Euthatal, Vericore Ltd, Dundee, UK). Each microPET list mode data set was reconstructed in to both a single 60-minute time frame and 6 x 10 minute time frames for analysis (section 2.1.3).

For each tumour the AUC90 of the central axial slice was calculated from the tumour ROI and divided by the cross-sectional area in order to give a value per unit area, see section 2.5.2 (figure 3.1). A region of interest (ROI) was drawn around the corresponding microPET slice to generate the mean SUV per unit area of tumour. When this involved the microPET images that had been framed in to 10-minute segments a single ROI was drawn on one of the images and copied identically across all time frames so that the same slice and ROI was chosen for each 10-minute image. The tumour SUV was calculated as described in section 2.1.5.

A more detailed grid analysis was not used for comparison of the microPET and MRI data due to limitations in the software available that were unable to set grid square elements that were identical across the two imaging modalities.

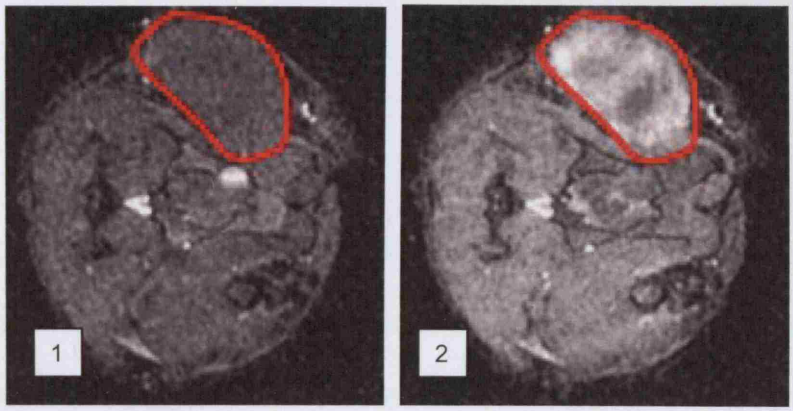

Figure 3.1 *Gadolinium-enhanced MRI image through mid-axial section of P22 tumour model. The tumour is outlined. The images were acquired 0 seconds (image 1) and 90 seconds (image 2) after the beginning of Gadolinium infusion. Image 2 shows the relatively greater increase in tumour signal intensity from the Gadolinium.*

Pearson's correlation coefficient was used to investigate a relationship between Gadolinium AUC90 and mean tumour SUV at 1 hour and measured for each of the 10-minute time frames.

3.4 Results

3.4.1 Tumour oxygenation

The results of the Eppendorf probe measurements revealed clinically significant tumour hypoxia based on the proportion of tumour with a pO_2 of less than 10mmHg. The percentage of each of the three tumours measured with a pO_2 of less than 10mmHg was 43.33%, 61.41%, 41.41%, giving a mean value of 48.72% (figure 3.2).

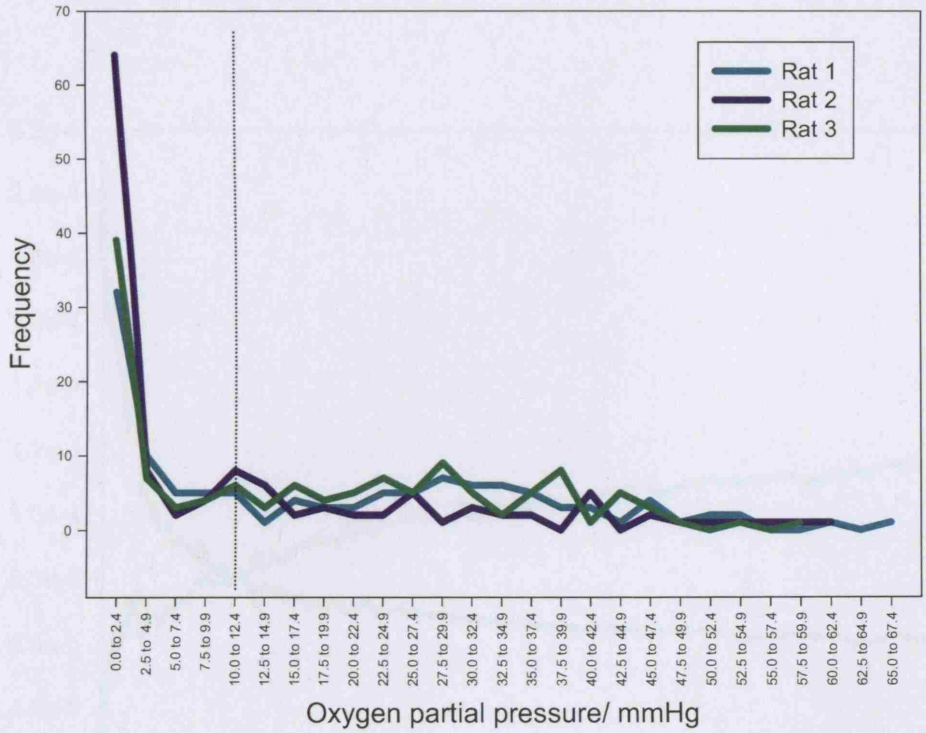

Figure 3.2 *Eppendorf probe measurements of P22 carcinosarcoma tumour oxygenation in the BD-9 rat. Dotted line represents level of pO_2 (10mmHg) below which effects of tumour hypoxia are seen clinically.*

3.4.2 Tracer uptake dynamics

The time-activity curves generated from the tumour and background ROIs demonstrated rapid tracer uptake by the tumour reaching a plateau during the latter stages of scanning (figure 3.3). Background tracer uptake was initially high however it fell to below tumour levels at approximately 20 minutes, and continued to fall thereafter. The tumour to background ratio was calculated to be a mean of 2.1 (range 1.6 to 3.1) 60 minutes after tracer injection. This ratio increased to a mean of 2.7 (range1.8 to 3.5) at the end of scanning. This experiment confirmed that ^{64}Cu-ATSM is tumour avid capable of producing tumour images (figure 3.4).

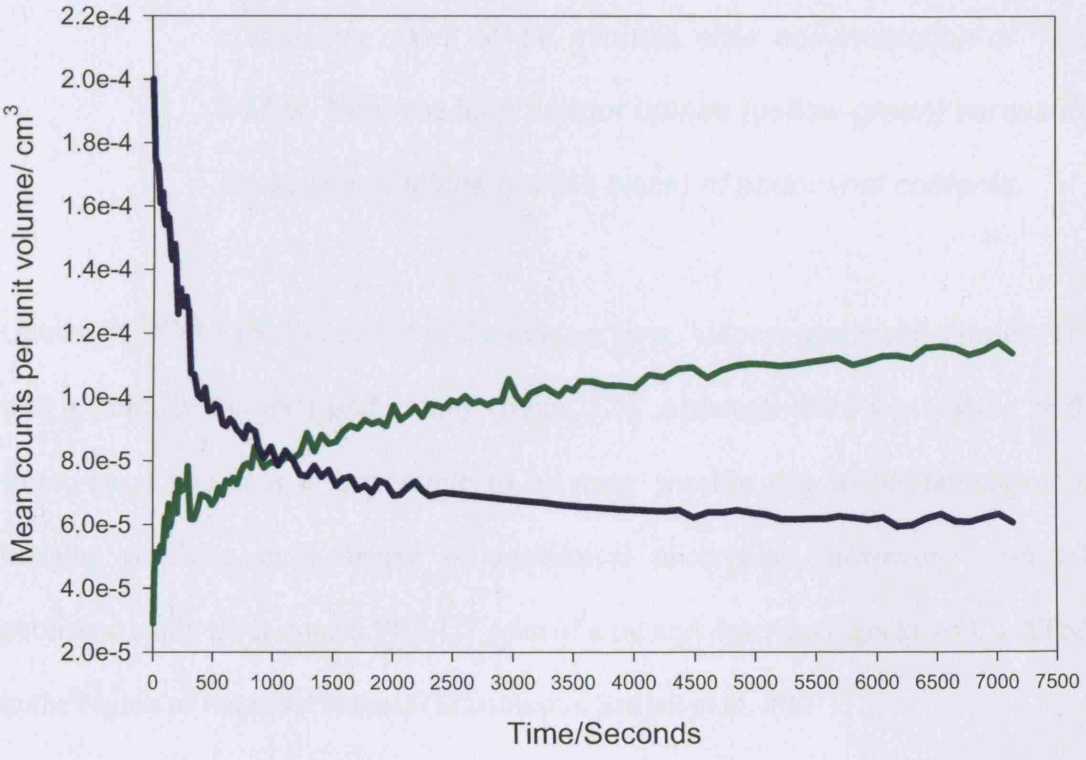

Figure 3.3 *Time-activity curve showing tumour (green) and background (blue) uptake of ^{64}Cu-ATSM (16.0 MBq)*

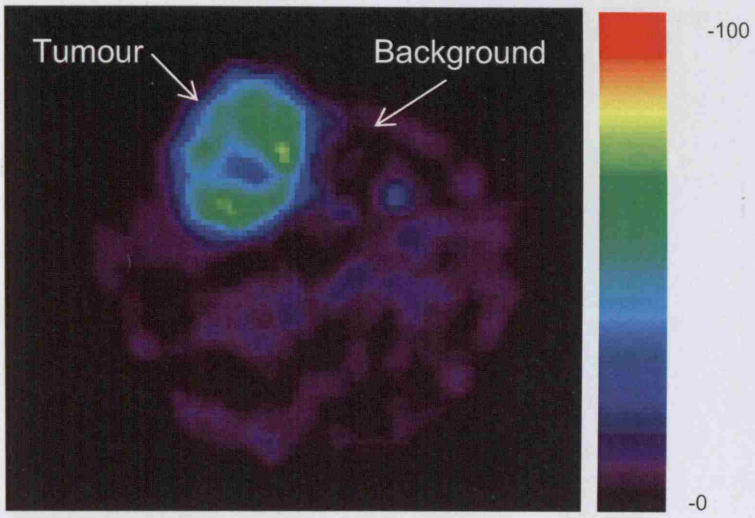

Figure 3.4 *A ^{64}Cu-ATSM PET image of a tumour bearing rat. 16.0 MBq of ^{64}Cu-ATSM was administered. This is the axial cross-section taken at the mid-point of the tumour and represents the cumulative count 50-60 minutes after administration of ^{64}Cu-ATSM. Note the high tumour uptake (yellow-green) versus the background uptake (purple-black) of abdominal contents.*

Uptake of ^{64}Cu-ATSM occurred in the tumour, liver, kidneys and facial sinuses. This was greatest in the liver and kidney (figure 3.5). Although there was uptake in the fronto-nasal region it is impossible to be more specific due to limitations of the imaging resulting in a degree of anatomical uncertainty, however, a recently published study performed a PET-CT scan of a rat and described uptake of Cu-ATSM in the region of the nasal sinuses (Matsumoto, Szajek et al. 2007).

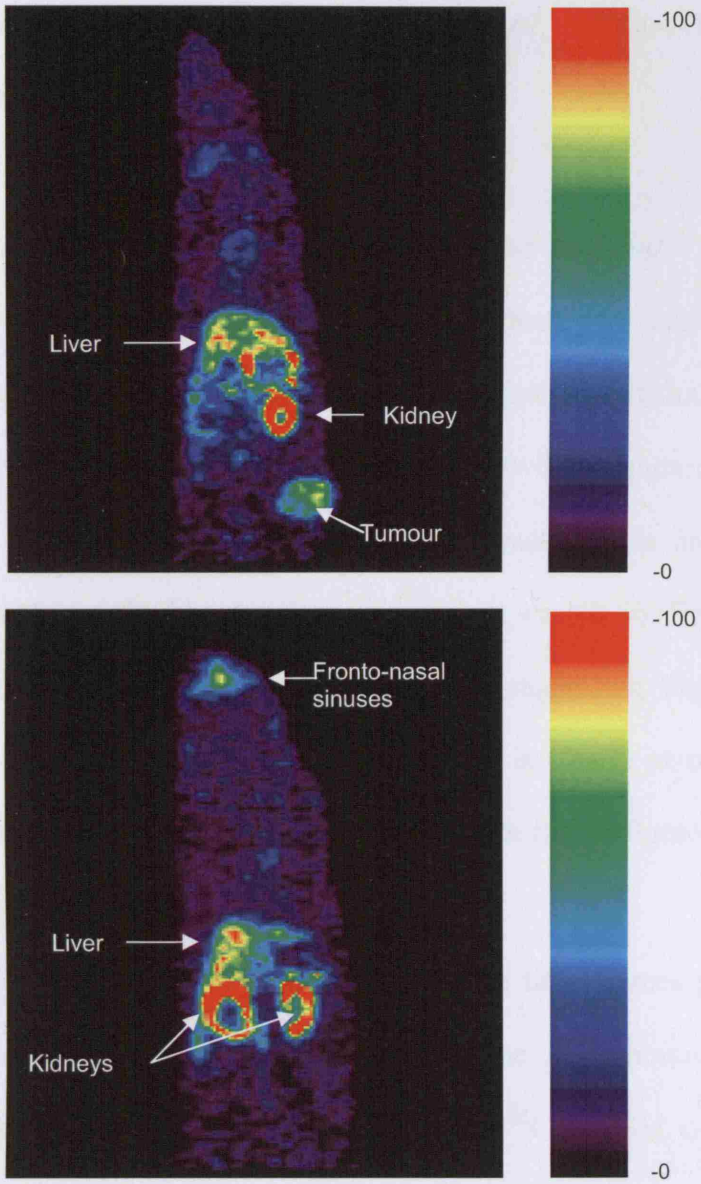

Figure 3.5 *Whole body ^{64}Cu-ATSM PET images of a tumour-bearing rat taken at different levels coronally to show distribution of the tracer in our tumour model. These images were generated from 3 separate images stitched together. Imaging of the head and neck region took place 0-20 minutes after injection of ^{64}Cu-ATSM, imaging of the thorax took place 20-40 minutes after tracer injection and imaging of the abdomino-pelvic region 40-60 minutes after tracer injection.*

3.4.3 Comparison of tumour uptake of ^{64}Cu-ATSM with immunohistochemical markers of hypoxia

3.4.3.1 Comparison of tumour SUV with pimonidazole staining

Sixteen datasets were used to compare the mean SUV of the central axial tumour slice with the pimonidazole-derived hypoxic fraction of the same slice. Combining the 16 datasets the overall mean tumour SUV at 1 hour was 2.19 with a standard deviation of 0.56 (figure 3.6). The overall mean tumour hypoxic fraction was 68.53% with a standard deviation of 14.64%. The correlation coefficient was –0.56 (figure 3.7) with a statistically significant two-sided p-value of 0.0237, suggesting that with larger hypoxic fractions have less ^{64}Cu-ATSM uptake, which is clearly at odds with the original proposition that ^{64}Cu-ATSM is retained in hypoxic tissue (figure 3.8).

The mean tumour SUVs generated from the 10-minute time frames progressively increased from the 0-10 minute time frame (1.293) to the 50-60 minute time frame (2.73) representing increased uptake and retention of ^{64}Cu-ATSM over the time course measured. Pearson's correlation was used to determine the correlation coefficient between hypoxic fraction and tumour SUV for each time frame. Again the correlation coefficients were negative for each of the time frames, each being statistically significant (table 3.1). This effect diminished somewhat over the 60-minute time course measured, however, remained significant.

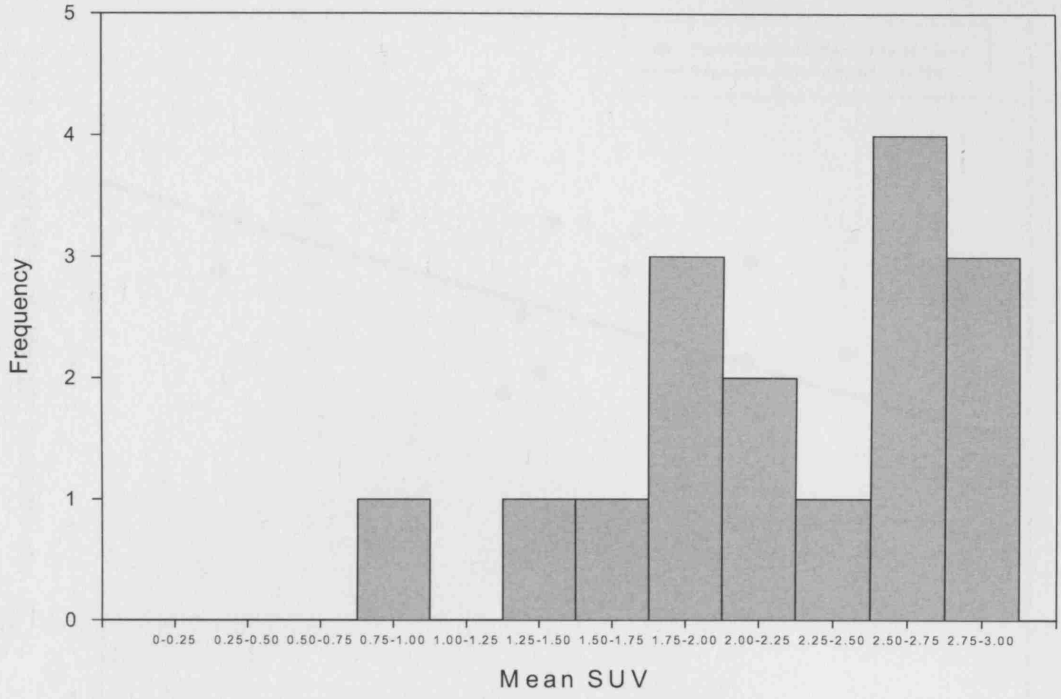

Figure 3.6 *Histogram of individual mean tumour SUV summed from the 0-60 minute PET data acquisition (n=16)*

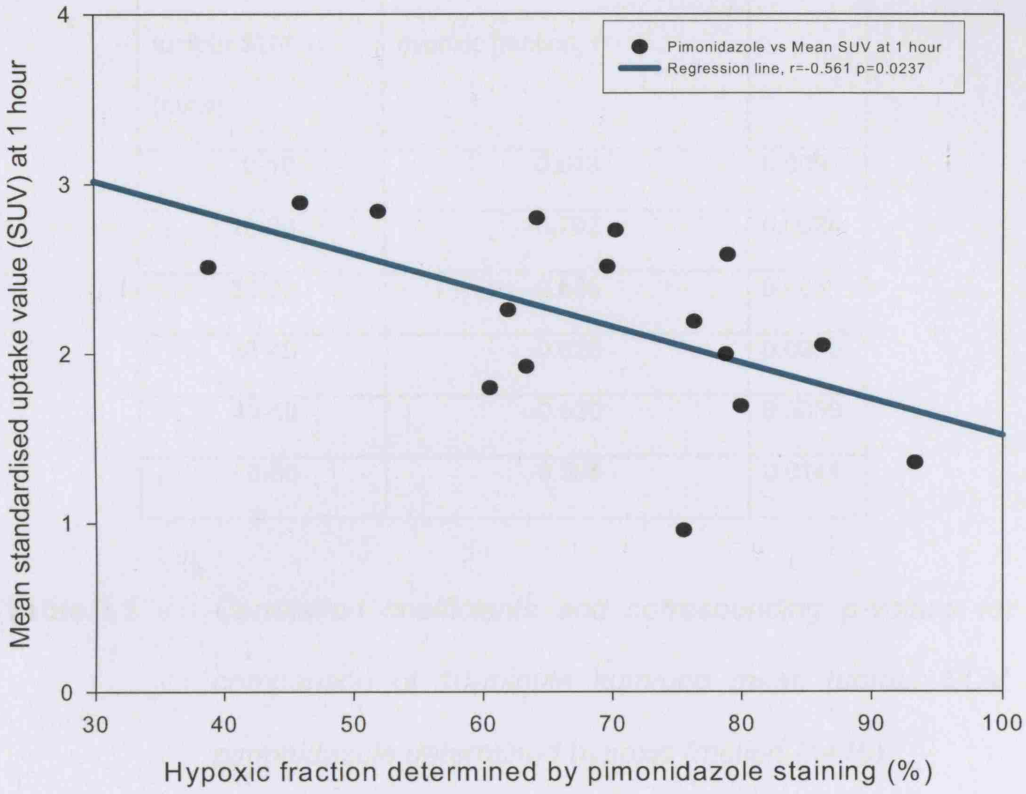

Figure 3.7 *Mean tumour SUV at 1 hour versus pimonidazole determined hypoxic fraction (n=16)*

Time frame for tumour SUV (mins)	Correlation coefficient with hypoxic fraction, r	P-value
0-10	-0.648	0.009
10-20	-0.702	0.0024
20-30	-0.636	0.008
30-40	-0.626	0.0095
40-50	-0.630	0.0089
50-60	-0.599	0.0141

Table 3.1 *Correlation coefficients and corresponding p-values for the comparison of 10-minute summed mean tumour SUV and pimonidazole determined hypoxic fraction (n=16).*

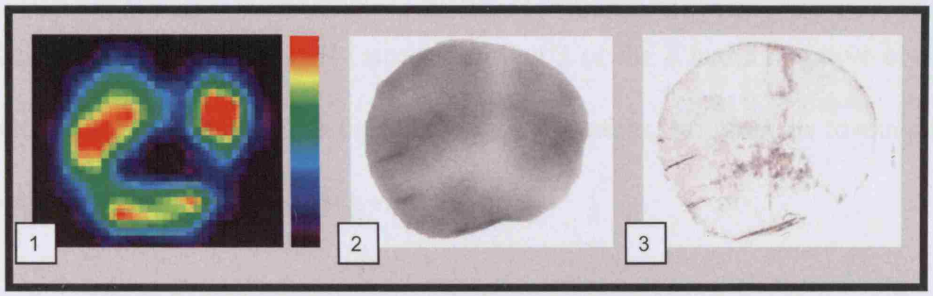

Figure 3.8 *Images of tumour section. Image (1) is the ^{64}Cu-ATSM microPET image. Uptake shown using a rainbow scale where red represents high uptake and black no uptake. Image (2) is the autoradiography image of the same tumour through the same plane and orientation. The darker areas represent greater uptake of ^{64}Cu-ATSM. Image (3) is the separated pimonidazole reference section showing regions of pimonidazole uptake only. Note the similarity of images (1) and (2) with an opposite distribution of pimonidazole seen in image (3).*

3.4.3.2 Pixel-by pixel comparison of ^{64}Cu-ATSM and pimonidazole distribution

There was a total of eleven paired datasets of sufficient quality for analysis with a minimum of one dataset from each of the seven rats. There were between 200 to 1800 points on each scattergram (figure 3.9). Of these 8 had a negative correlation value and 3 had a positive value (range 0.338 - -0.484). Seven of the eight negative correlations were statistically significant however, 4/7 had correlation coefficients less that –0.1 suggesting a weak albeit significant relationship. All 3 positive correlations were statistically significant, however again 2/3 had low values less than

0.11 (table 3.2). When 2 paired datasets were available for an animal the correlation coefficients were not necessarily similar, in fact 3 of the 4 had a negative correlation for one dataset and a positive correlation for the other, bringing in to question the importance of the results showing significance.

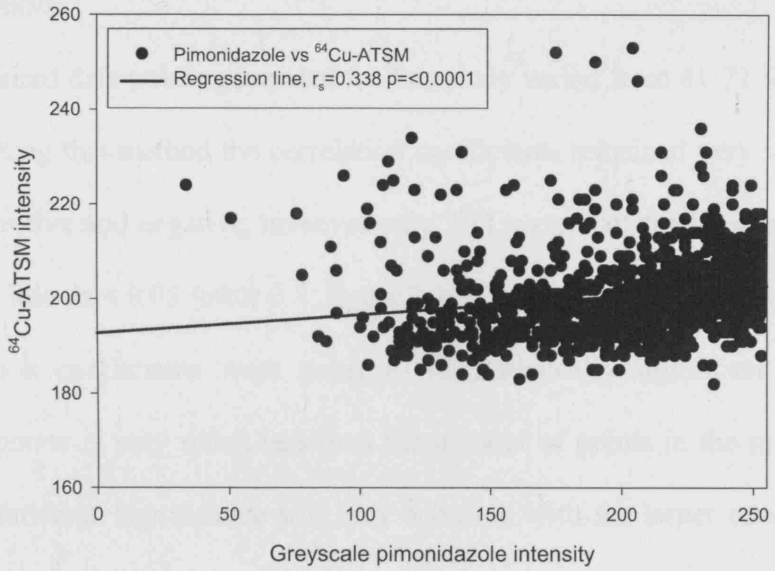

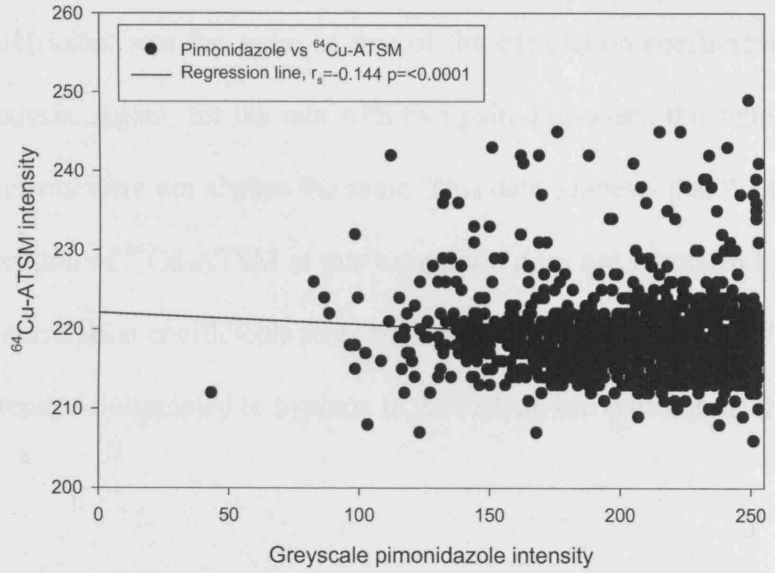

Figure 3.9 *Two examples of scattergrams comparing ^{64}Cu-ATSM intensity with greyscale pimonidazole intensity per pixel. The uppermost scattergram shows a positive correlation whereas the lowermost scattergram shows a negative correlation.*

3.4.3.3 *Grid comparison of ^{64}Cu-ATSM autoradiography with pimonidazole distribution*

The number of paired data points generated for this study varied from 41-71 for each paired dataset. Using this method the correlation coefficients remained very variable and were both positive and negative, however only 3/11 were statistically significant with a p-value of less than 0.05 (table 3.2, figure 3.10). It was less likely that the grid analysis correlation coefficients were going to be statistically significant as the number of data points is very much less than the number of points in the pixel-by-pixel analysis. Statistical significance was only achieved with the larger correlation coefficients. Two of the three correlation coefficients were significantly negative whereas one was significantly positive correlation. For each of these three the sign of the correlation coefficient was the same as that of the correlation coefficient in the pixel-by-pixel analysis. Again, for the rats with two paired datasets, the signs of the correlation coefficients were not always the same. This data suggests that the process of uptake and retention of ^{64}Cu-ATSM at this time-point does not represent hypoxia. The fact that the correlation coefficients were both positive and negative would point to a process of retention that related to hypoxia in, at best, an inconsistent manner.

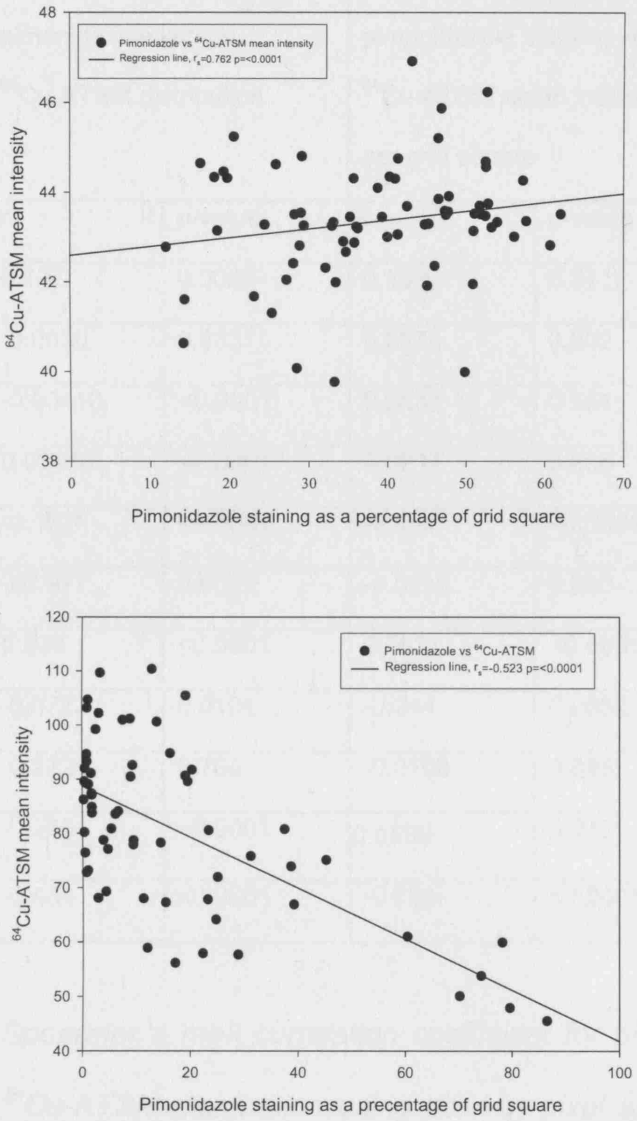

Figure 3.10 *Two examples of scattergrams comparing ^{64}Cu-ATSM mean intensity per grid square with pimonidazole staining as a percentage of grid square. Note the different intensity scales for the two graphs.*

	Pixel by pixel correlation of pimonidazole versus ^{64}Cu-ATSM distribution		Correlation of percentage pimonidazole staining versus ^{64}Cu-ATSM mean intensity per grid square	
	r	p-value	r	p-value
Rat 1	0.107	0.0003	0.139	0.341
	-0.0630	0.0331	0.0978	0.502
Rat 2	-0.00410	<0.0001	0.0833	0.564
	0.00100	<0.0001	0.0217	0.895
Rat 3	-0.182	<0.0001	-0.582	<0.0001
Rat 4	-0.0977	0.0022	-0.0256	0.880
Rat 5	0.338	<0.0001	0.762	<0.0001
	-0.0722	0.0101	-0.244	0.0652
Rat 6	-0.0224	0.764	-0.0198	0.885
	-0.235	<0.0001	0.0108	0.939
Rat 7	-0.484	<0.0001	-0.523	<0.0001

Table 3.2 *Spearman's rank correlation coefficient for pimonidazole and ^{64}Cu-ATSM distribution using pixel-by-pixel analysis and grid analysis.*

3.4.3.4 ^{64}Cu-ATSM uptake measured at a later time-point and its comparison with pimonidazole distribution

Autoradiography from all five tumour specimens was relatively homogeneous. The rare instance of some heterogeneity was on the background of very homogeneous high uptake, suggesting this heterogeneity was a result of artefact from the tissue mounting process as this was only seen in the sections that had been rapidly frozen.

Despite this homogeneity of uptake, pimonidazole distribution was heterogeneous with a mean area of staining of 54.01% (figure 3.11).

Figure 3.11 *Autoradiography image (1) 20 hours after administration of ^{64}Cu-ATSM showing a homogeneous distribution, compared with the pimonidazole separated reference image (2).*

The two tumours that were possible to compare in order to obtain a correlation coefficient were inconsistent in their results (table 3.3). For the pixel-by-pixel analysis there was a significant correlation for all four tumour sections. This was negative in sign for rat 1 and positive for rat 2, although all correlation coefficients were less than +/- 0.15 suggesting only a weak relationship. The sign of the correlation coefficients was the same for the grid analysis, however only the higher values were statistically significant, although this was to be expected due to the fact there were fewer points in the analysis.

	Pixel by pixel correlation of pimonidazole versus ^{64}Cu-ATSM distribution		Correlation of percentage pimonidazole staining versus ^{64}Cu-ATSM mean intensity per grid square	
	r	p-value	r	p-value
Rat 1	-0.144	<0.0001	-0.343	0.0087
	-0.0666	0.0339	-0.0986	0.469
Rat 2	0.116	0.0003	0.204	0.0882
	0.102	0.003	0.341	0.0112

Table 3.3 *Spearman's rank correlation coefficient for pimonidazole and ^{64}Cu-ATSM distribution approximately 20 hours after ^{64}Cu-ATSM administration using pixel-by-pixel analysis and grid analysis.*

3.4.4 Dynamic contrast-enhanced MRI

3.4.4.1 Comparison of Gadolinium AUC90 with mean tumour SUV at 1 hour

Fourteen tumour-bearing rats were used for this analysis. Pearson's correlation coefficient for mean AUC90 versus mean tumour SUV over one hour was 0.376 (p-value 0.145). The relationship between tumour blood flow and cumulative ^{64}Cu-ATSM uptake over the course of one hour is not statistically significant (see figure 3.12).

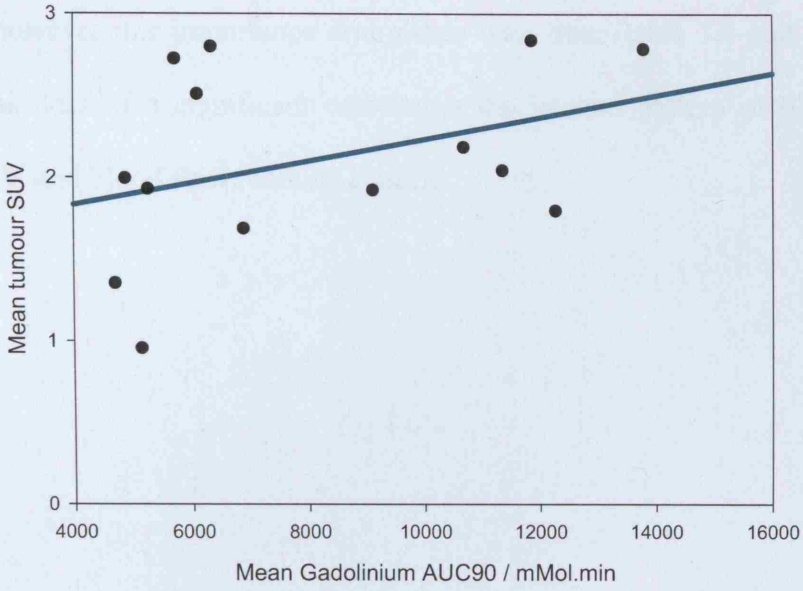

Figure 3.12 *Plot to evaluate the relationship between mean tumour SUV and AUC90 which is not statistically significant. The regression line is green (n=14).*

3.4.4.2 Comparison of Gadolinium AUC90 with mean tumour SUV in control animals from 10-minute time frames over the course of one hour

The mean tumour SUV of the central axial tumour slice was generated for each ten-minute time frame from 0 to 60 minutes for comparison with Gadolinium AUC90. This was performed to evaluate the effect of blood flow on uptake and retention of ^{64}Cu-ATSM at different times following its injection. The SUV for each time frame was plotted against AUC90 of the same slice and a correlation coefficient calculated. Pearson's correlation coefficient was generated which showed a statistically significant correlation for the 0 to 10 minute (0.580, p-value 0.0296) and 10 to 20 minute (0.566, p-value 0.0351) time frames (figure 3.13). After this time point the correlation coefficient diminished progressively indicating that blood flow is an

important determinant of ^{64}Cu-ATSM uptake and retention in the early phase after injection however this importance diminishes with time (table 3.4 and figure 3.14). Despite this loss of a significant correlation the general pattern of distribution of ^{64}Cu-ATSM and blood flow remained similar.

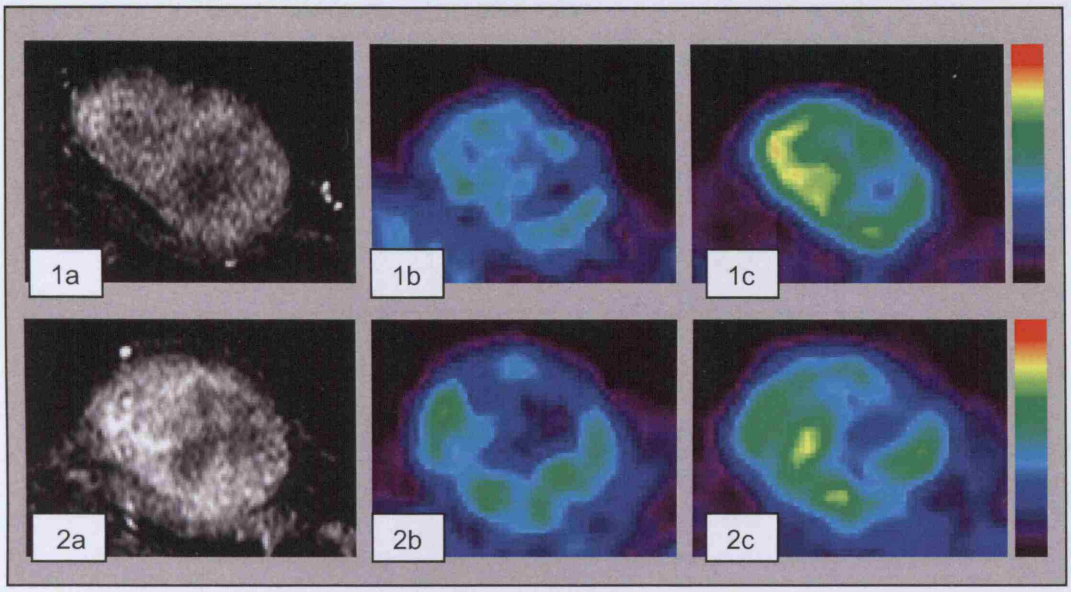

Figure 3.13 *Corresponding Gadolinium-enhanced MRI and microPET images. Images sets 1 and 2 represent two different control tumours. Image 1a and 2a are Gadolinium-enhanced images 90 seconds from the beginning of the Gadolinium infusion. The bright regions represent Gadolinium uptake, therefore blood flow. Images 1b and 2b are 0-10 minute microPET acquisitions and images 1c and 2c are 50-60 minute acquisitions. The ^{64}Cu-ATSM uptake in the 0-10 minute images was significantly similar to the Gadolinium uptake. Although the uptake of ^{64}Cu-ATSM in the 50-60 minute PET images was not significantly correlated the distribution looks similar to the distribution of Gadolinium even at this late stage.*

Time frames post-injection of ^{64}Cu-ATSM from which SUV is determined	Correlation coefficients between AUC90 and SUV in non-CA4P treated rats	
	Correlation coefficient, r	p-value
0-10 minutes	0.580	0.0296
10-20 minutes	0.566	0.0351
20-30 minutes	0.518	0.0576
30-40 minutes	0.459	0.0987
40-50 minutes	0.451	0.106
50-60 minutes	0.411	0.145

Table 3.4 *Pearson's correlation coefficients between AUC90 and mean tumour SUV from the 10-minute time frames reconstructed after microPET data acquisition. The correlation coefficients diminish with time and become less significant.*

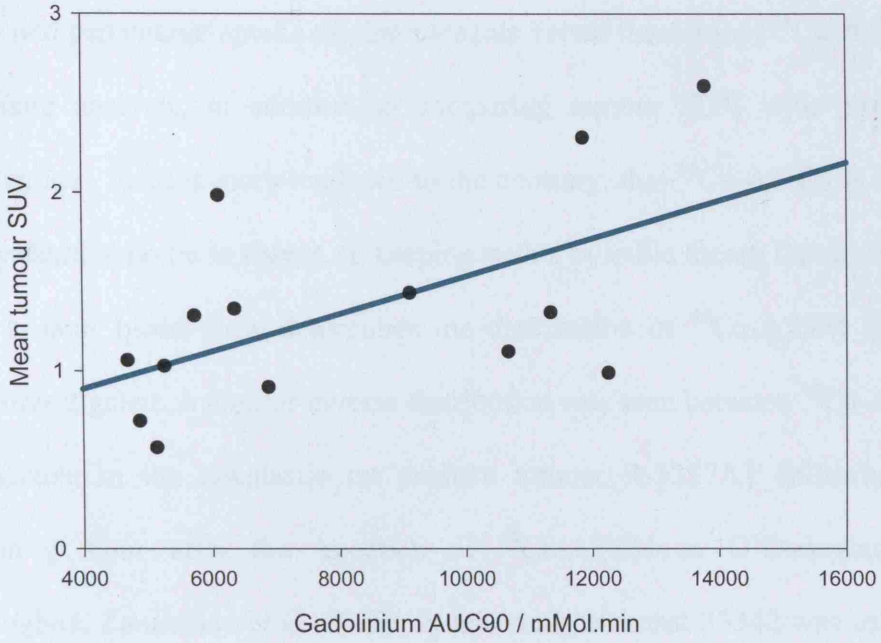

Figure 3.14 *Plot to evaluate the relationship between mean tumour SUV for an acquistion from 0 to 10 minutes post-injection of ^{64}Cu-ATSM and AUC90. The correlation coefficient is 0.580 which is statistically significant (0.0296). The regression line is green (n=14).*

3.5 Discussion

In the P22 carcinosarcoma tumour model ^{64}Cu-ATSM is undoubtedly tumour avid as the images show. However, whether or not this tumour avidity is as a result of tumour hypoxia is in question. In comparing the distribution of ^{64}Cu-ATSM using autoradiography with the well-validated immunohistochemical marker of hypoxia, pimonidazole, there is no convincing evidence to suggest the two co-segregate. This

has been investigated using both intensity of tumour uptake in the pixel-by-pixel analysis and percentage uptake of pimonidazole versus intensity of ^{64}Cu-ATSM in the grid square analysis, in addition to comparing tumour SUV with pimonidazole uptake. In fact, there is more evidence to the contrary, that ^{64}Cu-ATSM is retained in regions where hypoxia is absent, in keeping with a possible theory that in this tumour model, tumour blood flow determines the distribution of ^{64}Cu-ATSM in the time frames investigated. A similar inverse distribution was seen between ^{64}Cu-ATSM and pimonidazole in the anaplastic rat prostate tumour R-3327AT following tumour resection 1 hour after the injection of ^{64}Cu-ATSM in O'Donoghue's paper (O'Donoghue, Zanzonico et al. 2005). In this study Hoechst 33342 was used to look for tumour perfusion, however a correlation with ^{64}Cu-ATSM was not confirmed. The group went on to look at ^{64}Cu-ATSM distribution and its relationship with pimonidazole 24 hours following injection and found a correlation, however our study did not produce such results. In our study the autoradiography images of tumour exposed to ^{64}Cu-ATSM for a mean time of 20.5 hours were very homogeneous. There is as yet very little data that details the compositional integrity of ^{64}Cu-ATSM in vivo over this lengthy time period and a concern is that the copper may dissociate from the bis(thiosemicarbazone) structure with time. If this were the case autoradiography would be a mixture of the biodistributions of $CuCl_2$ and ^{64}Cu-ATSM which would likely be a homogenous distribution with no discernable functional specificity much like the images we obtained.

A further point is that the tumours evaluated were not exposed to pimonidazole and ^{64}Cu-ATSM for the same periods of time. Pimonidazole was injected 4 hours prior to tumour resection whereas ^{64}Cu-ATSM was administered at most 1.25 hours prior to

this, which may have introduced a discrepancy in the results obtained. In the tumour model used, pimonidazole needed a minimum of 4 hours viable tumour exposure for adequate staining to occur. The administration of pimonidazole closer to the time of resection would have resulted in poorly stained specimens in which the ability to discriminate between genuine cellular uptake and background would have been inadequate, therefore compromising the detection of the true distribution of cellular hypoxia. The administration of ^{64}Cu-ATSM at a later time-point was not thought to represent a problem as one of the earlier propositions about this hypoxic marker was its rapid uptake and distribution (Lewis 1999) thought to occur within our imaging time-frame. As both these markers were given at times that allowed them to distribute throughout the tumour in a manner representative of their proposed hypoxia-specific cellular retention patterns the different times of administration was thought to be unimportant and as such the distributions of both markers suitable for comparison.

Using DCE-MRI to evaluate the impact of blood flow on ^{64}Cu-ATSM uptake and retention it was demonstrated that uptake and retention of ^{64}Cu-ATSM in control animals within twenty minutes of its administration is similar to uptake of Gadolinium in regions of blood flow. After twenty minutes the statistically significant correlation between the two diminishes progressively over the course of the one-hour studied. This early similarity of tracer distribution to blood flow is not surprising as ^{64}Cu-ATSM is dependent on its delivery to the tumour via functioning vasculature. However, although a correlation was seen between blood flow and tumour SUV this was not absolute. In the high blood flow tumours where Gadolinium AUC90 was twice that of other tumours, the same factor increase in tumour SUV was not seen, indicating that there was not a one to one relationship between tumour blood flow and

^{64}Cu-ATSM and that even in the early phase of ^{64}Cu-ATSM uptake, which is strongly influenced by tumour blood flow, tumour uptake of ^{64}Cu-ATSM was not dependent on blood flow alone. The association between tumour blood flow and ^{64}Cu-ATSM uptake diminished with time as the dominant effect of blood flow is lost to the effects of intrinsic cellular handling in determining the ultimate tumour distribution of ^{64}Cu-ATSM. Despite the loss of a significant correlation between ^{64}Cu-ATSM and tumour blood flow after 20 minutes the general distribution of tracer remained similar to the distribution of blood flow seen with Gadolinium. As a result of these findings one would certainly recommend imaging of this tracer after 20 minutes if one wishes to see something different to blood flow, however longer periods may be required as the similarity between ^{64}Cu-ATSM and Gadolinium can clearly be seen for up to one hour following tracer administration. The application of a blood flow correction to the data may ultimately be required to generate distributions that are more representative of hypoxia, however evaluating this was beyond the scope of this current study.

The association described between ^{64}Cu-ATSM with tumour blood flow may explain the results described in this chapter in which ^{64}Cu-ATSM failed to segregate to areas of tumour hypoxia identified with pimonidazole staining an hour following administration of the tracer. In this tumour model it may take longer than one hour before the dominance of tumour blood flow in determining the distribution of ^{64}Cu-ATSM is lost. However, imaging at later time points negates one of the original benefits of imaging with this agent, and that was its proposed rapidity of delineating tumour hypoxia versus the slower time course of the alternative hypoxia imaging agent, ^{18}F-MISO (Lewis JL 1999). In addition, although we know that pimonidazole is retained in cells with a pO_2 of <10mmHg, the pO_2 at which ^{64}Cu-ATSM is retained

in cells is as yet unknown and may be different, generating a different pattern of uptake and retention from pimonidazole. This difference alone may explain some of the discrepancies seen between pimonidazole uptake and ^{64}Cu-ATSM uptake.

In summary, the study performed has not shown that ^{64}Cu-ATSM can be used as a marker of tumour hypoxia in this tumour model under the conditions set out. In the next chapter I will describe the effect of enhancing tumour hypoxia and its impact on ^{64}Cu-ATSM retention and blood flow.

References

Lewis JL, McCarthy D, McCarthy TJ, Fujibayashi Y, Welch MJ (1999). "Evaluation of ^{64}Cu-ATSM in vitro and in vivo in a hypoxic tumour model." J Nuc Med(40): 177-183.

Lewis JS, Herrero P, Sharp TL, Engelbacj JA, Fujibayashi Y, Laforest R, Kovacs A, Gropler RJ, Welch MJ. (2002). "Delineation of hypoxia in canine myocardium using PET and copper(II)-diacetyl-bis(N(4)-methylthiosemicarbazone)." J Nucl Med 43(11): 1557-69.

Lewis JS, Sharp TL, Laforest R, Fujibayashi Y, Welch MJ. (2001). "Tumor uptake of copper-diacetyl-bis(N(4)-methylthiosemicarbazone): effect of changes in tissue oxygenation." J Nucl Med 42(4): 655-61.

Matsumoto K,Szajek L Krishna MC, Cook JA, Seidel J, Grimes K, Carson J, Sowers AL, English S, Green MV, Bacharach SL, Eckelman WC, Mitchell JB. (2007). "The influence of tumor oxygenation on hypoxia imaging in murine squamous cell carcinoma using [64Cu]Cu-ATSM or [18F]Fluoromisonidazole positron emission tomography." Int J Oncol 30(4): 873-81.

O'Donoghue JA, Zanzonico P, Pugachev A, Wen B, Smith-Jones P, Cai S, Burnazi E, Finn RD, Burgman P, Ruan S, Lewis JS, Welch MJ, Ling CC, Humm JL. (2005). "Assessment of regional tumor hypoxia using 18F-fluoromisonidazole and 64Cu(II)-diacetyl-bis(N4-methylthiosemicarbazone) positron emission tomography: Comparative study featuring microPET imaging, Po2 probe measurement, autoradiography, and fluorescent microscopy in the R3327-AT and FaDu rat tumor models." Int J Radiat Oncol Biol Phys 61(5): 1493-502.

CHAPTER 4

Effect of combretastatin in enhancing tumour hypoxia on uptake of ^{64}Cu–ATSM

4.1 Combretastatin A4 phosphate

Modification of tumour oxygenation using the vascular disrupting agent combretatastatin A4 phosphate (CA4P) was performed in this tumour model in an attempt to evaluate the impact of a reduction in tumour oxygenation on uptake and retention of ^{64}Cu-ATSM. Combretastatin A4 (CA4) is a vascular targeting agent that was originally derived from the Cape Bushwillow tree *Combretum Caffrum* (Pettit 1987). This drug targets existing tumour vasculature resulting in rapid vascular shutdown and secondary tumour cell death.

CA4 has limited solubility in water unlike its sodium phosphate derivate, CA4P, which is the form of the drug currently used in clinical trials (Pettit 1995). CA4P is a pro-drug from which the phosphate group is cleaved under physiological conditions by non-specific phosphatases. CA4 binds to tubulin in the cytoskeleton and results in microtubule depolymerisation and morphological changes in endothelial cells. These changes cause an increase in vascular permeability and disrupt tumour blood flow

which has been demonstrated as early as 5 minutes following its administration with almost complete vascular shutdown in animal models at 20 minutes (Dark 1997; Beauregard 1998; Tozer 2001). The collapse of tumour blood flow is likely to occur as the result of morphological and functional changes of the endothelial cytoskeleton that cause the cell to change shape by rounding up and in some cases forming surface blebs, focal adhesions, loss of cell-cell junctions and an increased cell mono-layer permeability to macromolecules (Kanthou 2002). This acute increase in vascular permeability reduces plasma oncotic pressure as leakage of plasma proteins occurs causing a rise in interstitial fluid pressure, possibly sufficient to reduce vessel diameter. The loss of fluid may increase plasma viscosity and resistance to blood flow further. In addition, as blood flow slows down the red cells will arrange themselves in a rouleaux formation increasing viscous resistance (Milosevic 1999). A direct vasoconstrictor effect on arterioles has also been observed for CA4P which also reduces blood flow (Dark 1997; Tozer 1999).

In murine tumours the antivascular effects of CA4P are observed at a dose substantially less than the maximum tolerated dose (MTD) suggesting a safe therapeutic window. Following administration of the drug at $1/10^{th}$ the MTD a reduction in tumour blood flow of 93% was measured 6 hours following administration of drug. In the P22 rat tumour model a study showed that blood flow to the tumour decreased to near undetectable levels 6 hours after a single intraperitoneal injection of 100mg/kg CA4P, whereas the flow to normal tissues was much less affected (Tozer 1999). An additional study showed a significant increase in tumour hypoxic fraction 1 hour after administration of the drug in to mice bearing the mouse mammary carcinoma (Horsman 1998).

CA4P produces a much greater blood flow reduction in tumours than normal tissues (Tozer 1999). This tumour specificity is thought to reflect a difference between endothelial cells in tumours which are proliferating and fragile and normal tissue endothelial cells and their differing response to CA4P as a result of their microenvironments. In an animal model CA4P reduced tumour blood flow 100-fold compared with 7-fold in the spleen, the most sensitive tissue of those studied, no significant reduction was seen in the heart, kidney and small intestine (Tozer 1999).

An interesting feature of CA4P is that although profound anti-vascular effects occur within the centre of the tumour, the tumour rim is relatively spared. One explanation for this is that tumour cells in this region survive because they receive nutrients from non-tumour vasculature in the surrounding normal tissue. In addition, interstitial fluid pressure compounding vascular shutdown is likely to be less at the periphery than the centre of the tumour and small-calibre blood vessels found more frequently in the tumour centre are more likely to collapse than peripheral larger ones (Tozer 2005).

CA4P has direct toxic effects on proliferating endothelial cells (Dark 1997) and tumour cells (Boehle 2001). It is thought to cause spindle malformation in proliferating cells in mitosis leading to cell cycle arrest at the G2/M phase of the cell cycle and subsequent apoptosis. The effect of CA4P on endothelial cells in vitro is thought to be a lengthy process with apoptotic changes appearing at 2-4 hours after exposure to drug and reaching significance at 8 hours (Kanthou 2004). Considering the plasma half-life of CA4 in the rat (0.86 hours) it is unlikely this effect is relevant

and is likely to be of secondary importance unlike its effects on blood flow dynamics which occur within minutes of administration.

In the P22 rat tumour model a number of previous studies have looked at the impact of CA4P dose on temporal tumour vascular changes. Absolute tumour blood flow was measured using the freely diffusible tracer ^{125}I-iodoantipyrine in the P22 rat tumour model following CA4P administration at doses of 10mg/kg and 100mg/kg (Maxwell 2002). This study showed a greater than 8-fold reduction in tumour blood flow at 6h with a dose of 10mg/kg and a greater than 35-fold reduction at the same time in the animals treated with 100mg/kg. Tumour blood flow returned to control values at 24 hours in the animals treated with a dose of 10mg/kg, however no recovery was seen in those treated with 100mg/kg at 24 hours. In the same study a similar change in blood flow was measured by DCE-MRI using the parameters K^{trans} (a measure of blood flow rate and vascular permeability) and AUC from 0-94 seconds. In order to determine K^{trans} knowledge of the arterial input function is required. This would not have been possible in our study therefore AUC was chosen as a measure of tumour blood flow as this was readily measureable with no pre-requisites. In the study by Maxwell et al, although the magnitude of changes in AUC and K^{trans} values were less than the absolute measurement of blood flow the time-course and dose dependency was similar, in addition there was a strong correlation ($r=0.98$, $p<0.0001$) between absolute tumour blood flow and K^{trans}, suggesting these parameters can be used as a non-invasive indicator of tumour blood flow changes.

Tozer et al found that a CA4P dose of 100mg/kg reduced tumour blood flow to near undetectable at 6 hours with extensive tumour necrosis seen at 24 hours in the P22 rat tumour (Tozer 1999). In the same tumour model doses of 30mg/kg and 10mg/kg were

compared (Prise 2002). Tumour blood flow decreased to below 15% of the untreated control at 1 hour at both doses with a further drop at 6 hours to 2% of the control in the 30mg/kg dose arm. Vessel distension, coagulation and haemorrhage were seen histologically 1h and 6h after CA4P administration with necrosis appearing at 24 hours although this was less than that seen in the rats treated with 100mg/kg. Tumour blood flow recovery was complete at 24 hours for both doses.

As a result of previous studies CA4P at a dose of 10mg/kg was chosen to modulate oxygen delivery to the P22 rat tumour model. This dose was chosen to generate central tumour hypoxia but avoid the more extensive vascular disruption that would have been seen in higher doses. The effect of CA4P on the P22 rat tumour model has been studied extensively in this institute and the impact of CA4P on tumour blood flow assessed by DCE-MRI. In addition there is evidence to suggest that CA4P induces hypoxia in murine tumours (Horsman 1998). As such we used this agent to enhance tumour hypoxia in order to evaluate the impact of this on tumour uptake and retention of ^{64}Cu-ATSM and how this relates to tumour blood flow using DCE-MRI.

For this study the tumour sections were stained for GLUT-1 in addition to pimonidazole, due to concerns that the vascular disruption caused by CA4P may hinder the delivery of the extrinsic hypoxia marker pimonidazole. GLUT-1 was used because it is an intrinsic cellular marker thought to reflect tumour hypoxia (section 1.6.3.1) as such it was used as an additional marker to compare tumour hypoxia with ^{64}Cu-ATSM uptake, in the event that pimonidazole administered after CA4P did not represent true hypoxia.

4.2 Aims

For this study the effect of CA4P on tumour pO_2 was measured with an Eppendorf probe and immunohistochemical markers of hypoxia in the P22 rat tumour model. In addition, analysis of the distribution of ^{64}Cu-ATSM was compared with immunohistochemical hypoxia markers in order to evaluate the effect of increased hypoxia on tumour ^{64}Cu-ATSM distribution. The impact of tumour blood flow on the distribution of ^{64}Cu-ATSM following CA4P was evaluated using DCE-MRI.

4.3 Materials and methods

4.3.1 Eppendorf probe measurement of tumour pO_2 in animals treated with CA4P

This experiment was carried out to evaluate the degree of hypoxia in the P22 rodent tumour model following treatment with CA4P versus untreated control animals.

4.3.1.1 Experimental models

Six tumour bearing rats were chosen for this procedure. P22 tumour implantation was carried out as described in section 2.3.2. CA4P (10mg/kg i.p) was administered to each rat two hours prior to Eppendorf probe measurement of tumour oxygenation. Anaesthesia was administered as described in section 2.3.3. Following completion of the experiment the animals were sacrificed using cervical dislocation.

4.3.1.2 Experimental practise

Eppendorf probe measurement of tumour oxygenation is described in section 2.6. The median difference in tumour pO_2 values for the two different groups was compared using the Mann-Whitney U test.

4.3.2 Immunohistochemical determination of hypoxia in rats pre-treated with CA4P versus control

Immunohistochemical detection of tumour hypoxic fraction was determined using pimonidazole and GLUT-1 in animals pre-treated with CA4P and controls to assess the effect of CA4P on tumour hypoxic fraction measured immunohistochemically.

4.3.2.1 Experimental models

P22 tumour implantation in to male BD-9 rats was carried out as described in section 2.3.2. Pimonidazole (60mg/kg i.p) was injected in to control rats 4 hours prior to the sacrifice. In the treated rats CA4P (10mg/kg i.p.) was administered 4 hours prior to sacrifice and pimonidazole administered 3 hours prior to sacrifice.

Sacrifice of the animal was achieved with 0.2ml (200mg/ml) of intravenous pentobarbital sodium following which the tumour was resected as explained in section 2.3.3. Histological processing occurred as described in section 2.3.4 followed by staining for pimonidazole and GLUT-1 as described respectively in sections 2.3.6.1 and 2.3.6.2. Each slide was digitised as described in section 2.4.1 and separated reference images obtained in order to determine the percentage staining per tumour cross section (hypoxic fraction) as described in section 2.4.2. Thirty rats were

used as controls for pimonidazole staining and 11 for GLUT-1 staining, 14 rats treated with CA4P had pimonidazole staining and 9 had GLUT-1 staining. A minimum of two sections per tumour were stained for either GLUT-1 or pimonidazole although some slides weren't included in the analysis due to their inferior quality as a result of tears or the section becoming folded. There was a total of 56 pimonidazole and 21 GLUT-1 slides for the control rats, with 33 pimonidazole slides and 21 GLUT-1 slides for the CA4P treated animals.

The Mann-Whitney U test was used for comparing pimonidazole and GLUT-1 uptake in the CA4P-treated versus non-treated groups.

4.3.3 Comparison of mean tumour SUV in animals treated with CA4P versus controls

For this comparison the central axial tumour slice was selected from the microPET images of 16 untreated P22 tumour bearing rats. For each of these a one hour dynamic ^{64}Cu-ATSM PET image was generated with the centre of the field at the mid-point of the tumour (described in sections 2.1.3 and 2.3.3). A mean activity of 31.10MBq of ^{64}Cu-ATSM was administered (range 9.96-55.95MBq). Six animals were treated with CA4P (10mg/kg i.p.) 3 hours prior to sacrifice. For these animals the dynamic PET acquisition began 1.75 hours after administration of CA4P for a duration of 1 hour, followed by a 15 minute transmission scan, after which the animals were sacrificed with pentobarbital sodium i.v. The mean activity administered to these animals was 43.88MBq (range 25.22-58.37MBq). Image reconstruction is described in section 2.1.3. The mean SUV of the central axial slice

was generated from reconstructing the data in to a 1 hour time-frame (section 2.1.5). The SUVs generated from the more hypoxic tumours in the animals treated with CA4P were then compared with the control animals to see if there was a difference in uptake. The Mann-Whitney U test was used to compare SUV in those treated with CA4P versus those untreated.

4.3.4 Comparison of tumour SUV with immunohistochemical staining

One hour dynamic ^{64}Cu-ATSM PET images were obtained of six CA4P-treated tumour bearing rats following tumour implantation 10-14 days previously (for details see section 2.3.2) and the mean SUV of the central axial tumour slice was determined as described in section 4.3.3. The mean dose of ^{64}Cu-ATSM received was 39.05MBq (range 25.22-52.15MBq). CA4P (10mg/kg i.p.) was administered 4 hours prior to sacrifice, with pimonidazole (60mg/kg i.p.) administered one hour later. Pimonidazole and GLUT-1 staining was performed as described in section 4.3.2.1 to determine percentage uptake.

GLUT-1 staining (section 2.3.6.2) of the central axial tumour slice was carried out on 6 P22 tumour bearing rats as described above. MicroPET imaging was carried out in the hour prior to sacrifice and the rats received a mean ^{64}Cu-ATSM dose of 50.59MBq i.v.(range 46.88-58.37MBq) from which the mean SUV of the central axial slice was generated.

Pearson's correlation coefficient was used to determine the relationship between tumour SUV and pimonidazole uptake.

4.3.5 Comparison of immunohistochemical staining with ^{64}Cu-ATSM autoradiography in animals treated with CA4P

In this experiment CA4P was used to make the tumour model more hypoxic. This was performed to further investigate a possible association between ^{64}Cu-ATSM and hypoxia in this tumour model. Our end point in this study was to compare the distribution of ^{64}Cu-ATSM and pimonidazole on a pixel-by-pixel and grid basis to help further ascertain the nature of their relationship. Because there was concern that CA4P may reduce pimonidazole delivery to the tumour the intrinsic hypoxia marker GLUT-1 was also used to identify tumour hypoxia in some sections. Not all pimonidazole - ^{64}Cu-ATSM correlation analyses had corresponding GLUT-1 - ^{64}Cu-ATSM correlation analyses because tumour sections for GLUT-1 staining were used that were adjacent to the pimonidazole stained autoradiography slide. On occasions some of the GLUT-1 stained histology slides did not correspond sufficiently with the autoradiography image and were deemed unsuitable to be included in this analysis.

For this study there were three groups of rats. Each group was administered CA4P, pimonidazole and ^{64}Cu-ATSM in a different order sequentially in order to control for the possibility that CA4P was preventing adequate delivery of ^{64}Cu-ATSM and pimonidazole to the tumour. The first group (group 1) consisted of two rats. These rats received CA4P 4 hours prior to sacrifice (t=-4.0h), followed an hour later by pimonidazole (t=-3.0h) and then ^{64}Cu-ATSM (t=-1.25 hours) at an activity of 52.15MBq and 46.88MBq. Due to concerns that pimonidazole may not get to hypoxic tumour regions if given after CA4P, a second group (group 2) of 5 rats were given pimonidazole first (t=-4.0h), followed by CA4P (t=-3.0h) and subsequently ^{64}Cu-ATSM (t=-1.25h) at a mean activity of 47.96MBq (range 35.305 - 8.37MBq). In the

third group of 3 rats (group 3), both pimonidazole (t=-3.25 hours) and ^{64}Cu-ATSM (t=-3.0 hours) at a mean activity of 49.23MBq (range 47.38-51.33MBq) were given prior to CA4P (t=-2.75 hours) due to concerns that CA4P given beforehand could reduce delivery of both agents to the tumour.

^{64}Cu-ATSM and pimonidazole should only be retained in hypoxic cells therefore the timing of their administration in relation to the CA4P should be irrelevant. However both ^{64}Cu-ATSM and pimonidazole do need to gain access to the potentially hypoxic cell which was the rationale for giving them prior to CA4P.

For these experiments the P22 rat tumour model was prepared as described in section 2.3.2. CA4P (10mg/kg i.p.) and pimonidazole (60mg/kg i.p.) were administered at the times indicated above. Venous cannulation of the tail vein was carried out as described in section 2.3.3 for delivery of ^{64}Cu-ATSM. Following sacrifice of the rat the tumour was resected and with rapid formalin fixation and wax embedding as described in section 2.3.3 and 2.3.4. Four micrometre tumour sections were placed on slides which were then exposed to a storage phosphor screen (GE Healthcare, UK) in order to obtain autoradiography images for comparison with pimonidazole immunohistochemistry of the same slide (see sections 2.3.7 for details of autoradiography and 2.3.6 for details on immunohistochemical staining). The stained slides were digitised (section 2.4.1) and separated references obtained of the pimonidazole staining of these slides (section 2.4.2). Co-registration between the separated reference slide and the corresponding autoradiography image occurred as described in section 2.4.3. Comparison between the distribution of ^{64}Cu-ATSM and

cellular hypoxia as determined by pimonidazole staining was performed using pixel-by-pixel and grid analysis as described in section 2.4.4.

Spearman's rank correlation coefficient was used for this analysis to determine the relationship between hypoxia determined immunohistochemically and ^{64}Cu-ATSM uptake.

4.3.6 Dynamic contrast-enhanced MRI following CA4P

4.3.6.1 Comparison of blood flow using AUC90 in CA4P treated rats with controls

Twelve CA4P treated P22-bearing BD-9 rats were imaged in this experiment. CA4P (10mg/kg i.p.) was administered 2 hours prior to the Gadolinium-enhanced MRI acquisition. The tail vein and artery were cannulated prior to imaging in each rat. The rats were anaesthetised throughout using intra-peritoneal anaesthesia described in section 2.3.3. The AUC90 (section 2.5.2) for the central axial tumour slice was compared with that from 14 untreated controls.

The Mann-Whitney U test was used to compare AUC90 values in both groups.

4.3.6.2 Comparison of AUC90 with mean tumour SUV at 1 hour in animals treated with CA4P

Twelve animals were treated with CA4P (10mg/kg i.p.) two hours prior to Gadolinium-enhanced MRI immediately following which they were transferred to the microPET scanner for a one hour dynamic ^{64}Cu-ATSM PET scan (mean activity

41.26MBq, range 15.0-58.37MBq). Following this a 15-minute transmission scan was performed. The AUC90 was compared with the mean tumour SUV calculated from the 0-60 minute summed data to determine a possible correlation using Pearson's correlation coefficient.

The imaging process and image analysis process for generating the AUC90 and the mean tumour SUV is described in section 2.1.5 and 2.5.

4.3.6.3 Comparison of AUC90 in animals treated with CA4P with mean tumour SUV generated from 6 sequential 10-minute time frames

The one hour microPET data from 4.3.6.2 was summed in to 6x10 minute time-frames to determine a correlation between the mean tumour SUV and the AUC90 to investigate a possible temporal relationship between tumour uptake of ^{64}Cu-ATSM and blood flow. Pearson's correlation coefficient was used for determining the realtionship between AUC90 and tumour SUV.

4.4 Results

4.4.1 Eppendorf probe measurements of tumour pO_2 in animals treated with CA4P

The range of mean pO_2 for each of the six tumours measured was between 0.298-1.745mmHg. The proportion of tumour measurements that were below the clinically significant tumour pO_2 of 10mmHg for the six tumours measured were 91.7%,

96.4%, 98.8%, 98.8%, 100% and 100% in comparison to the control rats described in section 3.4.1 that were not treated with CA4P who had levels of 43.33%, 61.41% and 41.41% (figure 4.1). The difference in pO_2 between the two groups was statistically significant showing a median difference of 9.9mmHg (two-sided p-value <0.0001, confidence interval 9.5 to 10.3) confirming that administration of CA4P reduces tumour pO_2.

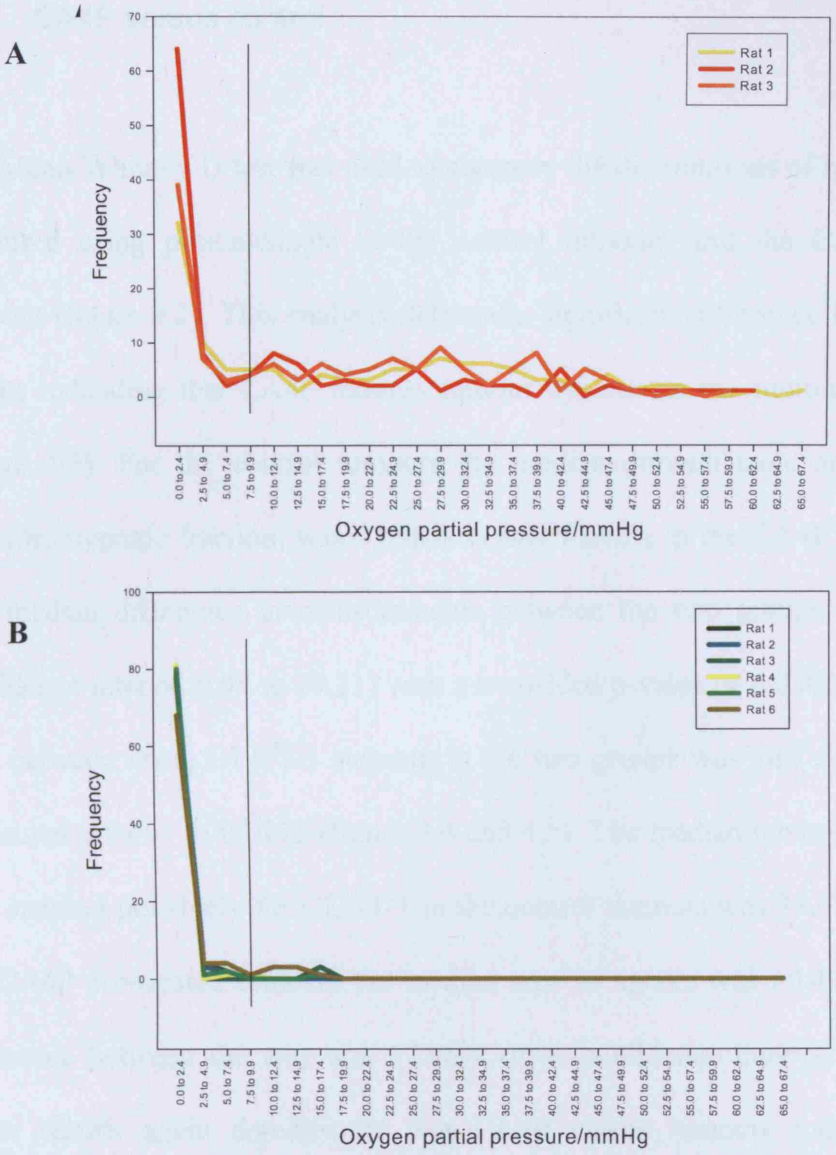

Figure 4.1 *Partial pressure of oxygen using the eppendorf probe in the tumour model. (A) demonstrates the pO_2 frequency measurements in 6 rats pre-treated with CA4P as compared with measurements in 3 control rats (B). The CA4P treated rats were significantly more hypoxic than the control rats. The lines on the graphs indicate the point at which hypoxia is radiobiologically and clinically significant (<10mmHg).*

4.4.2 Immunohistochemical determination of hypoxia in rats pre-treated with CA4P versus control

The Mann-Whitney U test was used to compare the distributions of hypoxic fractions measured using pimonidazole in the control tumours and the CA4P pre-treated tumours (figure 4.2). This analysis detected a significant difference between the two groups indicating that CA4P induces tumour hypoxia in the tumour model studied (figure 4.3). For the control tumours the median pimonidazole area stained, and therefore hypoxic fraction, was 63.98% versus 70.42% in the CA4P treated animals. The median difference in measurements between the two groups was 9.82 (95% confidence interval 0.98 to 19.21) with a two-sided p-value of 0.0303. The difference seen between using GLUT-1 staining in the two groups was also significant with a two-sided p-value of 0.0275 (figure 4.4 and 4.5). The median tumour cross-sectional area staining positively for GLUT-1 in the control tumours was 31.07%, whereas for the CA4P pre-treated tumours the median area of uptake was 50.49%. The median difference between the two was 17.96% (95% confidence interval 1.22 to 36.82). These results again demonstrate that CA4P makes tumours more hypoxic and supports our use of this agent in order to enhance tumour hypoxia to assess the effects of greater tumour hypoxia on uptake and retention of ^{64}Cu-ATSM.

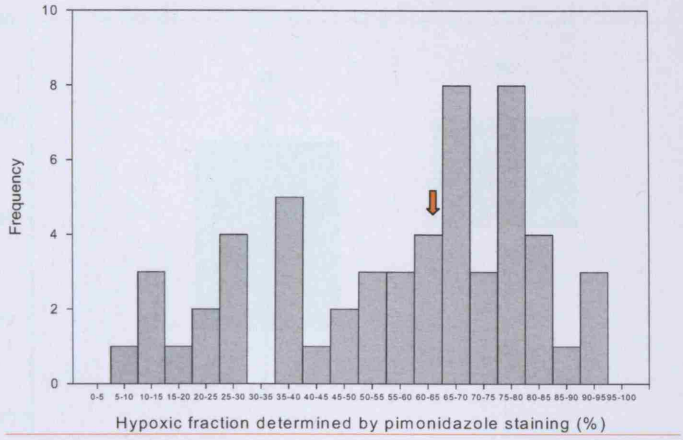

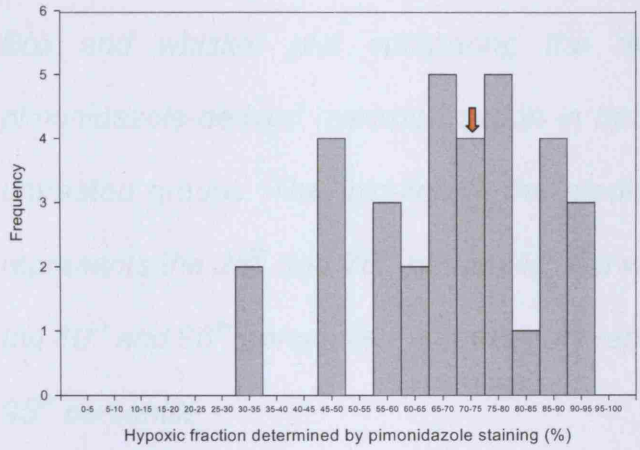

Figure 4.2 *Frequency histograms of pimonidazole derived tumour cross-section hypoxic fraction in control animals (n=30, 56 slides)(A), and those treated with CA4P (n=14, 33 slides)(B). The arrows mark the median pimonidazole staining fraction.*

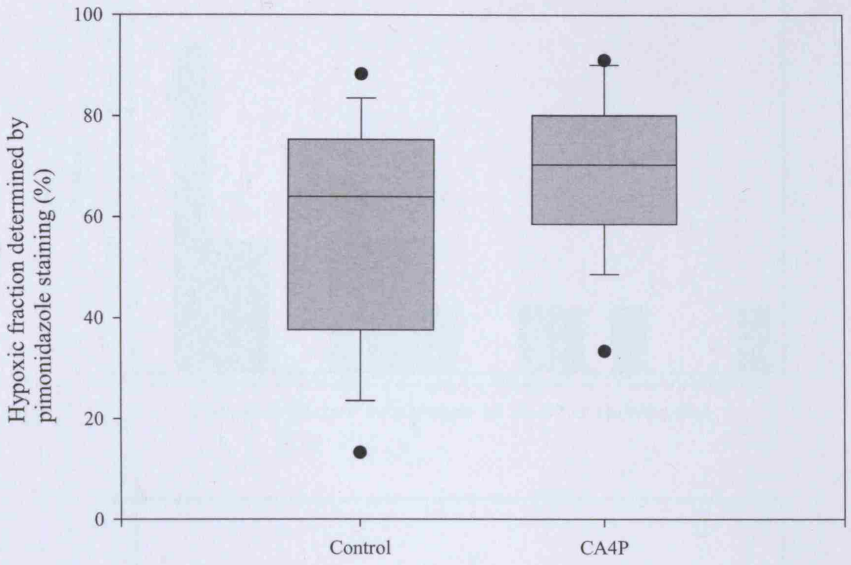

Figure 4.3 *Box and whisker plot comparing the distribution of the pimonidazole-derived hypoxic fraction in both the treated and untreated groups. The mid-line is the median value, the box represents the 25th and 75th percentile, the whiskers represent the 10th and 90th percentiles and the dots represent the 5th and 95th percentile.*

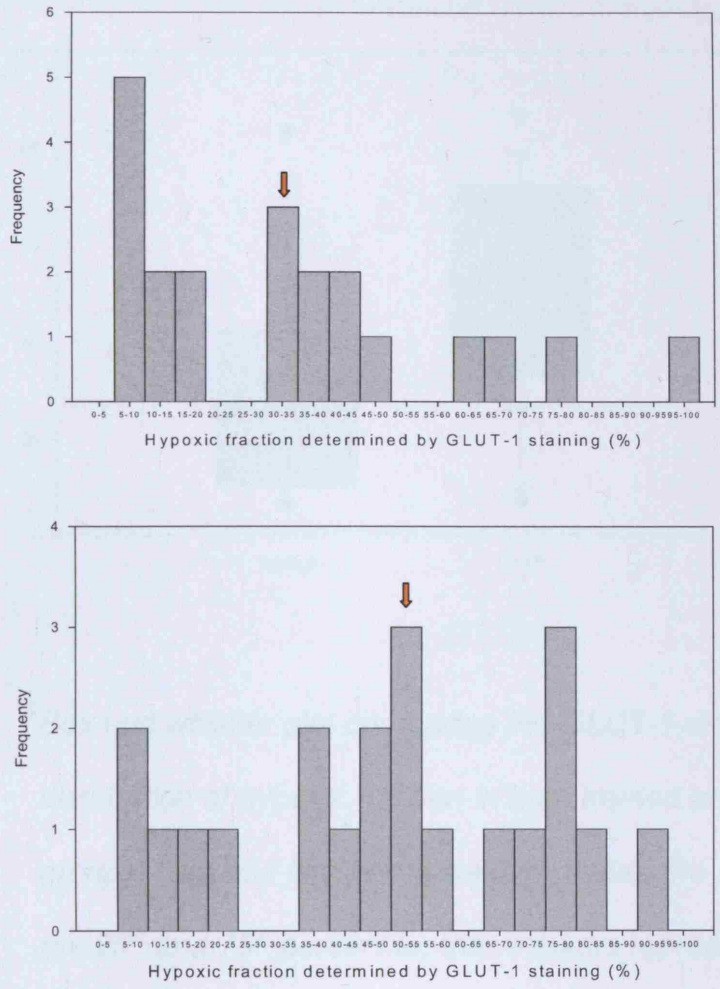

Figure 4.4 *Frequency histograms of GLUT-1 derived tumour cross-section hypoxic fraction in control animals (A) and those treated with CA4P (B). The treated group have a greater hypoxic fraction as illustrated by the arrow which is pointing to the median of the group.*

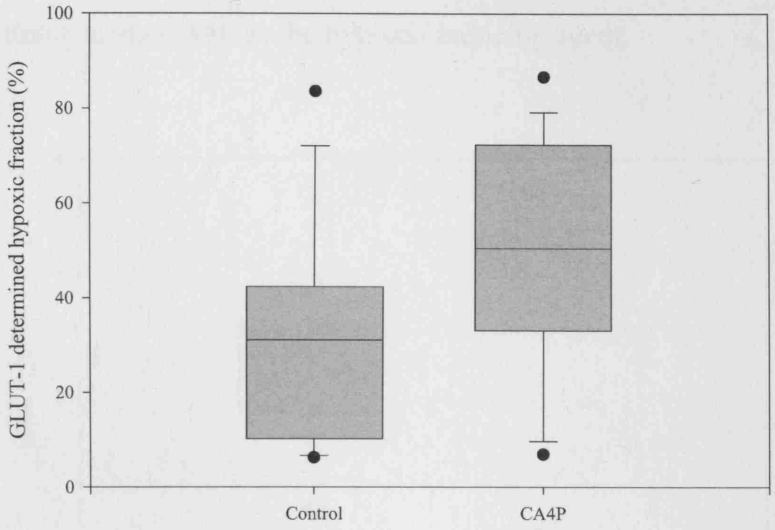

Figure 4.5 *Box and whisker plot comparing the GLUT-1-derived distribution of hypoxic fraction in both treated and untreated groups. The mid-line is the median value, the box represents the 25th and 75th percentile, the whiskers represent the 10th and 90th percentiles and the dots represent the 5th and 95th percentile.*

4.4.3 Comparison of mean tumour SUV in animals treated with CA4P versus controls

The mean tumour SUV was significantly lower for the CA4P treated group in whom the mean SUV was 0.489 (range 0.331 to 0.859) versus that of the control group, mean SUV 2.192 (range 0.956 to 2.891). The Mann-Whitney U test for calculating the difference between two groups showed a statistically significant median difference of 1.73 (95% confidence interval 1.39 to 2.16, $p<0.0001$) (figure 4.6).

These results are clearly contrary to the original premise that ^{64}Cu-ATSM is retained in hypoxic tissue using CA4P as the hypoxia inducing agent.

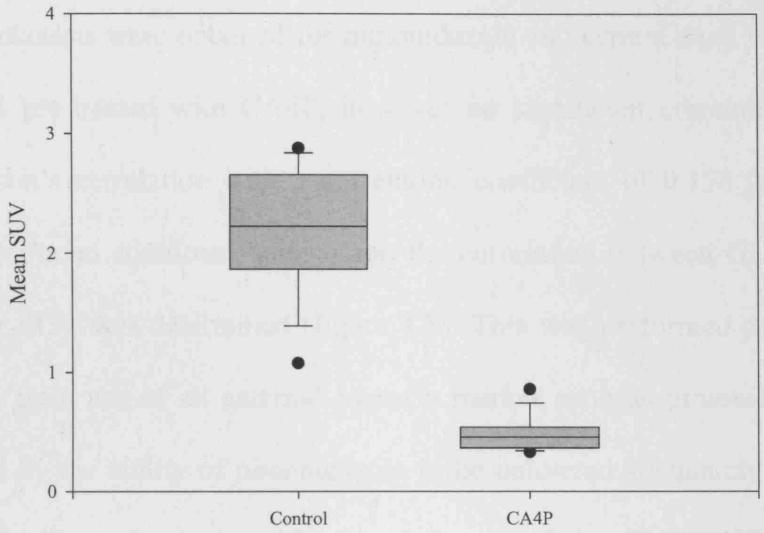

Figure 4.6 *Box and whisker plot of mean central axial tumour slice SUV 1 hour after injection of ^{64}Cu-ATSM in P22 rat tumour model treated with CA4P and controls. The significant difference between the SUVs of both groups was confirmed with the Mann-Whitney U test which calculated a median difference between the two datasets of 1.73 (95% confidence interval 1.39 to 2.16, $p<0.0001$). The mid-line is the median value, the box represents the 25th and 75th percentile, the whiskers represent the 10th and 90th percentiles and the dots represent the 5th and 95th percentile.*

4.4.4 Comparison of tumour SUV with immunohistochemical staining in the CA4P pre-treated tumour model

Six paired datasets were obtained for pimonidazole and central axial tumour SUV in the animals pre-treated with CA4P, however no significant correlation was found using Pearson's correlation with a correlation coefficient of 0.158 (p-value 0.766) (figure 4.7). As an additional comparison the correlation between GLUT-1 staining and tumour SUV was determined (figure 4.8). This was performed due to concerns that results from use of an external hypoxia marker such as pimonidazole may be confounded by the ability of pimonidazole to be delivered adequately to the tumour following CA4P administration. The correlation coefficient for GLUT-1 and tumour SUV was 0.00213 (p-value 0.979). These analyses are underpowered due to the small number of paired datasets available so should be interpreted with caution, however the results obtained are consistent with the findings in this thesis.

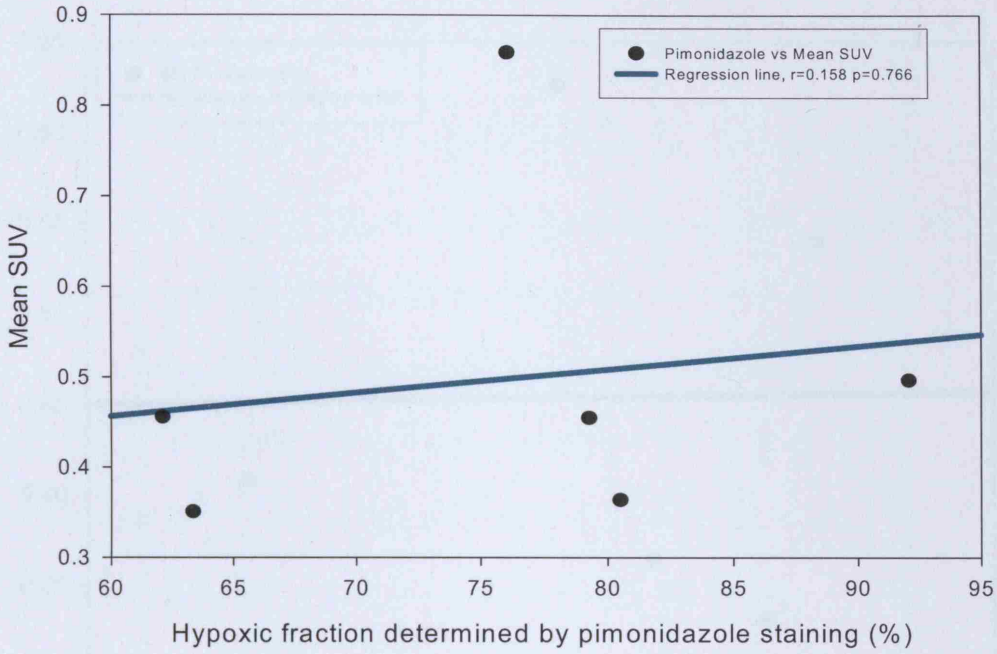

Figure 4.7 *Regression line showing relationship between axial central tumour slice SUV (0-60 minute summed data acquisition) and hypoxic fraction determined by pimonidazole staining. The correlation coefficient was 0.158 which was not statistically significant (p=0.766).*

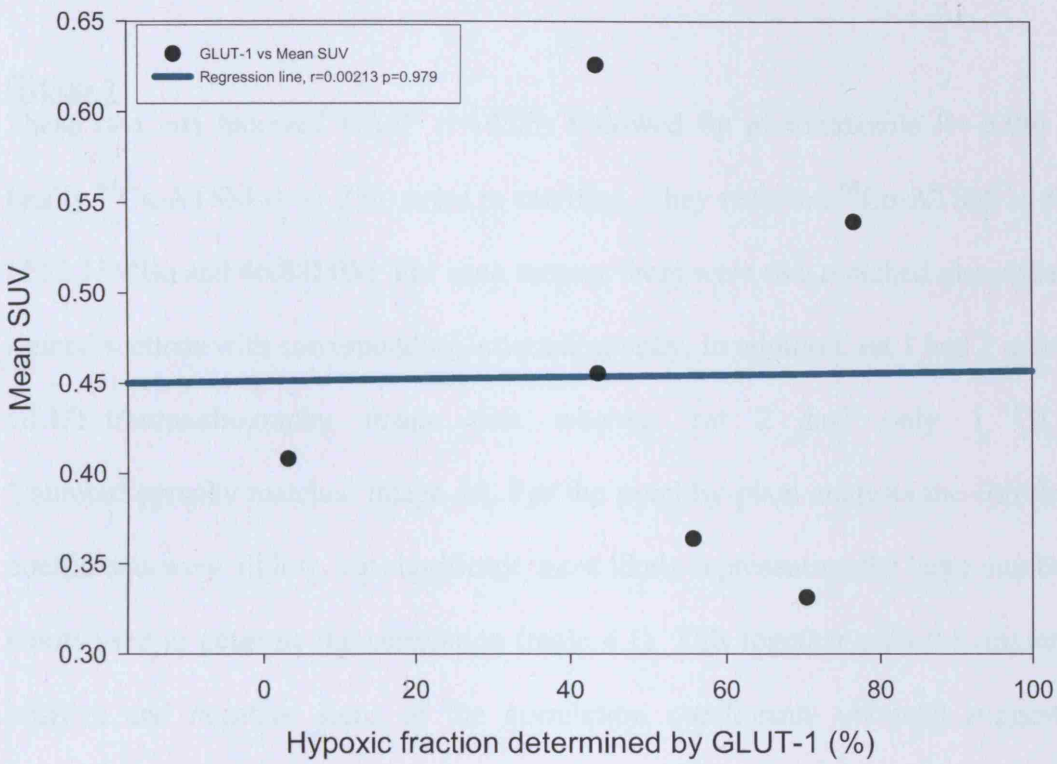

Figure 4.8 *Regression line showing relationship between axial central tumour slice SUV (0-60 minute summed data acquisition) and hypoxic fraction determined by GLUT-1 staining. The correlation coefficient was 0.00213 which was not statistically significant (p=0.979).*

4.4.5 Comparison of immunohistochemical staining with ^{64}Cu-ATSM autoradiography in animals treated with CA4P

Group 1

These two rats received CA4P (t=-4.0h) followed by pimonidazole (t=-3.0h) and finally ^{64}Cu-ATSM (t=-1.25h) prior to sacrifice. They received ^{64}Cu-ATSM at doses of 52.15MBq and 46.88MBq. For each tumour there were two matched pimonidazole stained sections with corresponding autoradiography. In addition, rat 1 had 2 matched GLUT-1/autoradiography image sets whereas rat 2 had only 1 GLUT-1/autoradiography matched image set. For the pixel-by-pixel analysis the correlation coefficients were all low, but significant, most likely representing the large number of points used to generate the correlation (table 4.1). This together with the mixture of positive and negative signs of the correlation coefficients obtained suggest no definitive co-segregation of ^{64}Cu-ATSM with pimonidazole when given after CA4P. The signs of the correlation coefficients were the same for corresponding grid analyses correlations however only one of the negative correlations was statistically significant. This lesser degree of statistical significance is likely due to the reduced number of data points in comparison with the pixel-by-pixel comparison. Glut-1 staining in this group produced similar correlations to pimonidazole staining (figure 4.9).

Figure 4.9 *Separated histology reference slides showing areas of similarity and difference between the distributions of pimonidazole (1) and GLUT-1 (2) in adjacent tumour sections and ^{64}Cu-ATSM autoradiography (image 3). The overall pattern is similar however uptake of ^{64}Cu-ATSM in the lower portion of the cross-section does not correspond with immunohistochemical staining. The pixel analysis of this (rat 2, table 4.1) shows there is a correlation ($r=0.181$, $p<0.0001$).*

Rat no.	Pixel by pixel correlation of pimonidazole versus ^{64}Cu-ATSM distribution		Correlation of percentage pimonidazole staining versus ^{64}Cu-ATSM mean intensity per grid square		Pixel by pixel correlation of GLUT-1 versus ^{64}Cu-ATSM distribution		Correlation of percentage GLUT-1 staining versus ^{64}Cu-ATSM mean intensity per grid square	
	r	p-value	r	p-value	r	p-value	r	p-value
1	-0.0931	<0.0001	-0.272	0.0593	-0.0430	0.152	-0.167	0.206
	-0.0659	0.0206	-0.54209	<0.0001	-0.196	<0.0001	-0.590	<0.0001
2	0.181	<0.0001	0.490	0.702	0.255	<0.0001	0.549	<0.0001
	0.285	<0.0001	0.00563	0.966	-	-	-	-

Table 4.1 *Table of correlation coefficients comparing ^{64}Cu-ATSM autoradiography with pimonidazole and GLUT-1 distribution in rats treated with CA4P (-4 hours) followed by pimonidazole (-3 hours) and ^{64}Cu-ATSM (-1.25 hours).*

Group 2

In this group receiving pimonidazole (t=-4.0h) prior to CA4P (t=-3.0h) and subsequently ^{64}Cu-ATSM (=-1.25h). Three of the rats had two matched pimonidazole/autoradiography image sets and 2 rats had 1 matched image set for comparison. The sign of the correlation coefficients generated using pixel-by-pixel analysis were mostly negative (7/8) (table 4.2). The one positive correlation coefficient (1/8) was not statistically significant. The values for the grid analysis were similar however only 4/7 negative correlations were statistically significant, again most likely due to the reduced number of points in this analysis versus the pixel-by-pixel comparison. The comparison between GLUT-1 staining and ^{64}Cu-ATSM

autoradiography was performed in 2 rats in this group. All the correlation coefficients were negative and statistically significant. These results were similar to the pimonidazole correlations from the same rats (figure 4.10).

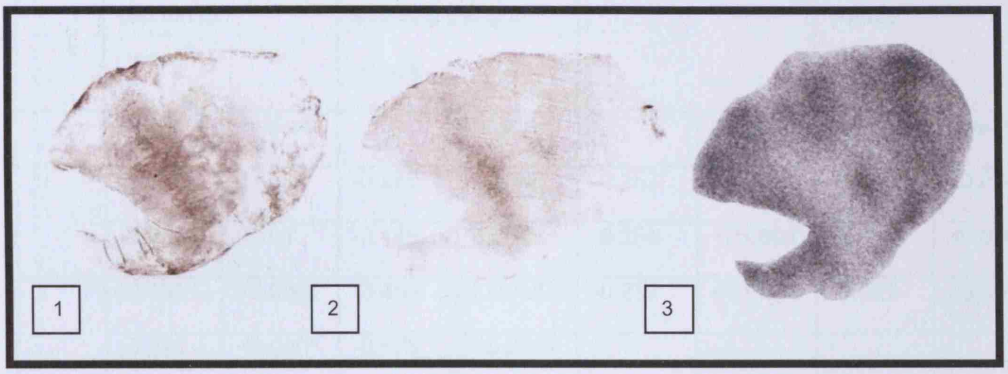

Figure 4.10 *Separated histology reference slides showing similar distribution of pimonidazole (1) and GLUT-1 (2) in adjacent tumour sections. Image (3) is a ^{64}Cu-ATSM autoradiography image of (1). Note in this tumour cross section the distribution of ^{64}Cu-ATSM and hypoxia markers is dissimilar. The pixel analysis of this (rat 2, table 4.2) shows there is a correlation ($r=-0.232$, $p<0.0001$).*

Rat no.	Pixel by pixel correlation of pimonidazole versus ^{64}Cu-ATSM distribution		Correlation of percentage pimonidazole staining versus ^{64}Cu-ATSM mean intensity per grid square		Pixel by pixel correlation of GLUT-1 versus ^{64}Cu-ATSM distribution		Correlation of percentage GLUT-1 staining versus ^{64}Cu-ATSM mean intensity per grid square	
	r	p-value	r	p-value	r	p-value	r	p-value
1	0.0255	0.435	-0.238	0.0588	-0.257	<0.0001	-0.579	<0.0001
	-0.0459	0.101	-0.149	0.254	-0.265	<0.0001	-0.557	<0.0001
2	-0.193	<0.0001	-0.459	0.0013	-0.232	<0.0001	-0.681	<0.0001
	-0.311	<0.0001	-0.675	<0.0001	-	-	-	-
3	-0.226	<0.0001	-0.312	0.0333	-	-	-	-
	-0.0766	0.0096	-0.136	0.317	-	-	-	-
4	-0.0739	0.0616	0.181	0.364	-	-	-	-
5	-0.455	<0.0001	-0.587	<0.0001	-	-	-	-

Table 4.2 *Table of correlation coefficents comparing ^{64}Cu-ATSM autoradiography with pimonidazole and GLUT-1 distribution in rats treated with pimonidazole (-4 hours) followed by CA4P (-3 hours) and ^{64}Cu-ATSM (-1.25 hours).*

Group 3

Three animals had pimonidazole (t=-3.25h) and ^{64}Cu-ATSM (t=-3.0h) administered prior to CA4P (t=-2.75h). All these correlations were significantly negative for each of the eight pimonidazole/autoradiography and GLUT-1/autoradiography matched image sets (figure 4.11, table 4.3). This was seen in both the pixel-by-pixel and grid comparisons of both pimonidazole and GLUT-1 stained sections.

An unpaired t-test was used to determine if tumour percentage uptake of pimonidazole was different between those treated with pimonidazole prior to versus post CA4P administration and there was no significant difference (p=0.2628).

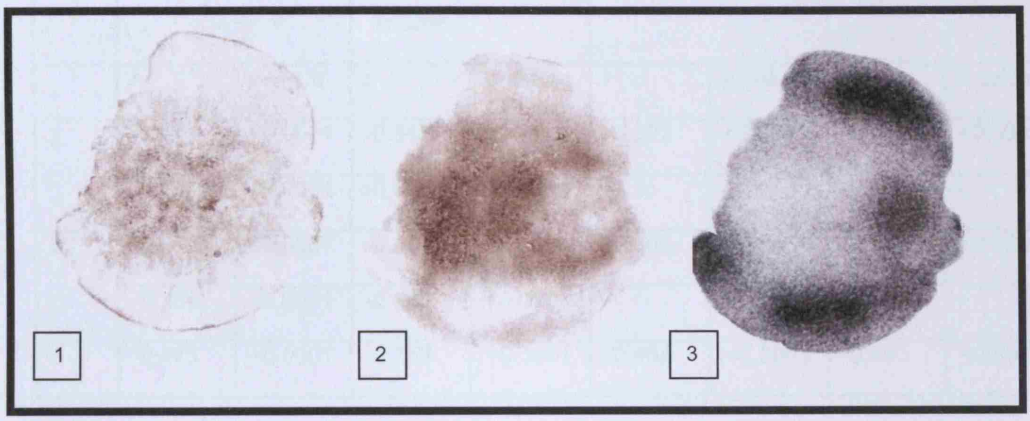

Figure 4.11 *Separated histology reference slides showing similar distribution of pimonidazole (1) and GLUT-1 (2) in adjacent tumour sections. Image (3) is a ^{64}Cu-ATSM autoradiography image of (1). Note in this tumour cross section the distribution of ^{64}Cu-ATSM and hypoxia markers is dissimilar. The pixel analysis of this (rat 3, table 4.3) shows there is a correlation ($r=-0.458$, $p<0.0001$).*

Rat no.	Pixel by pixel correlation of pimonidazole versus ^{64}Cu-ATSM distribution		Correlation of percentage pimonidazole staining versus ^{64}Cu-ATSM mean intensity per grid square		Pixel by pixel correlation of GLUT-1 versus ^{64}Cu-ATSM distribution		Correlation of percentage GLUT-1 staining versus ^{64}Cu-ATSM mean intensity per grid square	
	r	p-value	r	p-value	r	p-value	r	p-value
1	-0.271	<0.0001	-0.542	<0.0001	-0.592	<0.0001	-0.784	<0.0001
	-0.431	<0.0001	-0.603	<0.0001	-	-	-	-
2	-0.252	<0.0001	-0.538	<0.0001	-0.505	<0.0001	-0.710	<0.0001
	-0.239	<0.0001	-0.581	<0.0001	-	-	-	-
3	-0.443	<0.0001	-0.758	<0.0001	-0.458	<0.0001	-0.690	<0.0001

Table 4.3 *Table of correlation coefficients comparing ^{64}Cu-ATSM autoradiography with pimonidazole and GLUT-1 distribution in rats treated with pimonidazole (-3.25 hours) followed by ^{64}Cu-ATSM (-3.00 hours) and CA4P (-2.75 hours).*

4.4.6 Comparison of blood flow using AUC90 in CA4P treated rats and controls

To compare the effects of CA4P on tumour blood flow the mean AUC90 values from control rats were compared with those from rats pre-treated with CA4P. The median AUC90 for the treated animals was 1283 mMol.min whereas for the control group this was 6610 mMol.min. The two groups had statistically significant difference in AUC90 values with a median difference between the groups of 5452 (95% confidence interval 4235 – 9632 mMol.min, p-value <0.0001) (figure 4.12). This demonstrates that CA4P reduces blood flow in this tumour model. The pattern of loss observed with CA4P was similar to that described by others in that tumours pre-treated with CA4P had little evidence of blood flow centrally, however the tumour rim was spared (figure 4.13) (Prise VE 2002; Tozer GM 2005).

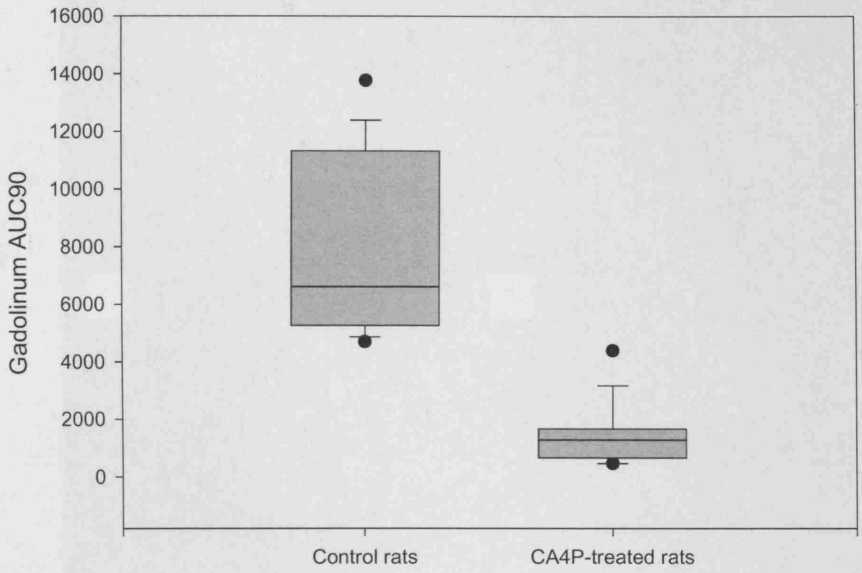

Figure 4.12 *Box plot to show the distribution of AUC90 in control rats and those treated with CA4P. The two groups have significantly different distributions confirming that CA4P reduces tumour blood flow. The mid-line is the median value, the box represents the 25th and 75th percentile, the whiskers represent the 10th and 90th percentiles and the dots represent the 5th and 95th percentile.*

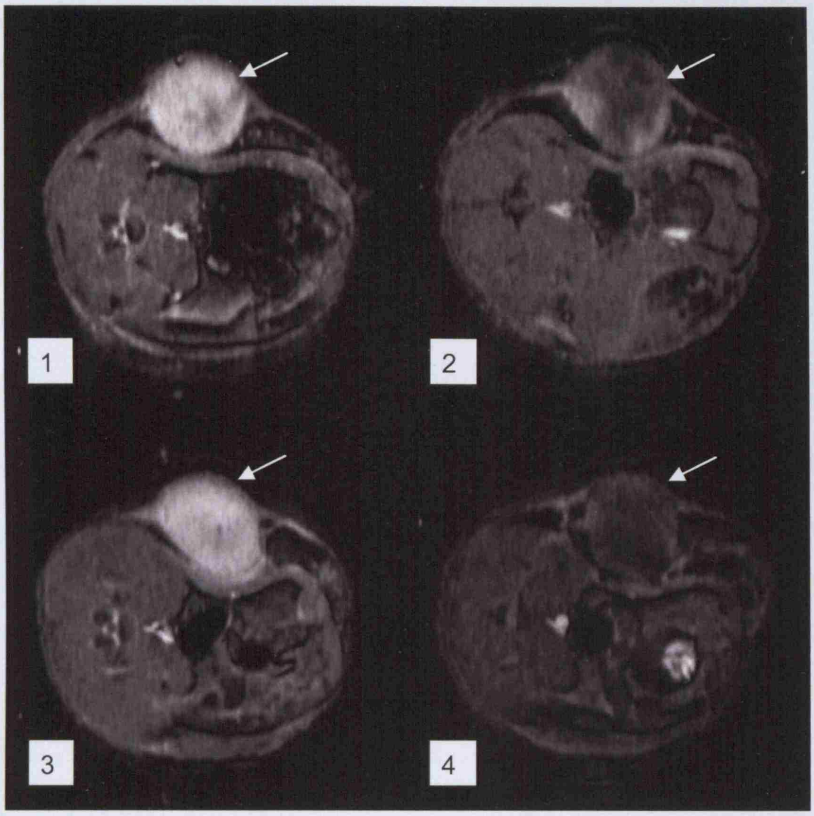

Figure 4.13 *Axial Gadolinium-enhanced MRI images taken through the level of the tumour mid-point. Images 1 and 3 are from control animals whereas images 2 and 4 are from CA4P treated animals. The signal intensity is much greater in the control tumours (see arrows) due to the greater accumulation of Gadolinium, unlike the CA4P-treated animals in whom uptake is limited to the peripheral tumour.*

4.4.7 Comparison of Gadolinium AUC90 with mean tumour SUV at 1 hour in animals treated with CA4P

Pearson's correlation coefficient was 0.836 (p-value 0.0007). There is clearly a statistically significant correlation between blood flow and ^{64}Cu-ATSM uptake and retention at one hour in these CA4P treated animals (figures 4.14 and 4.15) which is likely a result of the CA4P causing central tumour vascular shutdown leaving a rim of patent vasculature for circulation of ^{64}Cu-ATSM.

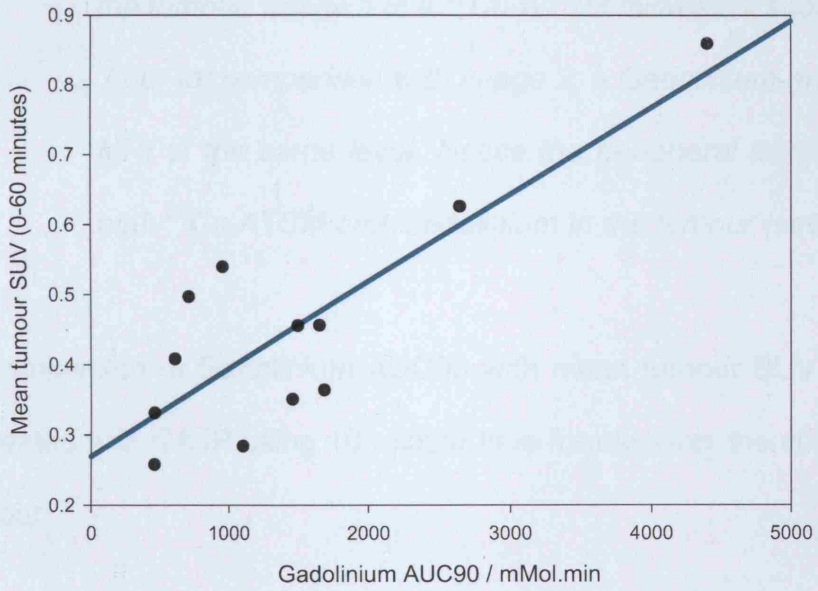

Figure 4.14 *Plot to evaluate the relationship between mean tumour SUV over one hour and tumour blood flow measured using AUC90 in animals pre-treated with CA4P*

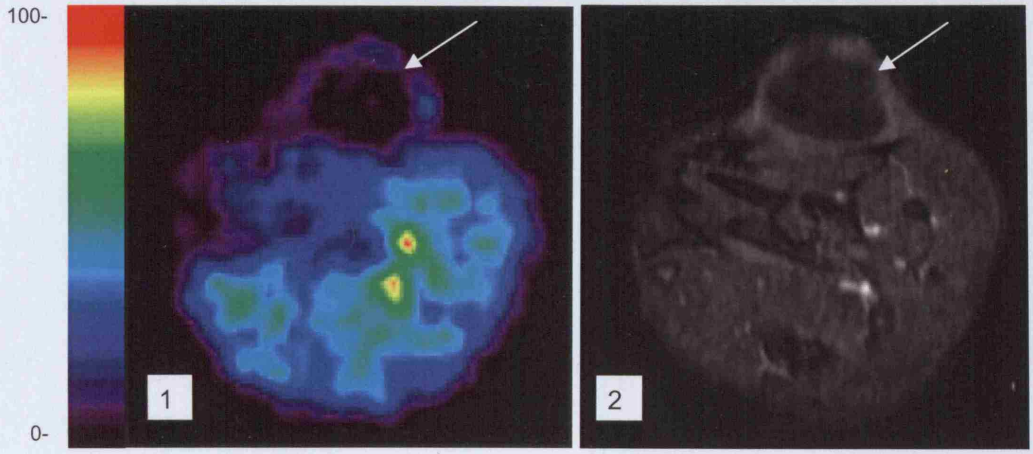

Figure 4.15 *Axial sections through the body of the rat at the mid-point of the tumour. Image 1 is a ^{64}Cu-ATSM microPET image at 1 hour for comparison with image 2, a Gadolinium-enhanced MRI at the same level. Notice the peripheral accumulation of both ^{64}Cu-ATSM and Gadolinium in the tumour (see arrows).*

4.4.8 Comparison of Gadolinium AUC90 with mean tumour SUV in animals treated with CA4P using 10-minute time frames over the course of one hour

For each ten-minute time frame from 0 to 60 minutes a statistically significant Pearson's correlation was seen between mean tumour SUV and tumour blood flow using AUC90 (table 4.4 and figure 4.16). This correlation neither increased nor decreased over the time course measured, unlike the correlation seen in control animals which became less significant with time. This suggests that blood flow is an important determinant of ^{64}Cu-ATSM uptake and retention in these animals treated with CA4P.

Time frames post-injection of ^{64}Cu-ATSM from which SUV is determined	Correlation coefficients between AUC90 and SUV in CA4P treated rats	
	Correlation coefficient, r	p-value
0-10 minutes	0.671	0.0168
10-20 minutes	0.581	0.0475
20-30 minutes	0.615	0.0333
30-40 minutes	0.654	0.0211
40-50 minutes	0.634	0.0267
50-60 minutes	0.776	0.003

Table 4.4 *This table shows the statistically significant correlation of all mean tumour SUV time frames with AUC90.*

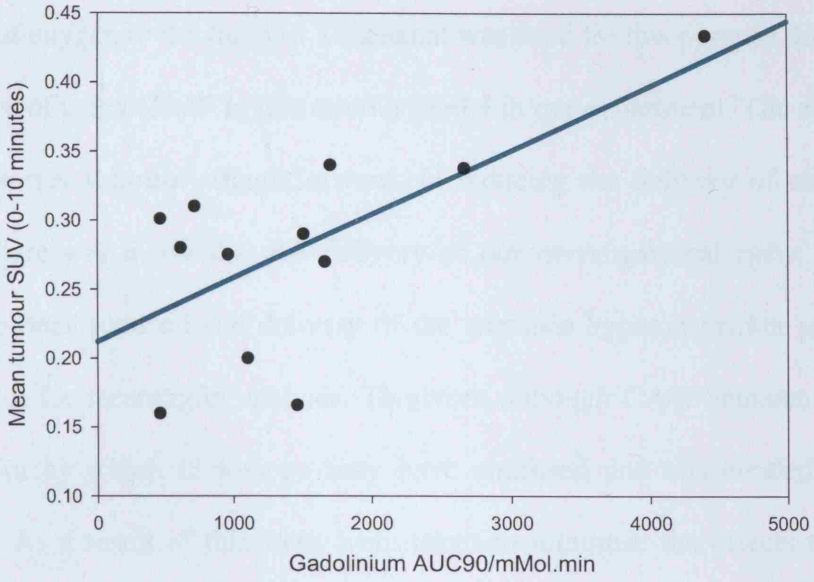

Figure 4.16 *Mean tumour SUV measured from 0 to 10 minutes post-injection of ^{64}Cu-ATSM versus AUC90 in animals treated with CA4P. This correlation was statistically significant (0.671, p-value 0.0168)*

4.5 Discussion

From the studies performed we have been able to confirm that treatment with CA4P induces tumour hypoxia measured both directly using Eppendorf probe measurements of tumour pO_2 and indirectly using the immunohistochemical markers of hypoxia pimonidazole and GLUT-1. The enhancement of tumour hypoxia was felt to be an important step to elucidating a possible association between tracer retention and hypoxia, particularly following the failure to demonstrate a relationship in control animals in experiments described in the previous chapter. The induction of hypoxia

using CA4P is through vascular disruption, reducing the flow of blood and therefore delivery of oxygen to the tumour. This agent was used for this purpose due to the vast experience of using CA4P in this tumour model in our department. The choice of this agent however was not straightforward. In reducing the delivery of oxygen to the tumour there was a risk that the delivery of our investigational agent ^{64}Cu-ATSM may have been reduced and delivery of the extrinsic hypoxia marker pimonidazole insufficient for meaningful analysis. Therefore although CA4P induces hypoxia the mechanism by which it does so may have confused and confounded any results obtained. As a result of this steps were taken to minimise the effects that vascular disruption may have had on the delivery and uptake of ^{64}Cu-ATSM and immunohistochemical hypoxia markers. For instance GLUT-1, an intrinsic marker of hypoxia, was used in addition to pimonidazole because it didn't require prior delivery to the tumour for its detection, pimonidazole was given prior to CA4P in a group of animals and in one experiment ^{64}Cu-ATSM was administered prior to CA4P to allow tumour circulation prior to vascular disruption.

The experiment performed to assess the impact of CA4P on uptake of ^{64}Cu-ATSM using SUV as a measure of uptake, showed that CA4P, despite making tumours more hypoxic, significantly reduced the uptake of ^{64}Cu-ATSM (sections 4.4.3). This is clearly not what was expected from a radiotracer thought to have an enhanced uptake in hypoxic tumours, however, this significant drop in tumour uptake of ^{64}Cu-ATSM was thought possibly to reflect the reduced vascular delivery of the agent to the tumour as a result of CA4P. Furthermore no correlation was seen between pimonidazole-derived hypoxic fraction and tumour SUV following treatment with CA4P. However this too may have been a reflection of inadequate tracer delivery. To

address possible vascular delivery problems pimonidazole and then ^{64}Cu-ATSM were administered to the rats prior to CA4P. In addition, the intrinsic hypoxia marker GLUT-1 was used for comparison with the tumour uptake of ^{64}Cu-ATSM, however similar results were seen with this as they were with pimonidazole. The administration of pimonidazole and then ^{64}Cu-ATSM prior to delivery of CA4P was to allow their circulation in the tumour before induction of hypoxia. Following CA4P a period of 2.75 hours was chosen to elapse before sacrifice of the animal and assessment of tracer distribution. Despite these manoeuvres the distribution pattern of ^{64}Cu-ATSM looked even less like the pattern of hypoxia seen with the immunohistochemical markers pimonidazole and GLUT-1. The negative correlation that had been seen previously was stronger and reached statistical significance in all tumour sections analysed, unlike the correlation coefficients calculated using alternative regimes. Statistical significance was seen using both the pixel and grid analysis. A concern was that ^{64}Cu-ATSM may have been trapped following administration of CA4P however that same trapping process may have affected the pimonidazole, in which case a more positive correlation would have been seen between the ^{64}Cu-ATSM and the pimonidazole. This was not so and both GLUT-1 and pimonidazole were seen to distribute similarly to regions of low ^{64}Cu-ATSM uptake and vice versa, suggesting that although ^{64}Cu-ATSM may be trapped in regions of functioning vasculature, pimonidazole is not and its greater lipophilicity and smaller size allow it superior access to non-perfused tumour regions. By way of further explanation, in the study in which ^{64}Cu-ATSM was administered 10 minutes prior to CA4P there was a strong negative correlation between ^{64}Cu-ATSM distribution and the immunohistochemical markers pimonidazole and GLUT-1. We know from chapter 3 that up to twenty minutes after its administration ^{64}Cu-ATSM

has a similar distribution to tumour blood flow, which may help to explain this strong and unexpected inverse relationship. At the time CA4P was administered ^{64}Cu-ATSM distribution would have reflected tumour blood flow. As CA4P exerts its vascular disrupting effects so rapidly it is likely that ^{64}Cu-ATSM was fixed in a vascular distribution following CA4P. A distribution likely to be contrary to the distribution we would expect of hypoxia. Despite the diminution in functioning vasculature following CA4P one would still have expected the proposed hypoxia radiotracer to circulate and be fixed and retained in regions of hypoxia, however this was clearly not the case and suggests that ^{64}Cu-ATSM relies heavily on its delivery to these regions using vessels as its dominant mode of transportation.

The effect of CA4P on the P22 tumour was to significantly diminish its blood flow and uptake of ^{64}Cu-ATSM as described (section 4.4.3 and 4.4.6). In these tumours uptake of ^{64}Cu-ATSM correlated significantly with tumour blood flow over the one-hour time course measured. This was quite different to the early correlation only that was seen in the control rats. In the CA4P treated rats both Gadolinium uptake and uptake of ^{64}Cu-ATSM were very similar, suggesting that ^{64}Cu-ATSM was taken up in regions with functioning vasculature only, and not in regions of CA4P driven vascular shutdown. As such, ^{64}Cu-ATSM uptake was limited to a rim around the tumour periphery in a distribution similar to that of Gadolinium-enhanced MRI post-CA4P (Prise 2002; Tozer 2005). These findings further demonstrate the dependence of ^{64}Cu-ATSM on tumour blood flow for its delivery and circulation within the tumour. Although a statistically significant similarity was seen between ^{64}Cu-ATSM and tumour blood flow in the first twenty minutes in control animals, this significant correlation persisted throughout the time course evaluated for the CA4P treated rats.

This similarity is likely to have persisted due to the inability of the tracer to redistribute to different tumour regions as a result of vascular shut down following the CA4P and its inability to circulate throughout the tumour without at least an initial delivery through blood vessels. Correction of ^{64}Cu-ATSM uptake for tumour blood flow may be required in this tumour model treated with CA4P however such a correction using either Gadolinium-enhanced MRI or PET imaging with perfusion radiotracers such as ^{15}O-H_2O or ^{11}C-acetate were beyond the scope of this study and was therefore not performed.

In conclusion, using both extrinsic and intrinsic immunohistochemical markers of hypoxia for comparison ^{64}Cu-ATSM does not appear to be a marker of hypoxia in this tumour model whether using CA4P to enhance tumour hypoxia or not. It would be a reasonable criticism to suggest that CA4P is preventing delivery of radiotracer and the extrinsic immunohistochemical marker, pimonidazole, however, correcting for this produced results that were even more strongly suggestive of the fact that ^{64}Cu-ATSM distributes to areas that are not hypoxic in this tumour model. The investigations described demonstrate that for ^{64}Cu-ATSM to circulate in this tumour model vascular delivery is a prerequisite.

References

Beauregard DA, Thelwall P., Chaplin DJ, Hill SA, Adams GE, Brindle KM (1998). "Magnetic resonance imaging and spectroscopy of combretastatin A4 pro-drug-induced disruption of tumour perfusion and energetic status." Br J Cancer 77: 1761-1767.

Boehle AS, Sipos B., Kliche U, Kalthoff H, Dohrmann P (2001). "Combretastatin A-4 prodrug inhibits growth of human non-small cell lung cancer in a murine xenotransplant model." Ann Thorac Surg 71: 1657-1665.

Dark GG, Hill S., Prise VE, Tozer GM, Pettit GR, Chaplin DJ (1997). "Combretastatin A4 phosphate (CA4P), an agent that displays potent and selective toxicity toward tumour vasculature." Cancer Res 57: 1829-1834.

Horsman MR, Ehrnrooth E., Ladekarl M, Overgaard J (1998). "The effect of combretastatin A-4 disodium phosphate in a C3H mouse mammary carcinoma and a variety of murine spontaneous tumours." Int J Radiat Oncol Biol Phys 42(4): 895-898.

Kanthou C, Greco O, Stratford A, Cook I, Knight R, Benzakour O, Tozer G (2004). "The tubulin binding agent A-4-phosphate arrests endothelial cells in mitosis and induces mitotic cell death." Am J Pathol 165: 1401-1411.

Kanthou C, Tozer. G. (2002). "The tumour vascular targeting agent combretastatin A-4-phosphate induces reorganization of the actin cytoskeleton and early membrane blebbing in human emdothelial cells." Blood 99: 2060-2069.

Maxwell RJ, Wilson J., Prise VE, Vojnovic B, Rustin GJ, Lodge MA, Tozer GM (2002). "Evaluation of the anti-vascular effects of combretastatin in rodent tumours by dynamic ontrast enhanced MRI." NMR Biomed 15: 89-98.

Milosevic MF, Fyles A., Hill RP (1999). "The relationship between elevated interstitial fluid pressure and blood flow in tumours: a bioengineering analysis." Int J Radiat Oncol Biol Phys 43: 1111-1123.

Pettit GR, Cragg G., Singh SB (1987). "Antineoplastic agents, 122. Constituents of Combretum caffrum." J Nat Prod 50: 386-391.

Prise VE, Honess D, Stratford MRL, Wilson J, Tozer GM (2002). "The vascular response of tumour and normal tissues in the rat to the vascular targeting agent, combretastatin A-4-phosphate, at clinically relevant doses." Int J Oncol 21: 717-726.

Tozer GM, Kanthou C., Baguley BC (2005). "Disrupting tumour blood vessels." Nat Rev Cancer 5: 423-435.

Tozer GM, Prise V, Wilson J, Cemazar M, Shan S, Dewhirst MW, Barber PR, Vojnovic B, Chaplin DJ (2001). "Mechanisms associated with tumour vascular shut-down induced by combretatstatin A-4 phosphate: intravital microscopy and measurement of vascular permeability." Cancer Res 61(17): 6413-6422.

Tozer GM, Prise V, Wilson J, Locke RJ, Vojnovic B, Stratford MR, Dennis MF, Chaplin DJ (1999). "Combretastatin A-4 phosphate as a tumour vascular-targeting agent: early effects in tumours and normal tissues." Cancer Res 59(7): 1626-1634.

CHAPTER 5

Concluding discussion

^{64}Cu-ATSM, a bis(thiosemicarbazone), was proposed as a tumour hypoxia marker demonstrable by positron emission tomography in the late 1990s (Fujibayashi 1997; Fujibayashi 1999; Lewis 1999; Lewis 2001). The discovery of such a non-invasive method of acquiring detailed information about the status of tumour oxygenation could make a significant impact in the management of malignant disease. Images detailing the distribution of tumour hypoxia could be used to aid physicians in making primary treatment decisions and would provide additional information for estimating prognosis. Radiotherapy dose-escalation to tumour sub-volumes is now feasible and providing tumour maps of hypoxia would allow the confident delineation of radioresistant sub-volumes for dose-escalation. Although radiotracers with similar imaging properties have been identified, most notably ^{18}F-FMISO, their introduction in to clinical practise has been hampered by low tumour:background ratios with poor resulting images and protracted imaging times. Following its original proposal ^{64}Cu-ATSM has provided information in patients with carcinoma of the lung and cervix consistent with tumour hypoxia (Dehdashti, Grigsby 2003; Dehdashti, Mintun 2003) however its evaluation in a number of different pre-clinical tumour models has had variable results depending on tumour type (Burgman 2005; O'Donoghue 2005; Matsumoto 2007).

MicroPET imaging of the P22 carcinosarcoma tumour model used in this study showed avid uptake of ^{64}Cu-ATSM by tumours with a cumulative tumour to

background ratio of 1.6, 60 minutes following its injection. Despite this, and together with the knowledge that a significant proportion of the control tumours were hypoxic from measurements taken with the eppendorf needle microelectrode, the experiments described in this thesis did not provide evidence for the use of ^{64}Cu-ATSM as a hypoxia marker in this rodent tumour.

^{64}Cu-ATSM uptake measured using mean tumour SUV increased as pimonidazole-determined hypoxic fraction decreased and a comparison at the cellular level of pimonidazole and ^{64}Cu-ATSM distribution from autoradiography demonstrated no consistent correlation at 75 minutes (section 3.4.3). A previous study using the anaplastic rat prostate tumour model described a similarly negative correlation between ^{64}Cu-ATSM and pimonidazole when compared 1 hour following injection of ^{64}Cu-ATSM. However in this same tumour model a correlation was seen 24 hours after its administration (O'Donoghue 2005). A similar comparison was performed in this study however the distribution of ^{64}Cu-ATSM 20 hours after its administration was homogeneous with no apparent delineation of hypoxic subvolumes despite the pimonidazole staining suggesting otherwise.

In order to assess the impact on ^{64}Cu-ATSM distribution of enhanced levels of hypoxia the vascular disrupting agent CA4P was administered. This made the tumours more hypoxic and the mean tumour percentage with a clinically significant partial pressure of oxygen of less than 10mmHg increased from 48.72% in control tumours to 97.62% in those treated with CA4P (section 4.4.1). This increased level of hypoxia was also demonstrated using immunohistochemical staining with the intrinsic marker of hypoxia GLUT-1 and the extrinsic marker of hypoxia

pimonidazole (section 4.4.2). Despite this increased level of hypoxia, tumour uptake of ^{64}Cu-ATSM was less than that of control animals (section 4.4.3). However, as the ^{64}Cu-ATSM was administered 3 hours after the CA4P, at a time when its vascular disrupting properties would have been at a maximum, the diminution in ^{64}Cu-ATSM was likely to have occurred due to a profound reduction in vascular delivery and tumour perfusion secondary to treatment with CA4P. Indeed the cellular distribution of ^{64}Cu-ATSM given after CA4P showed no consistent similarities of distribution with the immunohistochemical markers of hypoxia, GLUT-1 or pimonidazole (section 4.4.5). Furthermore, even when ^{64}Cu-ATSM was given prior to CA4P, along with pimonidazole, a very convincing negative correlation was seen in all tumour slices assessed, suggesting that ^{64}Cu-ATSM is retained in regions that are not hypoxic. Clearly this observation is contrary to the original proposition that Cu-ATSM is retained in hypoxic cells, but why should this be so?

In this study ^{64}Cu-ATSM seemed to be distributing in a contrasting pattern to hypoxia therefore being retained in more adequately oxygenated cells. An explanation for this would be that ^{64}Cu-ATSM is retained in regions of blood flow. This possibility was investigated using Gadolinium-enhanced MRI imaging and comparing its pattern of uptake with tumour ^{64}Cu-ATSM. In control rats ^{64}Cu-ATSM distribution and blood flow were similar up to 20 minutes after administration of the tracer, however after this time the association lost significance (section 3.4.4.2). Despite the loss of statistical significance the overall pattern of distribution of ^{64}Cu-ATSM did not change particularly, although tumour ^{64}Cu-ATSM activity increased over the 1 hour time-period measured. In rats pre-treated with CA4P, uptake of ^{64}Cu-ATSM was less than in control tumours (section 4.4.3). This was also observed with Gadolinium,

reflecting a reduced tumour blood flow as a result of CA4P (section 4.4.6). Unlike the control tumours in which association with blood flow diminished with time the correlation seen in CA4P-treated animals persisted over the 1-hour time course measured (section 4.4.8). This is likely to have occurred due to the inability for ^{64}Cu-ATSM to move beyond the rim of functioning vasculature remaining after treatment with CA4P, further suggesting a requirement for vascular delivery of the tracer to the tumour before re-distribution determined by individual tumour handling of ^{64}Cu-ATSM can occur.

The group of animals who received ^{64}Cu-ATSM prior to CA4P showed a very significant negative correlation between ^{64}Cu-ATSM retention with hypoxia determined by GLUT-1 and pimonidazole (section 4.4.5). In these animals there was only a 10 minute interval between administration of ^{64}Cu-ATSM followed by CA4P. The data obtained from the DCE-MRI experiments suggested that at 10 minutes ^{64}Cu-ATSM distribution is similar to blood flow. Therefore as CA4P begins to exert its effects within minutes it is likely that when vascular shutdown occurred the ^{64}Cu-ATSM was retained in the regions of prior vascular perfusion. These regions are unlikely to be hypoxic therefore the correlation between ^{64}Cu-ATSM and hypoxia was significantly negative. Further providing support to the proposition that the early distribution of ^{64}Cu-ATSM reflects blood flow. This initial dependence on blood flow needs to be taken in to account when imaging protocols are written in the future such that data acquisition should occur a minimum of 20 minutes after ^{64}Cu-ATSM administration. Indeed if distribution effects of blood flow remain a problem correction of images for blood flow may be required which could be performed by using either dynamic CT perfusion data from PET-CT scans or by using short lived

PET blood perfusion tracers such as ^{15}O-H_2O (half-life 2 minutes) or ^{11}C-acetate (half-life 20.3 minutes).

^{64}Cu-ATSM requires adequate vascular delivery to the tumour before a distribution representing its biological handling within the tumour is manifest. From the studies performed it is reasonable to assume that its early distribution is representative of blood flow, however over the course of time other biological processes may begin to dominate its pattern of distribution. In the tumour model evaluated ^{64}Cu-ATSM and blood flow were statistically similar for the first twenty minutes following administration of ^{64}Cu-ATSM, after which statistical significance was lost even though the distributions remained similar. In similar tumours resected 75 minutes after administration of ^{64}Cu-ATSM a consistent relationship failed to be seen between the distributions of ^{64}Cu-ATSM and pimonidazole. A possible explanation for this is that 75 minutes is insufficient time for the pattern of ^{64}Cu-ATSM-defined hypoxia to be realised in this tumour type and that blood flow still dominates the picture as is the case with ^{18}F-FMISO (Rajendran 2005). However, the tumours injected with ^{64}Cu-ATSM 20 hours prior to their resection still did not have a pattern of distribution that was similar to the pattern of pimonidazole-defined hypoxia. The original hypothesis for the mechanism of cellular retention of ^{64}Cu-ATSM suggested that lipophilicity of the molecule allowed its passive transfer in to cells, following which Cu(II) was reduced to Cu(I) which subsequently dissociated from the parent compound and was retained in the cell (Fujibayashi 1997; Dearling 2002). This process was only possible if the cell was hypoxic. It has become increasingly clear that this simple proposition for a mechanism of cellular retention is, in fact, more complex. Burgman et al performed a series of experiments and found that dissociated ^{64}Cu could be found

extracellularly as well as within the cell, suggesting a possible ^{64}Cu efflux mechanism that is likely to vary across tumour types (Burgman 2005). This mechanism may in part explain the homogeneous distribution of ^{64}Cu-ATSM seen in our tumours at 20 hours. A distribution that may occur if there is specific cellular retention followed by efflux of ^{64}Cu in to the extra-cellular space. Of course there could still be a time point in the P22 tumour model post-injection of ^{64}Cu-ATSM that reflects hypoxia, between the pattern of distribution dominated by blood flow and the homogeneous distribution seen at a later time point, however this was not determined in this study and remains only a theoretical possibility.

In conclusion, the specific cellular handling processes of ^{64}Cu-ATSM and its products of dissociation are bound to vary between tumour types and although ^{64}Cu-ATSM does not appear to reflect hypoxia in the tumour studied it has been shown to correlate in a number of others. It would be naive to think that a single radiotracer could be applied to any tumour to provide an accurate map of such a specific biological feature like hypoxia. Hypoxia is the end point of a number of different pathophysiological processes including those occurring at the cellular level of the tumour, those involving tissue architecture and perfusion and features such as haemoglobin level and lung capacity. Although Cu-ATSM may reflect hypoxia in a number of tumour types, it is unlikely to be useful on a global tumour scale. There is already evidence to suggest that Cu(I) handling differs between tumour types which re-enforces the likely existence of varied complex biological processes occurring in such disordered systems. However we are now beginning to see how radiotracers can be used to image very specific cellular processes that previously would have been impossible on a clinical scale which is an exciting prospect. Most of our current

understanding of Cu-ATSM is based on the important pre-clinical investigations that have been described, however, further evaluation of the behaviour of this agent in the clinical setting is required in order to fully evaluate the potential Cu-ATSM has of being one of the first non-invasive methods for identification of tumour hypoxia. The positive results obtained in the two clinical studies (Dehdashti, Mintun, 2003; Dehdashti 2008) that demonstrated the ability of Cu-ATSM PET to predict the response of both non-small cell lung cancer and cervical cancer to radiotherapy, together with the pre-clinical study described in this thesis have lead to the formation of a clinical trial in our institution to evaluate Cu-ATSM PET in patients with squamous cell carcinoma of the head and neck. For this study patients will have a Cu-ATSM PET-CT scan prior to surgical resection of their tumour. The tumours will be oriented with the PET-CT images to allow a comparison between pimonidazole immunohistochemistry with Cu-ATSM uptake. A sub-group of patients will have a dynamic contrast-enhanced CT scan to evaluate the effects of blood flow on Cu-ATSM distribution. The results of this study will be used to provide evidence for the feasibility of using Cu-ATSM PET images for radiotherapy tumour subvolume dose escalation in order to improve tumour control and survival in these patients in whom tumour hypoxia results in radiation-resistance and is a significant factor in determining prognosis.

References

Burgman P, O'Donoghue J., Lewis JS, Welch MJ, Humm JL, Ling C (2005). "Cell line-dependent differences in uptake and retention of the hypoxia-selective nuclear imaging agent Cu-ATSM." Nucl Med Biol **32**: 623-630.

Dearling JLJ, Lewis J., Mullen GED, Welch MJ, Blower PJ (2002). "Copper bis(thiosemicarbazone) complexes as hypoxia imaging agents: structure-activity relationships." J Biol Inorg Chem **7**: 249-259.

Dehdashti F, Grigs P., Lewis JS, Laforest R, Siegel BA, Welch MJ (2008). "Assessing tumour hypoxia in cervical cancer by PET with [60Cu]-labeled diacetyl-bis(N4-methylthiosemicarbazone)." Journal of nuclear medicine 49(2): 201-205.

Dehdashti F, Grigsby PW, Mintun MA, Lewis JS, Sigel BA, Welch MJ (2003). "Assessing tumor hypoxia in cervical cancer by positron emission tomography with 60Cu-ATSM: relationship to therapeutic response-a preliminary report." Int J Radiat Oncol Biol Phys 55(5): 1233-8.

Dehdashti F, Mintun MA, Lewis JS, Bradley J, Govindan R, Laforest R, Welch MJ, Siegel BA. (2003). "In vivo assessment of tumor hypoxia in lung cancer with 60Cu-ATSM." Eur J Nucl Med Mol Imaging 30(6): 844-50.

Fujibayashi Y, Cutler C., Anderson CJ, McCarthy DW, Jones LA, Sharp T, Yonekura Y, Welch MJ (1999). "Comparative studies of Cu-64-ATSM and C-11-Acetate in an acute myocardial infarction model: Ex vivo imaging of hypoxia in rats." Nucl Med Biol 26: 117-121.

Fujibayashi Y, Taniuchi H, Yonekura Y, Ohtani H, Konishi J, Yokoyama A. (1997). "Copper-62-ATSM: a new hypoxia imaging agent with high membrane permeability and low redox potential." J Nucl Med 38(7): 1155-60.

Lewis JL, McCarthy D., McCarthy TJ, Fujibayashi Y, Welch MJ (1999). "Evaluation of ^{64}Cu-ATSM in vitro and in vivo in a hypoxic tumour model." J Nuc Med(40): 177-183.

Lewis JS, Sharp TL, Laforest R, Fujibayashi Y, Welch MJ. (2001). "Tumor uptake of copper-diacetyl-bis(N(4)-methylthiosemicarbazone): effect of changes in tissue oxygenation." J Nucl Med 42(4): 655-61.

Matsumoto K, Szajek L, Krishna MC, Cook JA, Seidel J, Grimes K, Carson J, Sowers AL, English S, Green MV, Bacharach SL, Eckelman WC, Mitchell JB. (2007). "The influence of tumor oxygenation on hypoxia imaging in murine squamous cell carcinoma using [64Cu]Cu-ATSM or [18F]Fluoromisonidazole positron emission tomography." Int J Oncol 30(4): 873-81.

O'Donoghue JA, Zanzonico P, Pugachev A, Wen B, Smith-Jones P, Cai S, Burnazi E, Finn RD, Burgman P, Ruan S, Lewis JS, Welch MJ, Ling CC, Humm JL. (2005). "Assessment of regional tumor hypoxia using 18F-fluoromisonidazole and 64Cu(II)-diacetyl-bis(N4-methylthiosemicarbazone) positron emission tomography: Comparative study featuring microPET imaging, Po2 probe measurement, autoradiography, and fluorescent microscopy in the R3327-AT and FaDu rat tumor models." Int J Radiat Oncol Biol Phys 61(5): 1493-502.

Rajendran JG, Krohn KA (2005). "Imaging hypoxia and angiogenesis in tumors." Radiol Clin North Am 43(1): 169-87.